

Proceedings of the
11th International Magnet Measurement Workshop
(IMMW-XI)

Brookhaven National Laboratory, Upton, NY 11973-5000, USA
September 21-24, 1999

- **Foreword**
- **Organizing Committee**
- **Abstracts (sorted by author)**
- **Program**
- **Session Summaries**
- **List of Participants**
- **List of Exhibitors**

Proceedings of the
11th International Magnet Measurement Workshop (IMMW-XI)
Brookhaven National Laboratory, Upton, NY 11973-5000, USA
September 21-24, 1999

F O R E W O R D

The 11th International Magnet Measurement Workshop (IMMW-XI) was held at Brookhaven National Laboratory, Upton, USA, during September 21-24, 1999. There were 52 registered [participants](#), 22 of them from seven countries outside the United States. Also, 7 of the participants were from the industry.

The format of the workshop [program](#) was similar to other workshops in this series. The scientific [program](#) consisted of oral presentations and visits to various laboratory facilities. The speakers at this workshop were encouraged to submit their presentations in electronic format, so that the proceedings could also be published as a CD-ROM, along with a paper version. It was encouraging to note that a good fraction of the contributions (26 out of 36) were received in electronic form. Three of the contributions were not received in any form, and hence could not be included in these proceedings. The remaining 7 contributions were converted from paper copies to PDF files. Some of the contents in these 7 files is searchable, but a large fraction is not.

In addition to the presentations included in these proceedings, there were two other important technical components of the program. One was visits to various laboratory facilities of interest, and the other was display of magnetic measurements related instruments by [vendors](#). The visits included the magnet test and construction facilities in building 902 (where nearly all the magnet measurement work related to RHIC was done), the measurement laboratory at the Alternating Gradient Synchrotron, and the magnet alignment and survey stations at the National Synchrotron Light Source. The STAR and the PHENIX experimental halls at RHIC were also visited. We thank Albert Prodell, John Jackson, George Rakowski, Robert Ruland and Timothy Hallman for their efforts to make these visits a success. On the industrial exhibits side, 4 [vendors](#) had set up displays at the Workshop. Apart from providing an opportunity to look at the latest product offerings by the leading manufacturers and to discuss individual needs, the exhibits also helped defray some of the cost of hosting the Workshop.

We would like to thank the members of the [International Advisory Committee](#) for their valuable input in the organization of this Workshop. Sincere thanks are due to the Workshop Secretary, Diana Votruba, who efficiently handled all the administrative matters and to David McChesney for his skilled computer support towards the organization of this Workshop, as well as the publication of these proceedings. We also acknowledge very useful discussions and support from Robert Ruland and Foster Thompson of SLAC in regard to creating the CD-ROM version of these proceedings.

[Animesh Jain](#)
Proceedings Editor

[Peter Wanderer](#)
Workshop Chairman

11th International Magnet Measurement Workshop (IMMW-XI)

**Brookhaven National Laboratory, Upton, NY 11973-5000, USA
September 21-24, 1999**

International Advisory Committee

Michael I. Green, LBNL

Knud Henrickson, CERN

Peter O. Mazur, FNAL

Gebhard Moritz, GSI

Malgorzata Tkatchenko, LNS-Saclay

Louis Walckiers, CERN

Peter Wanderer, BNL

Zachary Wolf, SLAC

Local Organizing Committee

Peter Wanderer (Workshop Chair)

Diana Votruba (Workshop Secretary)

Animesh Jain (Program & Proceedings)

David McChesney (Computer Support)

Joseph Muratore (Industrial Exhibits)

11th International Magnet Measurement Workshop (IMMW-XI)
Brookhaven National Laboratory, Upton, NY 11973-5000, USA
September 21-24, 1999

PROGRAM

Monday, September 20, 1999:

6:00 PM to 8:00 PM REGISTRATION (Brookhaven Center, Bldg.30)

Tuesday, September 21, 1999:

8:15 AM to 8:45 AM REGISTRATION (Berkner Hall lobby)

8:45 AM to 8:55 AM Welcome address (M. Harrison)

8:55 AM to 1:30 AM **Session TU1** (Chair: Knud Henrichsen)

8:55 AM **PRI01:** *Shimming the Superferric Storage Ring Magnet for the Brookhaven Muon g-2 Experiment*, Ralf Prigl, BNL. (60 min)

9:55 AM **COR01:** *Field Map of the LEP Spectrometer With A Moving Carbon Fiber Arm*, Didier Cornuet, CERN. (20 min)

10:15 AM **BRO01:** *Analytic Form for Fitting Hysteretic Magnet Strength*, Bruce Brown, FNAL. (15 min)

10:30 AM to 11:00 AM BREAK (30 min)

11:00 AM to 12 noon **Session TU2** (Chair: Knud Henrichsen)

11:00 AM **KUM01:** *Magnetic Field Measurement By Digital Integration Of A Repetitive Magnetic Field*, M. Kumada, K. Nishikigoori, T. Togasi and Takashi Aoki, NIRS and AEC. (20 min)

11:20 AM **THO01:** *AC Loss Measurements in RHIC Arc Dipoles*, Richard Thomas, BNL. (15 min)

11:35 AM **COR02:** *NMR Probe As A Field Marker In A Quadrupole*, Didier Cornuet and Fritz Caspers, CERN. (15 min)

11:50 AM **WOL01:** *Overview Of Magnetic Measurements At SLAC*, Zachary Wolf, SLAC. (10 min)

12 noon to 1:30 PM LUNCH (90 min)

1:30 PM to 3:00 PM **Session TU3** (Chair: Malgorzata Tkatchenko)

1:30 PM **TRB01:** *Magnet Alignment of the RHIC Magnets and Operational Experience*, Dejan Trbojevic, BNL. (40 min)

2:10 PM **THO02:** *Rotating Hall Probe System for Polarity Checks in RHIC Magnets*, Richard Thomas, BNL. (15 min)

Session TU3 Continued (Chair: Malgorzata Tkatchenko)

- 2:25 PM **MAK01:** *Magnetic Calibration Stands for Irradiation Influence on Magnetic Field Sensors*, V. K. Makoveev, N. I. Balalykin, A.V. Karpukhin, S. I. Kukarnikov, V. M. Lachinov, V. G. Shabratov, JINR, Dubna. (20 min)
- 2:45 PM **JAI01:** *Measurement of Integral Field of Helical Dipoles*, Animesh Jain, BNL. (15 min)
- 3:00 PM to 3:30 PM BREAK
- 3:30 PM to 5:00 PM **Session TU4 (Chair: Gebhard Moritz)**
- 3:30 PM **GRE01:** *Status of Magnetic Measurements at LBNL*, Michael I. Green, LBNL. (15 min)
- 3:45 PM **BIL01:** *Search Coils for LHC*, Jacques Billan, CERN. (20 min)
- 4:05 PM **EVA01:** *Magnet Measurements for the ISAC Project at TRIUMF*, Doug Evans, TRIUMF. (20 min)
- 4:25 PM **WOL02:** *Magnetic Measurements for the PEP II Interaction Region Permanent Magnets*, Zachary Wolf, SLAC. (20 min)
- 4:45 PM **DEN01:** *Effect of Rectangular Coil Windings on Magnetic Field Measurement using Rotating Coils System*, Laurent Deniau, CERN LHC-MTA. (15 min)
- 6:00 PM onwards: Welcoming Reception (Berkner Hall lobby)

Wednesday, September 22, 1999:

- 8:30 AM to 12 noon: **Session WE1 (Chair: Doug Evans)**
- 8:30 AM **WAL01:** *Measurements for the Acceptance Tests of the LHC Superconducting Magnets*, Louis Walckiers, CERN. (40 min)
- 9:10 AM **SCH01:** *Measurements of FNAL HGQ Model Magnets*, Phil Schlabach, FNAL. (30 min)
- 9:40 AM **SIM01:** *Magnetic Measurement on LHC Prototype Quadrupoles at Room Temperature*, Fabrice Simon, CEA. (20 min)
- 10:00 AM BREAK & VISITS TO **VENDOR** DISPLAYS*
- 11:30 AM **SCH02:** *Plans for Measurements of LHC IR Quads During Production*, Phil Schlabach, FNAL. (30 min)
- 12 noon to 1:00 PM LUNCH (60 min)
- 1:00 PM onwards Visits to Magnet Labs, followed by excursion and dinner.

(***Vendor** exhibits were set up during most of the duration of the workshop.)

Thursday, September 23, 1999:

- 8:30 AM to 10:00 AM **Session TH1** (Chair: Louis Walckiers)
- 8:30 AM **SCH03:** *Stretched Wire System at FNAL*, Phil Schlabach, FNAL. (25 min)
- 8:55 AM **RAK01:** *Trajectory Straightening, Fiducialization and Alignment of the Strong-Focusing VISA Undulator, using Pulsed Wire and Interferometric Techniques: Part I*, George Rakowsky, BNL, and Robert Ruland, SLAC(20 min)
- 9:15 AM **RAK02:** *Trajectory Straightening, Fiducialization and Alignment of the Strong-Focusing VISA Undulator, using Pulsed Wire and Interferometric Techniques: Part II*, George Rakowsky, BNL, and Robert Ruland, SLAC(20 min)
- 9:35 AM **DEN02:** *Finding Magnetic Axis of LHC Superconducting Dipoles in Warm Conditions*, Laurent Deniau, CERN LHC-MTA. (25 min)
- 10:00 AM to 10:30 AM BREAK (30 min)
- 10:30 AM to 12 noon **Session TH2** (Chair: Heiner Brueck)
- 10:30 AM **TEM01:** *Magnetic Center Finding using Vibrating wire technique*, Alexander Temnykh, Cornell. (20 min)
- 10:50 AM **BUZ01:** *The Mole: A Travelling Probe for Warm Magnetic and Optical Measurements of LHC Dipoles*, L. Bottura(1), M. Buzio(1), G. Deferne(1), H. Jansen(2), C. Glöckner(2), A. Köster(2), P. Legrand(1), A. Rijllart(1), P. Sievers(1)
(1) CERN, (2) Fraunhofer Institut, IPT, Aachen, Germany (30 min)
- 11:20 AM **MOR01:** *Pulsed Wire System for Magnetic Measurement at SLAC*, Gebhard Moritz, GSI. (20 min)
- 11:40 AM **BIL02:** *An AC Field Static System for Measuring the Magnetic Axis of LHC Superconducting Magnets In Warm Condition*, Jacques Billan, CERN. (20 min).
- 12 noon to 1:30 PM LUNCH (90 min)
- 1:30 PM to 2:30 PM **Session TH3** (Chair: Bruce Brown)
- 1:30 PM **GAR01:** *Development of a Measurement System for the Magnetic Field Geometry of LHC Magnets*, Jacques Billan and Juan Jose Garcia Perez, CERN. (20 min)
- 1:50 PM **EVE01:** *A New Challenge in Magnetic Axis Transfer*, Corinne Evesque, CNRS-IN2P3. (20 min)

Session TH3 Continued (Chair: Bruce Brown)

- 2:10 PM **WOL03: *Magnet Alignment Tools Developed At SLAC***, Zachary Wolf, SLAC. (20 min)
- 2:30 PM to 3:00 PM BREAK (30 min)
- 3:00 PM to 5:00 PM VISITS TO NSLS AND RHIC

Friday, September 24, 1999:

- 8:30 AM to 10:30 AM **Session FR1 (Chair: Didier Cornuet)**
- 8:30 AM **GUR01: *Magnet Mapping of the PHENIX Magnets Using Surface Method***, Wlodek Guryn, BNL. (60 min)
- 9:30 AM **WOL04: *The Babar Detector Solenoid Field Map***, Zachary Wolf, SLAC. (20 min)
- 9:50 AM **RON01: *High Accuracy Field Mappings Using a Laser Monitored Traveling Mole***, B. Dehning, G. Mugnai, F. Roncarolo, CERN. (20 min)
- 10:10 AM **SCH04: *Recycler Measurements***, Phil Schlabach, FNAL. (20 min)
- 10:30 AM to 11:00 AM BREAK (30 min)
- 11:00 AM to 12 noon **Session FR2 (Chair: Michael I. Green)**
- 11:00 AM **BRO02: *Top Ten Things to Learn at IMMW***, Bruce Brown, FNAL. (15 min)
- 11:15 AM **Summaries of various sessions by respective chairpersons.** (45 min)
- 12 noon Workshop ends.

11th International Magnet Measurement Workshop (IMMW-XI)
Brookhaven National Laboratory, Upton, NY 11973-5000, USA
September 21-24, 1999

SUMMARIES OF SESSIONS

Summaries of all the sessions were presented by the respective chairpersons at the concluding session of the Workshop on September 24, 1999. Summaries of the following sessions were made available for inclusion in the proceedings:

[Session TU3](#), Tuesday, September 21, 1999, 1:30 PM to 3:00 PM.
(Chair: Malgorzata Tkatchenko, CEA, Saclay)

[Session TU4](#), Tuesday, September 21, 1999, 3:30 PM to 5:00 PM.
(Chair: Gebhard Moritz, GSI)

[Session WE1](#), Wednesday, September 22, 1999, 8:30 AM to 12:00 noon.
(Chair: Doug Evans, TRIUMF)

11th International Magnet Measurement Workshop (IMMW-XI)
Brookhaven National Laboratory, Upton, NY 11973-5000, USA
September 21-24, 1999

Abstracts of Presentations

BIL01: Search Coils for LHC

Jacques Billan, CERN

No abstract received.

BIL02: An AC Field Static System for Measuring the Magnetic Axis of LHC Superconducting Magnets In Warm Condition

Jacques Billan, CERN

The choice of a 3D-laser tracker for controlling several delicate operations during the fabrication process of the LHC magnets gave the idea to measure simultaneously, with a single mole, the centre axis of the cold bore tube and the magnetic axis of the magnet. This mole houses at the same cross-section point four tangential coils for detecting the magnetic axis, a corner cube for detecting the centre of the mole and a mechanical system to centre the mole inside the cold bore tube. This contribution described the principle, the equipment and the preliminary results related especially to the magnetic axis measurement.

BRO01: Analytic Form for Fitting Hysteretic Magnet Strength

Bruce Brown, FNAL

I presented analytic forms for fitting magnet strength with hysteresis. It will provide fits to MI Dipole strength at the 3E-4 level.

BRO02: Top Ten Things to Learn at IMMW

Bruce Brown, FNAL

It will reflect on various successes and mostly failures, some of which we were warned about at previous IMMW's.

BUZ01: The Mole: a Travelling Probe for Warm Magnetic and Optical Measurements of LHC Dipoles

L. Bottura(1), M. Buzio(1), G. Deferne(1), H. Jansen(2), C. Glöckner(2), A. Köster(2), P. Legrand(1), A. Rijllart(1), P. Sievers(1)

(1) CERN, (2) Fraunhofer Institut, IPT, Aachen, Germany

A novel kind of harmonic coil probe (the Mole) has been developed for the measurement, in warm conditions, of magnetic field quality, field direction and axis of the superconducting LHC dipoles and associated sextupole and decapole corrector windings. The Mole houses a set of radial rotating coils and travels inside the magnet aperture by means of an externally driven two-way traction belt. The coil rotation is driven by an ultrasonic piezoelectric motor, being tested in view of future devices for cold measurements as the only type of electrical motor compatible with a strong magnetic field. A light spot is generated by a LED source and projected optically into the coil center on the coil rotation axis. The position of this virtual light spot is measured by an optical system that includes a telescope, a CCD camera and a DSP carrying out image processing algorithms. The position is then transferred with high accuracy to the magnet fiducial reference

line by means of a system of jigs. In this paper we describe the characteristics of the Mole, its capability in terms of resolution and accuracy of measured harmonics, field direction and magnetic axis position, and a comparative analysis of the results obtained on a LHC dipole using the Mole as well as other measurement systems.

COR01: Field Map of the LEP Spectrometer With A Moving Carbon Fiber Arm

Didier Cornuet, CERN

To measure the energy of the LEP machine (Large Electron Positron collider) at high energies, a spectrometer is installed in the tunnel because the polarization is working well under 60 GeV. Field maps of the spectrometer have been undertaken so that the ratios of integrals Bdz can be known with a precision of few $10E-5$. The previous LEP magnetic measurement stand has been modified by including a carbon fiber arm which is practically not sensitive to temperature fluctuations. A description of the stand is given with first measurement results.

COR02: NMR Probe As A Field Marker In A Quadrupole

Didier Cornuet and Fritz Caspers, CERN

To improve the reproducibility from cycle to cycle of an accelerator a B_train is implemented and refined with the help of NMR (Nuclear Magnetic Resonance probes) markers. This B-train is linked to the field of the main bending magnets. For the Cern-SPS machine it is also proposed to improve the reproducibility of the focusing elements by including a "G_train" linked to the gradient of the main quadrupoles. The evaluation of different options will be presented.

DEN01: Effect of Rectangular Coil Windings on Magnetic Field Measurement using Rotating Coils System

Laurent Deniau, CERN LHC-MTA

This talk will present the influence of different coil winding approximations (sector, sector with same center of mass, rectangular and rectangular with tilt) in the computation of coil geometric factors used in the magnetic field measurement of the LHC magnets. Results are provided for tangential coil 15m long shaft used at CERN.

DEN02: Finding Magnetic Axis of LHC Superconducting Dipoles in Warm Conditions

Laurent Deniau, CERN LHC-MTA

This talk will present a method proposed for finding in warm condition the magnetic axis of the 15m long dipole magnets built for the LHC. The goal of the method is to improve the accuracy of the measurement of the magnetic field of dipoles in warm condition (low current, low field) in order to compute their harmonics with a good enough accuracy to be able to find the magnetic axis. The method involves the use of low AC current using the current frequency as an amplifier (derivate of flux proportionnal to the frequency) and a signal processing method (synchronous demodulation) to recover the harmonics from the modulated signal read by the rotating coils.

EVA01: Magnet Measurements for the ISAC Project at TRIUMF

Doug Evans, TRIUMF

This would include a brief overview of the expansion at Triumf with the building of the ISAC project, focusing on some of the major magnets, the equipment used to measure them, and the results for both dipoles and multipole magnets. All these magnets are DC and room temperature.

EVE01: A New Challenge in Magnetic Axis Transfer

Corinne Evesque, CNRS-IN2P3

No abstract received.

GAR01: Development of a Measurement System for the Magnetic Field Geometry of LHC Magnets

Jacques Billan and Juan Jose Garcia Perez, CERN

In the context of the LHC superconducting dipoles production it is foreseen to perform acceptance tests, including field measurements of the collared coils assembly to estimate, at an early production stage, the possible significant deviations from the expected multipole component value of these magnets. A sensitive measuring probe and efficient data acquisition are the consequence of a low magnetisation current necessary to limit the coils heating. The knowledge of the magnetic field geometry is very important, especially for multipole magnets. In order to get this information two systems have been conceived. First, a mole miming the magnetic one but equipped only with position sensors laser beam as reference line, target and CCD camera) to complement the magnetic measurement. A second system equipped with magnetic sensors (4 static tangential coils and AC excitation current for the magnet) and position sensors (3D-laser tracker and light reflector) allow the detection of the magnetic field axis and the cold bore axis. Another capability of this system is to work for several field configurations ($n=1, 2, 3, 4$ and 5). This conference contribution describes these two systems and gives the preliminary performance results.

GRE01: Status of Magnetic Measurements at LBNL

Michael I. Green, LBNL

No abstract received.

GUR01: Magnet Mapping of the PHENIX Magnets Using Surface Method

Wlodek Guryń, BNL

We shall describe the mapping procedure, setup and give preliminary results of the magnet mapping of the PHENIX magnets. We used the surface mapping technique, where the flux of the magnetic field through the closed surface surrounding the volume of interest is measured. Given the absence of the current sources inside the surface, the magnetic potential satisfies Laplace equation, which is solved using Green's function method. Reconstructed field is compared to the measurements made on the inside of the volume of interest and to TOSCA simulations.

JAI01: Measurement of Integral Field of Helical Dipoles.

Animesh Jain, BNL

Helical dipoles with 360 degrees rotation of the dipole field over 2.4 m length are being built for the RHIC spin physics program. The integral dipole field for such magnets is ideally zero, and should be below 0.05 T.m for central dipole field strength of 4 T. The integrated dipole field is measured using a long rotating coil. Errors introduced in the measurement of integral field due to typical coil construction errors will be presented, and illustrated using experimental data.

KUM01: Magnetic Field Measurement By Digital Integration Of A Repetitive Magnetic Field

M.Kumada, K.Nishikigoori, T.Togasi and Takashi Aoki, NIRS(National Institute of Radiological Sciences) and AEC(Accelerator Engineering Corporation)

In conventional magnetic measurement using search coil, an integrator using operational amplifier or Voltage to Frequency Converter with a combination of counter is used to acquire magnetic field information. The purpose of integration is not only to get the magnetic information but to improve Signal to Noise ratio. The Integrator, however, usually has a difficulty in reducing long term drift of the operational amplifier. The voltage to frequency converter also has similar problem as well as a resolution. We have developed a new technique by applying a digital processing capability of FFT analyzer to integrate the output voltage of search coil. This is very useful to diminish drift effect when magnets are excited periodically as in most of the accelerator.

MAK01: Magnetic Calibration Stands for Irradiation Influence on Magnetic Field Sensors

V.K. Makoveev, N.I.Balalykin, A.V.Karpukhin, S.I.Kukarnikov, V.M.Lachinov, V.G. Shabratov, Joint Institute for Nuclear Research, Dubna, Russia

Parameters of modern experimental set-ups depend on the precision of the magnetic field monitoring in the conditions of a real experiment. As a rule, the conditions of modern experiments (ATLAS, CMS, ALICE, LHC-B) have their special requirements to radiation hardness of the magnetometric apparatus used in the given set-up. Specialized magnetic-calibration stands have been manufactured (0.025÷5T) to investigate sensors of the magnetic field for radiation hardness at the Joint Institute for Nuclear Research (JINR). The superconducting stand has a magnet fields up to 5 T with a field homogeneity up to 0.001%/cm in a warm work volume of 60 cm³. The warm stand has a function of a magnet fields up to 2 T with a field homogeneity up to 0.01%/cm in a gap 30 mm and diameter 50 mm. Characteristics of different magnetic field sensors were studied before exposure and after it.

The work is supported by projects ISTC # 639.

MOR01: Pulsed Wire System for Magnetic Measurement at SLAC

Gebhard Moritz, GSI

A 'pulsed wire' bench was built at SLAC. We used the system for two measurements: Finding the axis of a quadrupole and determination of the transverse fields of a permanent magnet stack.

PRI01: Shimming the Superferric Storage Ring Magnet for the Brookhaven Muon g-2 Experiment

Ralf Prigl, BNL

A C-shaped storage ring magnet with a circumference of 45m and powered by superconducting coils has been built and operated for the Muon g-2 experiment currently in progress at BNL. The goal of this experiment is to measure the Anomalie $a = (g-2)/2$ to a precision of 0.35 ppm, a 20-fold improvement over the previous experiment done at CERN about 25 years ago. This requires good field homogeneity and precise field measurements in the muon storage region which has a circular aperture of 9cm diameter. The field measurement equipment and the shimming tools used will be discussed.

RAK01: Trajectory Straightening, Fiducialization and Alignment of the Strong-Focusing VISA Undulator, using Pulsed Wire and Interferometric Techniques: Part I (presented by G. Rakowsky)

George Rakowsky, BNL, and Robert Ruland, SLAC

Brief description of the VISA FEL experiment. Design of the in-vacuum undulator and its vacuum vessel. Alignment tolerance and error budget. Magnet sorting and matching. Pulsed wire measurements. Trajectory shimming. Determining the magnetic axis.

RAK02: Trajectory Straightening, Fiducialization and Alignment of the Strong-Focusing VISA Undulator, using Pulsed Wire and Interferometric Techniques: Part II (presented by R. Ruland)

George Rakowsky, BNL, and Robert Ruland, SLAC

Fiducialization concept. Description of the straightness interferometer, the optical wire finders and the zero-force gauge bar. Referencing the magnetic axis to fiducials. Alignment concept. The two-axis straightness interferometer. Aligning the undulator sections to the beamline.

RON01: High Accuracy Field Mappings Using a Laser Monitored Traveling Mole

B. Dehning, G. Mugnai, F. Roncarolo, CERN

A spectrometer has been installed along the beam path of the LEP accelerator in order to measure the beam energy with a relative accuracy of $10e-4$. A bending magnet is flanked on either side by three beam position monitors (BPM) used to determine the deflection angle of the beam. This angle, together with the integral of the magnetic field along the beam trajectory, allows the calculation of the beam energy. In order to reach the desired accuracy on the energy a relative precision of a few $10e-5$ on the magnetic field integral is necessary. The field inside the magnet has been mapped first in a dedicated laboratory setup based on a moving arm equipped with one NMR and two Hall probes. In the same laboratory another system was setup to cross check the magnetic field integral and perform the mapping again after the magnet transportation and positioning in the LEP ring. This measurement was carried out using a mole sliding inside the vacuum pipe. Two NMR probes as well as a search coil were mounted on the mole and used to sample the field value every 10 mm. The longitudinal position was monitored by a laser interferometer while the transverse positioning was ensured by the precise mechanical construction of the mole running in the vacuum chamber. Several field maps have been carried out at different field levels and at different temperatures in order to ensure a good extrapolation to the actual run conditions. Four NMR probes were installed in between the vacuum chamber and the lower pole, in four fixed locations. Those same probes remain available during the normal spectrometer operation and are used to extrapolate the real field integral. A full description of the mapping mole system together with the measurement procedure is given. A summary of the results is also presented with particular focus on the reproducibility and accuracy of this technique. A comparison with the results of the first system used in the laboratory is provided.

SCH01: Measurements of FNAL HGQ Model Magnets

Phil Schlabach, FNAL

No abstract received.

SCH02: Plans for Measurements of LHC IR Quads During Production

Phil Schlabach, FNAL

No abstract received.

SCH03: Stretched Wire System at FNAL

Phil Schlabach, FNAL

No abstract received.

SCH04: Recycler Measurements

Phil Schlabach, FNAL

No abstract received.

SIM01: Magnetic Measurement on LHC Prototype Quadrupoles at Room Temperature

Fabrice Simon, CEA

No abstract received.

TEM01: Magnetic Center Finding using Vibrating wire technique

Alexander Temnykh, Cornell

No abstract received.

THO01: AC Loss Measurements in RHIC Arc Dipoles

Richard Thomas, BNL

No abstract received.

THO02: Rotating Hall Probe System for Polarity Checks in RHIC Magnets

Richard Thomas, BNL

No abstract received.

TRB01: Magnet Alignment of the RHIC Magnets and Operational Experience

Dejan Trbojevic, BNL

No abstract received.

WAL01: Measurements for the Acceptance Tests of the LHC Superconducting Magnets

Louis Walckiers, CERN

No abstract received.

WOL01: Overview Of Magnetic Measurements At SLAC

Zachary Wolf, SLAC

No abstract received.

WOL02: Magnetic Measurements for the PEP II Interaction Region Permanent Magnets

Zachary Wolf, SLAC

No abstract received.

WOL03: Magnet Alignment Tools Developed At SLAC

Zachary Wolf, SLAC

No abstract received.

WOL04: The Babar Detector Solenoid Field Map

Zachary Wolf, SLAC

No abstract received.

11th International Magnet Measurement Workshop (IMMW-XI)
Brookhaven National Laboratory, Upton, NY 11973-5000, USA
September 21-24, 1999

List of Participants

- 1. Jeffrey Aspenleiter** 1-631-344-4590
BNL, NSLS aspenlei@bnl.gov
Bldg. 725A, Upton, NY 11973, USA
- 2. Ken Atchue** 1-508-852-3674
Walker Scientific Inc. walkrsci@world.std.com
Rockdale Street, Worcester, MA 01606, USA
- 3. Ulf Bechstedt** +49 2461 61 3624
Forschungszentrum Juelich GmbH u.bechstedt@fz-juelich.de
IKP-COSY, Postfach 1913
Leo-Brand Strasse, Juelich, NRW D-52425, Germany
- 4. Jacques Billan** 00 41 22 767 5977
CERN, LHC Jacques.Billan@cern.ch
1211 Geneva 23, Switzerland
- 5. Bruce Brown** 1-630-840-4404
Fermilab bcbrown@fnal.gov
Beams Division/Main Injector
MS341
PO Box 500, Batavia, IL 60510, USA
- 6. Heiner Brueck** +49 40 8998 3944
DESY, MKS brueck@herant.desy.de
Notkestr 85, Hamburg 22607, Germany
- 7. Marco Buzio** +4122 767 3724
CERN LHC MTA marco.buzio@cern.ch
Magnet tests & Analysis
CERN LHC Division
CH 1211 GENEVA 23
Meyrin, GENEVA 1211, Switzerland

IMMW-XI: List of Participants (Page 2 of 6)

- 8. Didier Cornuet** 00 41 22 767 2551
CERN Didier.Cornuet@cern.ch
SL Division, Meyrin site
Bldg 23-1-032
Geneva, CH-1211, Switzerland
- 9. Laurent Deniau** +4122 767 4647
CERN LHC MTA laurent.deniau@cern.ch
Magnet Tests & Analysis
CERN LHC DIVISION
CH 1211 GENEVA 23
Meyrin, Geneva 1211, Switzerland
- 10. Doug Evans** 1-604-222-1047 local 6423
Triumf devans@triumf.ca
Magnet Measurement
4004 Wesbrook Mall
Vancouver, B.C. V6T-2A3, Canada
- 11. Corinne Evesque** 331.69.08.90.02
CNRS-IN2P3 cevesque@cea.fr
SEA/LMM - L'Orme des Merisiers - Bat 701
CEA SACLAY
91191 Gif SUR YVETTE, France
- 12. Juan Jose Garcia Perez** 41-22-767.3762
CERN Juan.Garcia.Perez@cern.ch
LHC/MMS
Meyrin, Geneva 1211, Switzerland
- 13. James Gentile** 1-407-678-6900
F. W. Bell
Div. of Bell Technologies
6120 Hanging Moss Road
Orlando, FL 32807, USA
- 14. Michael Green** 1-925-254-0609
Lawrence Berkeley National Laboratory MIGreen@lbl.gov
117 Rheem Boulevard
Orinda, CA 94563-3620, USA
- 15. Wlodek Guryn** 1-631-344-3878
Brookhaven National Laboratory gurun@bnl.gov
Physics, 510C
Upton, NY 11973, USA

IMMW-XI: List of Participants (Page 3 of 6)

- 16. Ping He** 1-631-344-2042
BNL, NSLS
B.820/ATF
Upton, NY 11973, USA
phe@bnl.gov
- 17. Knud Henriksen** +41 22 767 3284
CERN, LHC
CH-1211, Geneva 23, Switzerland
knud.henrichsen@cern.ch
- 18. John Herrera** 1-631-344-7763
Brookhaven National Laboratory
Bldg. 902A, Cornell Ave.
Upton, NY 11973, USA
- 19. Ted Hunter** 1-505-665-8975
Los Alamos National Laboratory
LANSCCE-1, P.O. Box 1663
MS H817, Los Alamos, NM 87545, USA
thunter@lanl.gov
- 20. Peter Hwang** 1-610-266-2840
Everson Electric Company
Engineering
2000 City Line Road, Bethlehem, PA 18017, U.S.A.
phwang@eversonelec.com
- 21. John Jackson** 1-631-344-4695
Brookhaven National Laboratory
AGS, Upton, NY 11973-5000, USA
jackson@bnl.gov
- 22. Animesh Jain** 1-631-344-7329
Brookhaven National Laboratory
Superconducting Magnet Division
Building 902A, PO Box 5000
Upton, NY 11973-5000, USA
jain@bnl.gov
- 23. Jeff Karn** 1-757-269-7010
Jefferson Lab
Accelerator Engineering
12000 Jefferson Ave.
MS 4A, Newport News, VA 23606, USA
karn@jlab.org
- 24. Masayuki Kumada** +81 43 251 2111 x6872
Nat'l Inst. of Radiological Sciences
4-9-1 anagawa, inage
3-15-13 kasuga, Tsukuba, Ibaraki, Japan
chiba, chiba 263-8555, Japan
kumada@nirs.go.jp

IMMW-XI: List of Participants (Page 4 of 6)

- 25. Patrick Legrand** +4122 767 5761
CERN LHC MTA
Magnet Tests & Analysis
CERN, Meyrin Site LHC Division
CH 1211 GENEVE 23
Meyrin, Geneva 1211, Switzerland
patrick.legrand@cern.ch
- 26. Michael Lehecka** 1-631-344-4590
BNL, NSLS
Bldg. 725A, Upton, NY 11973, USA
lehecka@bnl.gov
- 27. Vladimir Makoveev** +7-096-21-63056
Joint Institute for Nuclear Research
Particle Physics Laboratory
Leader of Magnetometry Group, PPL, JINR
Dubna, Moscow Region 141980, Russia
makoveev@sunse.jinr.ru
- 28. David McChesney** 1-631-344-4623
Brookhaven National Laboratory
Superconducting Magnet Division
Building 902A, P.O. Box 5000
Upton, New York 11973-5000, USA
mcchesne@bnl.gov
- 29. Gebhard Moritz** 49 615 971 2368
GSI, BTE
Planckstrasse 1, Darmstadt, 64291, Germany
g.moritz@gsi.de
- 30. Giuseppe Mugnai** +41 22 767 5593
CERN, SL Division
1211 Geneva 23, Switzerland
mugnai@cern.ch
- 31. Joseph Muratore** 1-631-344-2215
Brookhaven National Laboratory
Superconducting Magnet Division
PO Box 5000, Building 902A
Upton, NY 11973, USA
muratore@bnl.gov
- 32. James Murphy** 1-407-678-6900 Ext. 216
F. W . Bell
Div. of Bell Technologies
6120 Hanging Moss Road
Orlando, FL 32807, USA
jmurphy@belltechinc.com
- 33. Oreste Pagano** +4122 767 5934
CERN, LHC Division
Rte De Meyrin
1211 Geneva 23
Meyrin, Geneva 1211, Switzerland
oreste.pagano@cern.ch

IMMW-XI: List of Participants (Page 5 of 6)

- 34. Ralf Prigl** 1-631-344-6035
BNL, AGS prigl@bnl.gov
Building 911B
Upton, NY 11973, USA
- 35. George Rakowsky** 1-631-344-5298
BNL, NSLS rakowsk1@bnl.gov
Bldg. 725-D, P.O. Box 5000
Upton, NY 11973-5000, USA
- 36. Claude Reymond** +41 22 884 33 13
MetroLab Instruments SA creymond@metrolab.ch
110, Pont-du-Centenaire
CH-1228, Geneva, Switzerland
- 37. Brian Richter** 1-650-802-8292
GMW Associates brian@gmw.com
P.O. Box 2578
Redwood City, CA 94064, USA
- 38. Federico Roncarolo** +390322804258
CERN, SL/BI federico.roncarolo@cern.ch
via vignale 32
Borgomanero, 28021 ITALY
- 39. Robert Ruland** 1-650-926-3468
SLAC, Metrology ruland@slac.stanford.edu
P.O. Box 4349, Stanford, CA 94309, USA
- 40. Phil Schlabach** 1-630-840-5037
Fermilab schlabach@fnal.gov
Technical Division, Dev.&Test
Fermilab, MS316
PO Box 500, Batavia, IL 60510, USA
- 41. Thomas Schultheiss** 1-631-345-6264 Ext. 3012
Advanced Energy Systems Inc. Tom_Schultheiss@mail.aesys.net
Engineering Analysis
27 Industrial Blvd., Unit E, Medford, NY 11763, USA
- 42. Fabrice Simon** +33 1.69.08.33.28
CEA simonf@hep.saclay.cea.fr
DAPNIA/STCM
CEA-Saclay, GIF SUR YVETTE, 91191, France
- 43. Charles Spataro**
Brookhaven National Laboratory, AGS spataro@bnl.gov
Upton, NY 11973-5000, USA

IMMW-XI: List of Participants (Page 6 of 6)

- 44. Alexander Temnykh** 1-607-255-4882
Cornell University st@lns.cornell.edu
Physics, Wilson Lab
Ithaca, NY 14850, USA
- 45. Richard Thomas** 1-631-344-3534
Brookhaven National Laboratory thomas1@bnl.gov
Bldg. 902A, Upton, NY 11973-5000, USA
- 46. Malgorzata Tkatchenko** 01 69 08 73 06
CEA (Commissariat a L'Energie Atomique) tkatchenko@dapnia.cea.fr
DSM/DAPNIA/SGPI
CEA Saclay, bat.123
GIF SUR YVETTE, 91191 France
- 47. Gueorgui Velev** 1-630-840-3630
Fermilab velev@fnal.gov
Technical Division-Dev & Test
P.O. Box 500 - MS 316, Batavia, IL 60510, USA
- 48. Louis Walckiers** +4122 767 6945
CERN LHC-MTA Louis.Walckiers@cern.ch
Magnet Tests & Analysis
CERN LHC DIVISION
CH 1211 Geneva 23
Geneva, Geneva 1211, Switzerland
- 49. Peter Wanderer** 1-631-344 7687
Brookhaven National Lab wanderer@bnl.gov
Superconducting Magnet Division
Building 902A
PO Box 5000, Upton, NY 11973-5000, USA
- 50. Zachary Wolf** 1-650-926-2576
SLAC wolf@slac.stanford.edu
Magnetic Measurements, MS 87
P.O. Box 4349, Stanford, CA 94309, USA
- 51. Chen Yan** 1-757-269 7349
Thomas Jefferson National Accelerator Facility Yan@jlab.org
Physics
12000 Jefferson Avenue, Newport News, VA 23606, U.S.A.
- 52. Janos Zichy** +41 56 310 3596
Paul Scherrer Institut (PSI) zichy@psi.ch
Swiss Light Source (SLS)
WLGA/C11
Villigen, CH-5232, Switzerland

11th International Magnet Measurement Workshop (IMMW-XI)
Brookhaven National Laboratory, Upton, NY 11973-5000, USA
September 21-24, 1999

Vendors who had set up exhibits at IMMW-XI

Lake Shore Cryotronics, Inc.

575 McCorkle Blvd.
Westerville, OH 43082, USA
Phone: 1-614- 891-2243
Fax: 1-614- 891-1600

Represented at IMMW-XI by
Andy Ian

IAN Technology Solutions

15 Indian Ridge Rd.
Atkinson, NH 03811, USA
Phone: 1-603-362-5971
1-603-362-5117

FW Bell, Div. of Bell Technologies

6120 Hanging Moss Rd.
Orlando, FL 32807, USA
Phone: 1-407-678-6900 ext 216
Fax: 1-407-677-5765

Represented at IMMW-XI by
James Murphy
Product Manager - Gaussmeters
jmurphy@belltechinc.com

Walker Scientific

Corporate Office: Rockdale Street,
Worcester, MA 01606, USA
walkrsci@world.std.com
info@walkerscientific.com
Phone: 1-508-852-3674
1-800-W-MAGNET
Fax: 1-508-856-9931

Represented at IMMW-XI by
Ken Atchue

GMW Associates

P.O. Box 2578
Redwood City, CA 94064, USA
Phone: 1-650-802-8292, Ext: 12
Fax: 1-650-802-8298

Represented at IMMW-XI by
Brian Richter
e-mail: brian@gmw.com

Shimming the superferric storage ring magnet for the Brookhaven Muon g-2 Experiment

R. Prigl, BNL

I. Introduction

The muon g-2 experiment at Brookhaven National Laboratory has the goal of determining the muon anomalous g-value, $a_\mu = (g_\mu - 2)/2$, to a precision of 0.35 ppm (parts per million) and thus requires a storage ring magnet with great field stability and homogeneity. A superferric storage ring with a radius of 7.11m and providing a field of 1.45 Tesla has been constructed and is in operation since 1996. The experiment started taking data in summer 1997 and the result of this engineering run together with a brief description of the experiment can be found in [1]. In this talk, the tools used to shim the magnet to the required homogeneity, and the field measurements at various stages of the shimming process are presented.

II. The g-2 Storage Ring Magnet

The storage ring magnet has been designed and constructed with maximum attention to azimuthal symmetry and with a number of shimming tools to allow obtaining a homogeneous magnetic field. An extensive article describing the details of the design and construction is still in preparation ([2]), but most of the design considerations and features are discussed in [3, 4]. The cross section of the 'C'-shaped storage ring magnet is shown in Figs. 1,2. It is excited by superconducting coils which carry a current of 5177 A. The yoke consists of twelve 30 degree sections bolted together at the four corners, see Fig. 1, with azimuthal gaps of less than 1 mm. Easily removable/adjustable steel plates on the top and bottom of the yoke, 15 degrees wide, allow adjustments of the total yoke reluctance for a coarse reduction of the field inhomogeneity in azimuth. The pole pieces are 10 degrees long and aligned with the yoke sectors. The azimuthal gap between adjacent pole pieces of about $75 \mu\text{m}$ is filled with insulating Kapton foils to avoid irregular eddy current effects. The vertical gap between pole and yoke decouples the field between the poles, which are fabricated from very pure vacuum cast iron steel, from imperfections in the magnet yoke, which is fabricated from conventional 1006 steel. It also allows the insertion of iron wedges to compensate for the quadrupole moment in the magnetic field due to the C-shaped yoke.

The 10 cm wide wedges are radially adjustable to improve the field homogeneity in azimuth. The four edge shims, 5 cm wide and initially 3.2 mm (outer radius) and 4.3 mm (inner radius) high, are the main tool for reducing field variations over the beam cross section. The wedge angle provides a parameter for an almost pure adjustment of the normal quadrupole but it turned out that the design angle was close to perfect and there was no need to ground the

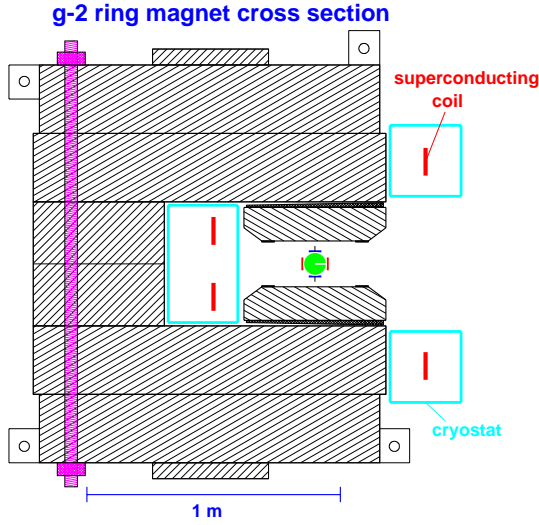


Figure 1: Magnet cross section.

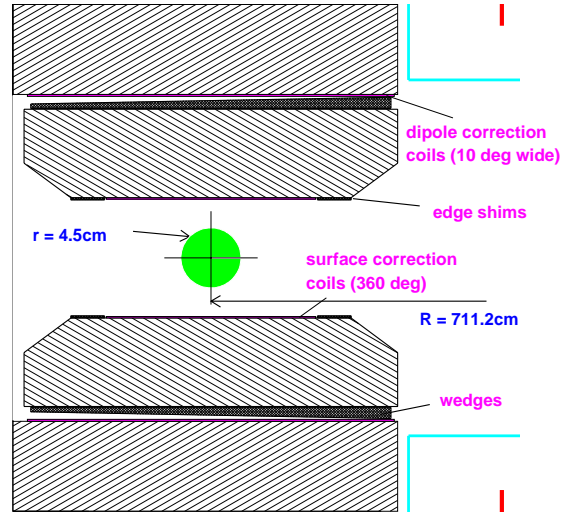


Figure 2: Main shimming tools.

wedges. Continuous current shims on the poles in form of printed circuit boards that were glued onto the pole faces between the inner and outer edge shims are used to further reduce the inhomogeneity in the integrated field.

III. Magnetic field characterization

Multipole analysis in two dimensions was used to study the field distribution over the cross section of the muon storage region. As the diameter of 9 cm of the toroidal muon storage region is very small compared to the ring magnet circumference of 4469 cm (44.7m), it can be approximated by a straight section. We denote x as the radial, y as the vertical, and z as the azimuthal coordinate. For most of the circumference it can be assumed that the dependence of the magnetic field $B(x,y,z)$ on z is small compared to the field variations in the x - and y -direction. In this case the magnetic field can be approximated by a 2-dimensional series of multipoles

$$B_y = \sum_{n=0}^{\infty} C_n r^n \cos(n\phi) - \sum_{n=0}^{\infty} D_n r^n \sin(n\phi) \quad (1)$$

$$B_x = \sum_{n=0}^{\infty} C_n r^n \sin(n\phi) + \sum_{n=0}^{\infty} D_n r^n \cos(n\phi), \quad (2)$$

where r and ϕ are polar coordinates, $x = r \cdot \cos \phi$ and $y = r \cdot \sin \phi$. The coefficients C_n and D_n refer to the normal and skew multipoles respectively. Note that according to our definition a positive skew quadrupole component C_1 refers to higher field values towards the negative y -direction, i.e. the lower pole. In the $(g-2)$ storage ring magnet the dominant field component

is the normal dipole term C_0 , subsequently referred to as the dipole field. The skew dipole term D_0 , or radial field, as well as all higher order terms ($C_n, D_n, n = 1, 2, 3, \dots$), will be expressed in ppm relative to the dipole field C_0 . All multipoles other than dipole will be presented as amplitudes at $r_0 = 4.5 \text{ cm}$, the edge of the muon beam aperture:

$$B_y = B_{dipole} + B_{quad}^{norm} \left(\frac{r}{4.5}\right) \cos \phi + B_{sext}^{norm} \left(\frac{r}{4.5}\right)^2 \cos 2\phi + B_{octu}^{norm} \left(\frac{r}{4.5}\right)^3 \cos 3\phi + B_{decu}^{norm} \left(\frac{r}{4.5}\right)^4 \cos 4\phi + \dots \quad (3)$$

$$-B_{quad}^{skew} \left(\frac{r}{4.5}\right) \sin \phi - B_{sext}^{skew} \left(\frac{r}{4.5}\right)^2 \sin 2\phi - B_{octu}^{skew} \left(\frac{r}{4.5}\right)^3 \sin 3\phi - B_{decu}^{skew} \left(\frac{r}{4.5}\right)^4 \sin 4\phi - \dots \quad (4)$$

$$B_x = B_{radial} + B_{quad}^{norm} \left(\frac{r}{4.5}\right) \sin \phi + B_{sext}^{norm} \left(\frac{r}{4.5}\right)^2 \sin 2\phi + B_{octu}^{norm} \left(\frac{r}{4.5}\right)^3 \sin 3\phi + B_{decu}^{norm} \left(\frac{r}{4.5}\right)^4 \sin 4\phi + \dots \quad (5)$$

$$B_{quad}^{skew} \left(\frac{r}{4.5}\right) \cos \phi + B_{sext}^{skew} \left(\frac{r}{4.5}\right)^2 \cos 2\phi + B_{octu}^{skew} \left(\frac{r}{4.5}\right)^3 \cos 3\phi + B_{decu}^{skew} \left(\frac{r}{4.5}\right)^4 \cos 4\phi + \dots \quad (6)$$

Since the beam aperture is relatively small compared to the size of the pole pieces and far away from the pole edges, see Fig. 2, the multipole amplitudes can be expected to fall off rapidly with increasing multipole order. Also, the average field seen by the muons whose spin precession is measured in the experiment, is obtained by folding the magnetic field with the distribution of the muons over the beam aperture. Although the muon distribution is not uniform, it is relatively smooth and high order terms in the field expansion have little effect on the average field. Thus we usually truncated the field expansion after the decupole term.

IV. The field measurement equipment

All measurements of the main field component were done with NMR (nuclear magnetic resonance) probes using a magnetometer specifically designed and built for the $(g-2)$ experiment. Details of the magnetometer, which is based on the principle of pulsed NMR, can be found in [5]. The active volume of the NMR probes was a cylindrical water sample with a diameter of 2.5mm and a length of 15mm, aligned along the azimuthal or z-direction, the direction along which the field was expected to be very flat. The fact that the NMR frequency does not yield the vertical field component, which determines the $(g-2)$ frequency, but rather the absolute magnetic field, is not a problem in our case. In the $(g-2)$ magnet the minor field components are of order of 100 ppm or less, and thus

$$|\vec{B}| = \sqrt{B_y^2 + B_x^2 + B_z^2} \approx |B_y| \times \left(1 + \frac{B_x^2 + B_z^2}{2B_y^2}\right) = |B_y| \times (1 + O(0.01 \text{ ppm})). \quad (7)$$

The error due to the measurement of $|\vec{B}|$ rather than $|B_y|$ on average is more than a factor of ten smaller than the desired measurement accuracy of 0.1 ppm and thus negligible.

The setup during the magnet shimming period is shown in Fig. 3 An array of 25 NMR

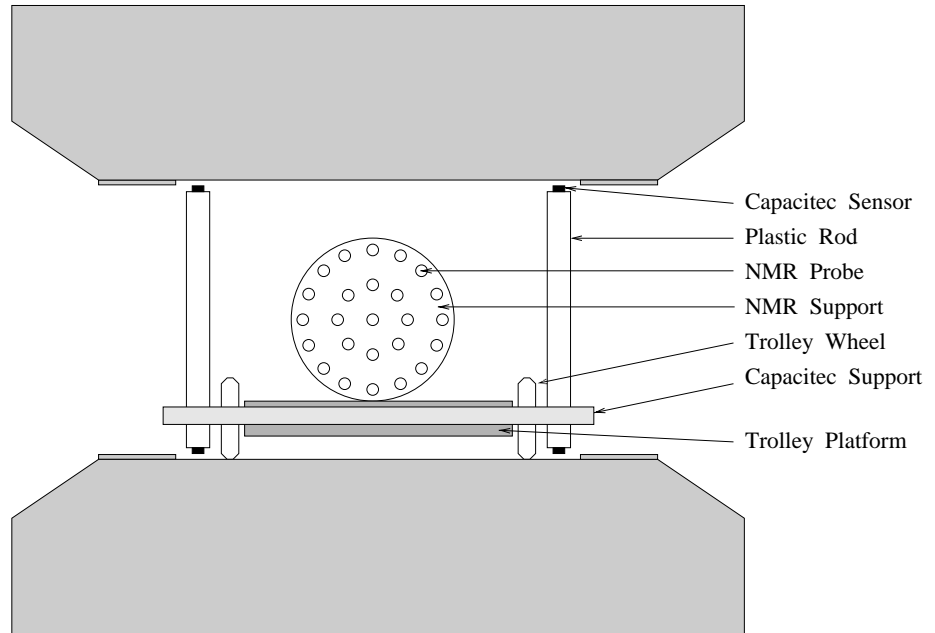


Figure 3: NMR and Capacitac probe setup during magnet shimming.

probes, one in the center, 8 and 16 on circles of 2.25 and 4.5 cm radius, respectively, was mounted on a plastic *shimming trolley*. The trolley was attached to the arm of a turntable in the center of the ring magnet. This turntable had been used throughout the construction of the magnet and its axis of rotation defined the center of the ring magnet. Therefore, once the trolley was set up at the correct radius at any location in azimuth, we could be sure that it would ride along the center orbit as the turntable rotated without the need for readjustments or even measurements of its radial position. Actually, the arm of the turntable, an aluminum beam, did change its length by up to 1mm over a few days due to room temperature changes, but over the duration of a trolley measurement, typically 1 hour for a full 360 degree map, the change in radius was negligible. For an accurate measurement of the variation of the vertical pole to pole gap as a function of the azimuthal position, two pairs of capacitive sensors (HPB-150A-A-L2-10-B-D, *Capacitac*, MA, USA) were mounted onto two plastic rods at one end of the shimming trolley. The absolute length of the plastic rods was not important to us, as we were interested in the gap variations rather than its absolute value, but the length of the inner relative to the outer rod could be measured easily by flipping the rod support by 180 degree.

A completely different setup was used to check the minor field components, particularly the radial field. This will be discussed in section VI.

After the installation of the muon beam vacuum chambers at the beginning of 1997, field measurements were done using a hermetically sealed NMR magnetometer housed in an aluminum case [6]. This magnetometer, referred to as the beam tube trolley, is pulled through the vacuum chamber by two cables and can map the field in the muon storage region with full 360 degree coverage in azimuth. It carries 17 NMR probes, 12 of them at $r = 3.5\text{ cm}$, and is used

to map the field every 2-3 days during a physics run. Data taking has to be disrupted for 3-4 hours for a field map, but most times they can be done while the beam is off for other reasons.

V. Field measurements

After seven years of construction, a major part of it being the fabrication of the world's largest diameter superconducting coils, the magnet was powered for the first time in January 1996. At that time we were not able to run the magnet to full field and had to settle for initial measurements at half field. The problem was a radial instability that drove the outer coil into an oval shape at about 70% of full current. During the cooldown this coil shrinks by 30mm in radius and then expands by 3mm in radius when the magnet is powered. As it shrinks, it catches onto radial stops mounted on the inner cryostat wall. To limit the stress on the cryostat while the coil is cold but not powered, only four radial stops were used initially. This turned out to be insufficient to prevent distortions.

The first field measurement over the whole circumference of the ring magnet is shown in Fig. 4(a). The total field variation is about 1500 *ppm*. Relatively dramatic field changes can be seen at multiples of 10 degree reflecting the structure of the poles which are constructed from 10 degree wide sections. There is no pronounced structure with a periodicity of 30 degree, the segmentation of the yoke, verifying the decoupling of the yoke structure from the field in the storage region due to the small air gap between yoke and pole pieces.

In Fig. 4(b) the results of the vertical gap measurements are shown. There is a clear correlation between the variation in the dipole field and the vertical gap. Particularly, most of the field jumps near the pole ends correspond to a jump in the vertical gap due to a small misalignment of adjacent pole pieces. We did not measure the gap at the same radius as the magnetic field, see Fig. 3, which most likely would have enhanced the correlation between vertical gap measurement and field strength over short intervals in azimuth. The total field variation is significantly larger than the total gap variation. Contributions to the field variations include (1) various holes in the magnet yoke, for pump and lead ports to the outer cryostat as well as a hole for beam injection, (2) variations in the gap between the upper and lower yoke sections, (3) temperature gradients, (4) variations in the coil positions as a function of azimuth, (5) other mechanical tolerances on all steel parts.

To fix the problem with the outer coil, the upper yoke pieces had to be removed to gain access to the cryostat. Four spring loaded radial stops were added to the four rigid ones to improve the mechanical stability of the coil. This will be discussed in detail in [2]. After the reassembly of the yoke, the magnet was successfully commissioned, without a single training quench, to full field, $B = 1.45 T$, in late June, 1996. The dipole field variation for the first measurement at full field is shown in Fig. 5. The total field range is about the same, but a detailed comparison to the January 1996 field map is not possible due to the work that was

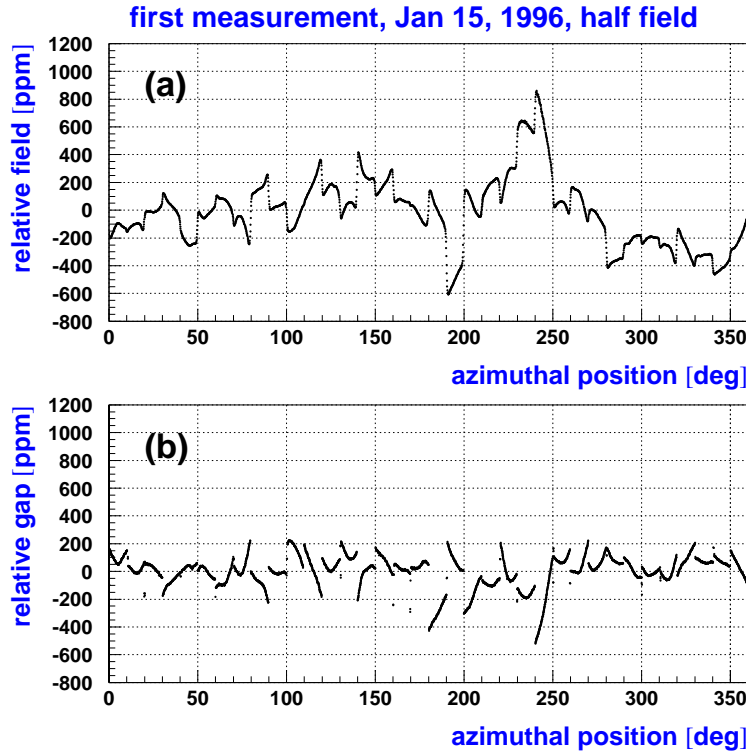


Figure 4: (a) Magnetic field, in *ppm* relative to the mean value, as a function of the azimuthal position at half field, January 15, 1996. (b) Vertical gap, in *ppm* relative to the average gap, as a function of the azimuthal position. Shown is the average value between the two measurements at the inner and outer radius, see Fig. 3

done on the magnet inbetween.

To reduce the large field variations near the pole ends, the vertical position of the pole pieces was readjusted by changing the thickness of the spacers between yoke and pole, with the goal of matching it to its neighbours to within $10\ \mu\text{m}$ corresponding to about $50\ \text{ppm}$ of the total gap. This difficult task took about three month to complete but at the end the tightened tolerance was met in most of the pole sections. Figs. 6 (a) and (b) show the field and gap variation at the end of the first shimming period. By that time, the field had been flattened in the azimuthal direction. Coarse adjustments were made by adding nonmagnetic spacers between the steel plates on top/bottom and the main yoke, see Fig. 1, in regions where the field had been high. Further improvements were achieved by moving the wedges between pole and yoke radially in or out. These methods lead to field changes over some range in azimuth with an approximately Gaussian profile, roughly 30 degree wide in the case of local yoke reluctance manipulations and 10 degree in the case of a single wedge movement. Thus none of them is suited for local field

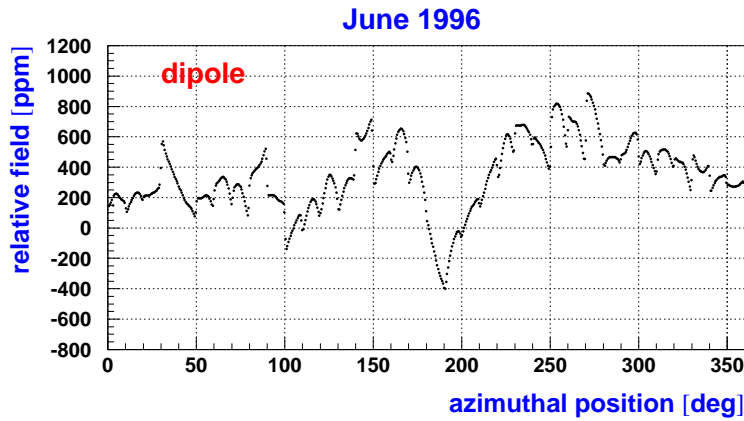


Figure 5: Magnetic field as a function of azimuth, June 1996.

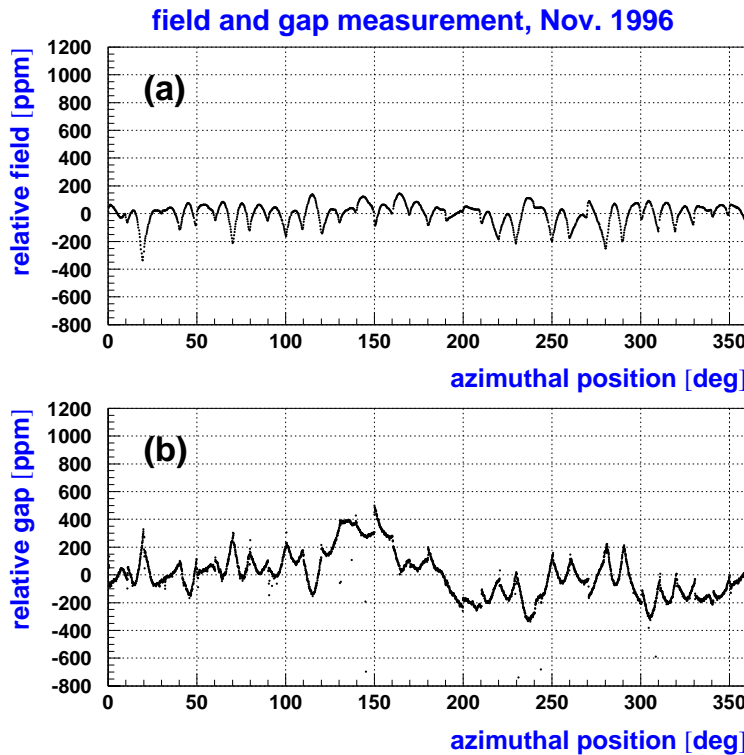


Figure 6: (a) Magnetic field, in *ppm* relative to the mean value, as a function of the azimuthal position at half field, November 10, 1996. (b) Vertical gap, in *ppm* relative to the average gap, as a function of the azimuthal position. Shown is the average value between the two measurements at the inner and outer radius, see Fig. 3.

adjustments and the field still changes by several hundred *ppm* over short distances in azimuth. A comparison between Figs. 6 (a) and (b) shows that most of the residual field variations are due to the slope or curvature of the pole faces. At this point we had to stop the shimming work to prepare the experiment for the first beamtime in June/July 1997. The azimuthal field variation during this run is shown in Fig. 7. It is very similar to Fig. 6 (a) confirming the good mechanical stability of the magnet assembly.

After the run in 1997, further improvements in the azimuthal field homogeneity were achieved by adding stripes of 1 mil (25 μm) thick steel shims of varying width to the pole faces. These stripes were sandwiched in between two Aluminum plates and then glued to the surface correction coil boards which had been installed already, see Fig. 8. With this method the field variations were reduced by another factor of four, excluding the angle interval between 10 and 35 degree, where the fringe field from the inflector magnet dominates, and a pole section at 270 deg where the field was already too high near the pole ends. We avoided to add any shims on the pole faces in the middle in order not to compromise the accuracy of the NMR probes that are used to measure and stabilize the magnetic field during physics running. These probes are located in groves in the outside wall of the beam vacuum chamber and are only about 1 cm away from the pole surface. Some probes near the pole ends did fail after the addition of the steel shims, but in most cases the higher field gradients towards the pole ends had compromised the precision of these probes even before the shims were installed.

As outlined in section III, the field distribution in x and y, the radial and vertical coordinates, was analysed using a 2-dimensional multipole expansion. In a typical field map, the shimming trolley would move at a constant speed of about 0.5 cm/sec. The NMR probes on the trolley were read out in sequence at a rate of 10 Hz. Thus every probe was read out every 1-2 cm in the azimuthal direction z. To prepare the data for multipole analysis, linear interpolation was used to calculate the field on a regular grid in z for each of the NMR probes. Subsequently, a multipole function of specified order in the normal and skew moments, typically up to decupole, was fitted to the interpolated field values using the CERN library function HFITV. The fit parameters as a function of the azimuthal trolley position for the first field map at full field in June 1996 are shown in Figs.10-13.

Normal quadrupole and octupole were negative due to the thicker edge shims at the inner radius (negative x). Since grinding the edge shims is much cheaper than producing a new set, all four had been fabricated somewhat thicker than the best calculated values resulting in strong positive sextupole and decupole moments. Apart from the normal quadrupole, which is extremely sensitive to pole tilts, all normal multipoles were rather uniform in azimuth, verifying the high quality/uniformity of the pole steel and the validity of the 2-dimensional multipole expansion. The spikes at multiples of 10 deg are due to the breakdown of the 2-D approximation at the ends of the pole piece sections, enhanced by an increased error from the linear interpolation.

The skew moments, particularly the higher moments, were small, although the variation in

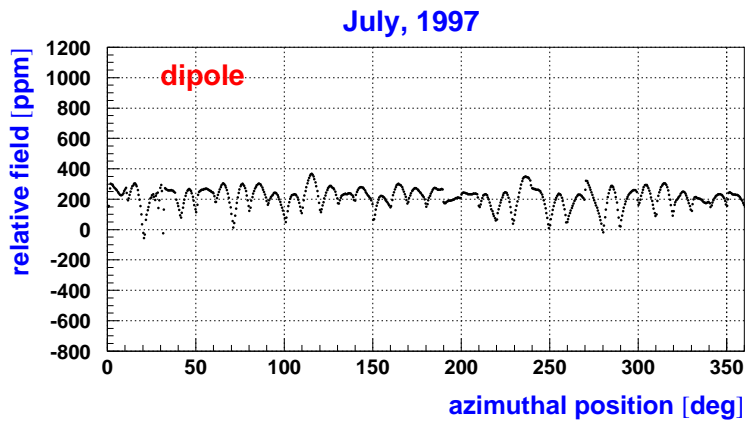


Figure 7: Magnetic field as a function of azimuth, July 1997.

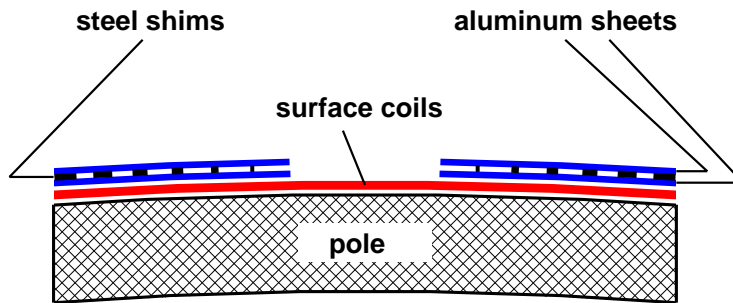


Figure 8: Schematic longitudinal pole cross section showing the steel shims used to compensate for the curvature of the pole surface.

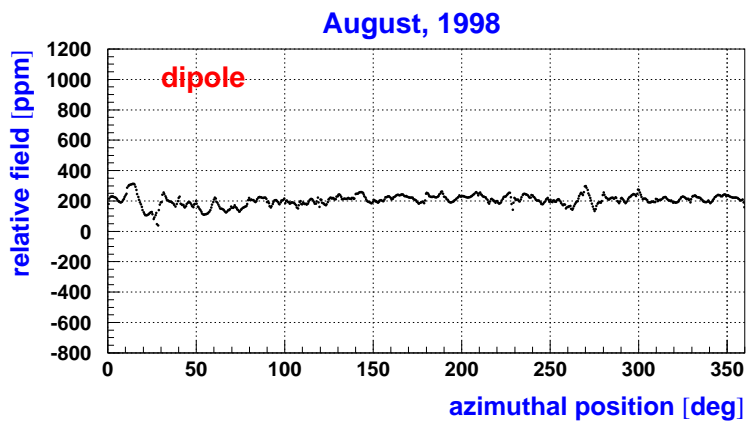


Figure 9: Magnetic field as a function of azimuth, August 1998.

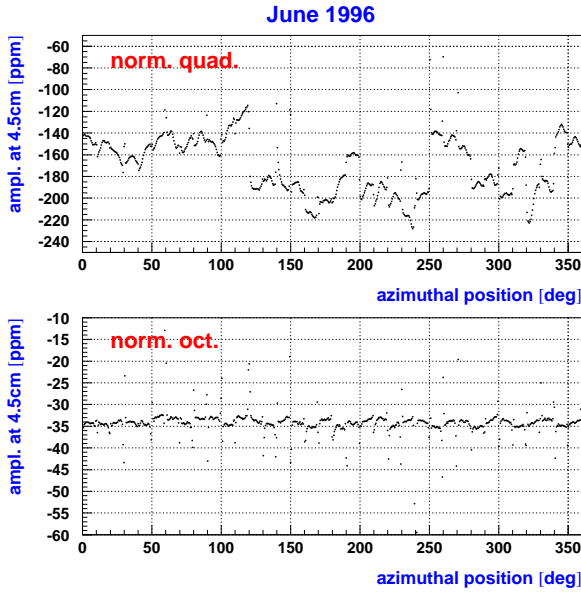


Figure 10: Normal quadrupole and octupole, in *ppm* at 4.5cm radius, as a function of azimuth for the first measurements at full field (June 1996).

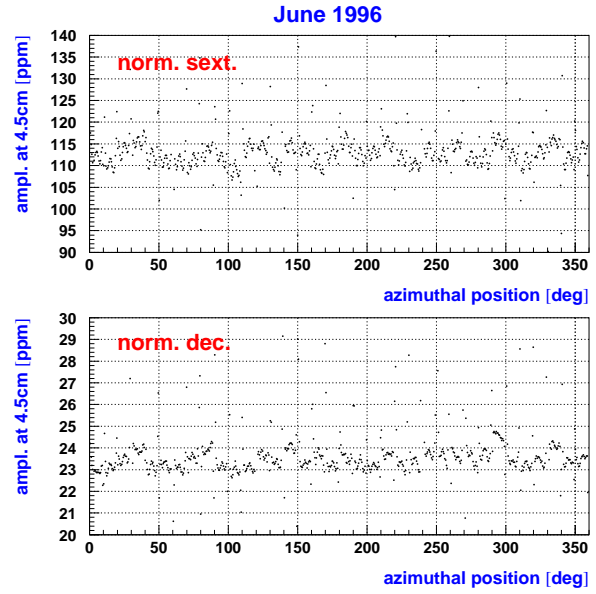


Figure 11: Normal sextupole and decupole.

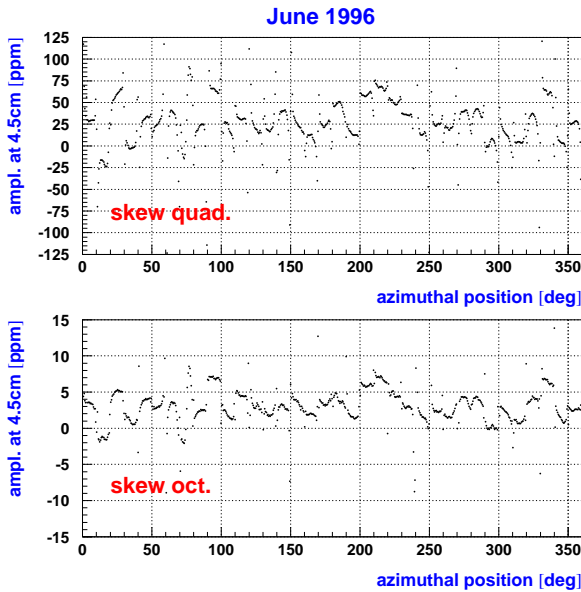


Figure 12: Skew quadrupole and octupole.

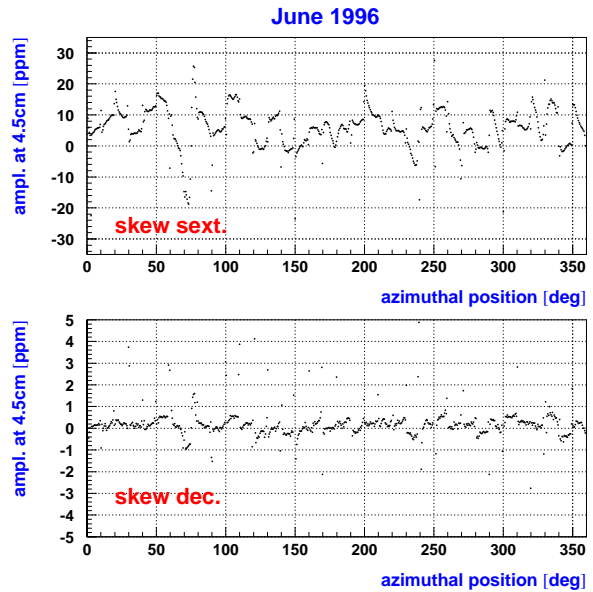


Figure 13: Skew sextupole and decupole.

the skew quadrupole, as well as its mean value, was larger than expected.

By November 1996, all multipole coefficients were reduced to less than 10 *ppm* on average by grinding the edge shims, see Figs. 14-17. Note that all vertical scales are now centered with respect to "0". A small up/down asymmetry was introduced to reduce the average value of the skew quadrupole. The positive sign of the even normal multipoles, sextupole and decupole, indicates that the shims were still oversized allowing future adjustments by additional grinding. Also the thickness of the four edge shims was still uniform in azimuth. The dramatic change of the normal quadrupole variation in azimuth, as compared to the June 1996 map, was a result of the realignment of the pole pieces.

Figs. 18-21 show the multipoles for a field map taken with the beam tube trolley inside the vacuum chamber during the first data taking run in July 1997. There is relatively little change from the November 1996 map, a proof of the excellent mechanical stability of the magnet. There is also no indication of any significant field distortions caused by the vacuum chambers, mainly aluminum, or the electron detectors thanks to a careful choice of the materials used in and close to the pole gap. The apparent gap in the data between 20 and 30 degree marks the location of the inflector magnet. Its fringe field causes dipole field changes in excess of 1000 *ppm*, towards the outer edge of the aperture, over a few degree in azimuth and in a quite irregular pattern. Here again the 2-D multipole expansion fails to describe the data. As an example, Fig. 22 shows the relative field as a function of azimuth for two probes in the inflector region, one towards the inside at $x=-3.5\text{cm}$, the other towards the outside, closer to the inflector channel. Another irregularity near 70 degree, visible mainly in the skew multipoles, marks the location of the current leads to the outer coils.

After the run in summer 1997, the edge shims were optimized pole section by pole section, mainly to flatten the skew moments. Some of the pole pieces were tilted by adjusting the spacers between pole and yoke, with typical tilts of 50 μrad , to reduce the normal quadrupole variation. As a result, the total variation of the multipoles along the circumference of the ring magnet is now comparable to the variation within the 10 degree pole sections, see Figs. 23-26.

The history of the multipole coefficients, averaged in azimuth, is summarized in Table 1 and Figs. 27-30. The coefficients for the August 8, 1998 map are the final results of the static shimming. After August 8, we commissioned the surface coils and then used them to reduce the average values of the normal quadrupole and sextupole. Due to the lack of time for a calibration of the NMR trolley prior to the run, as well as insufficient knowledge of the inflector fringe field, no effort was made to adjust the other multipoles which were sufficiently small anyway. About half of the probes on the trolley dropped out in the inflector fringe field and a different set of probes had to be used later to fill this gap in the data. The curves shown in Fig. 22 are from data taken in this dedicated inflector fringe field measurement. In the August 22, 1998 trolley map, all multipole coefficients, with the exception of the quadrupole moments, are sufficiently small and do not compromise the goal of the experiment to know the average magnetic field seen by the stored muon beam to an accuracy of about 0.1 *ppm*. The quadrupole moments

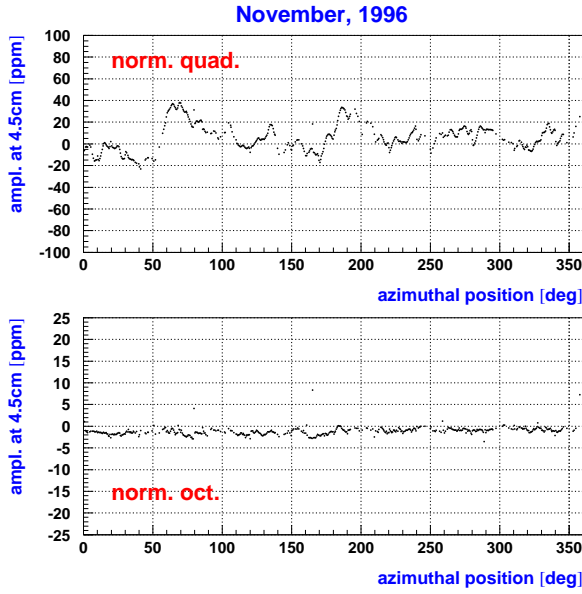


Figure 14: Normal quadrupole and octupole, in *ppm* at 4.5cm radius, as a function of azimuth (November 1996).

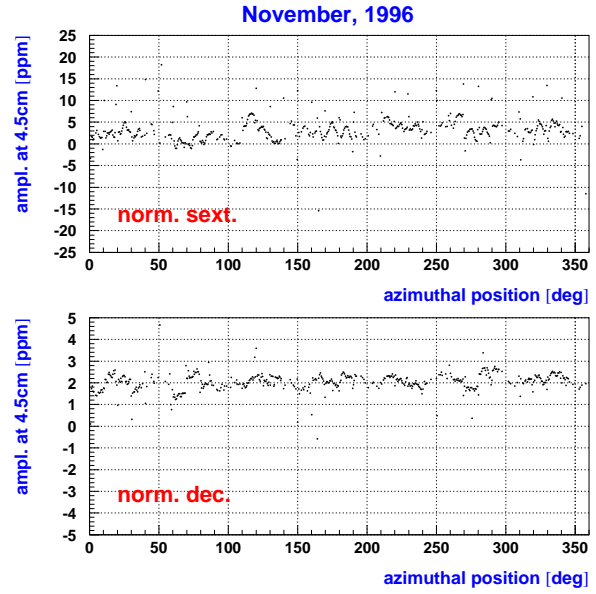


Figure 15: Normal sextupole and decupole.

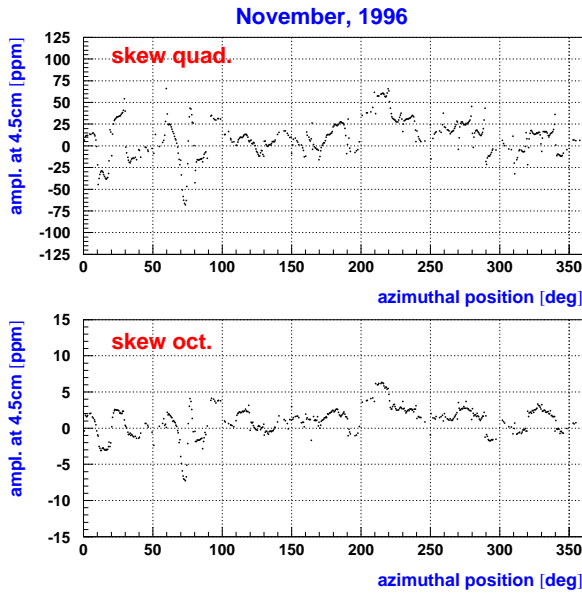


Figure 16: Skew quadrupole and octupole.

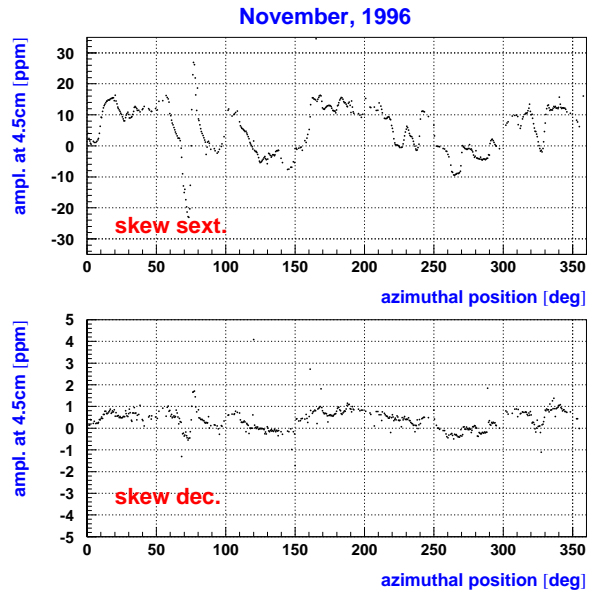


Figure 17: Skew sextupole and decupole.

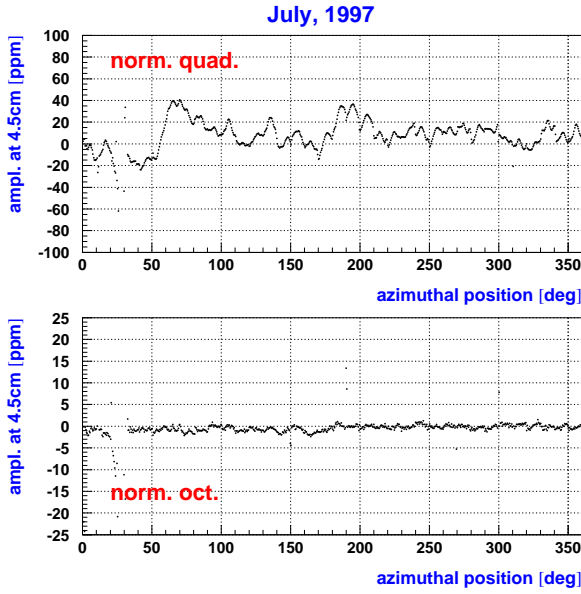


Figure 18: Normal quadrupole and octupole, in *ppm* at 4.5cm radius, as a function of azimuth (July 1997).

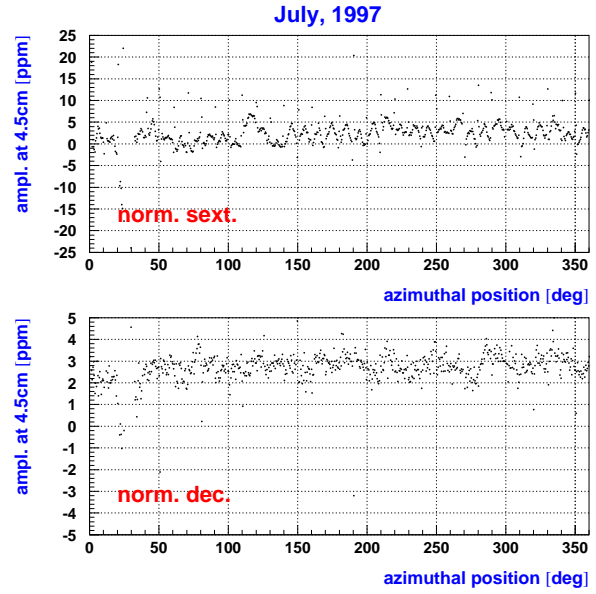


Figure 19: Normal sextupole and decupole.

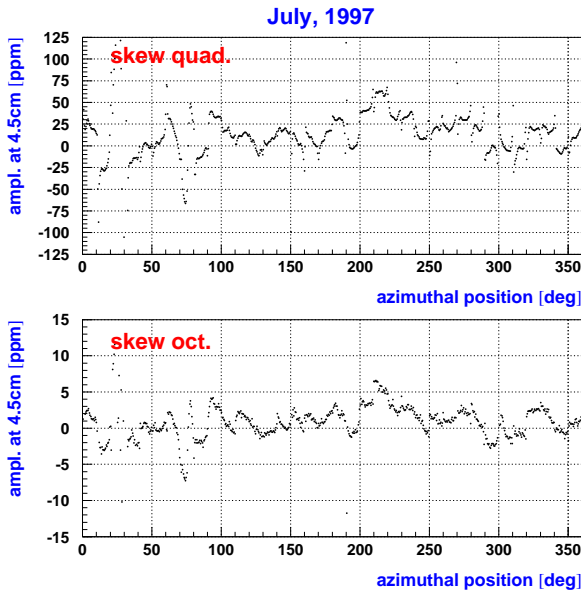


Figure 20: Skew quadrupole and octupole.

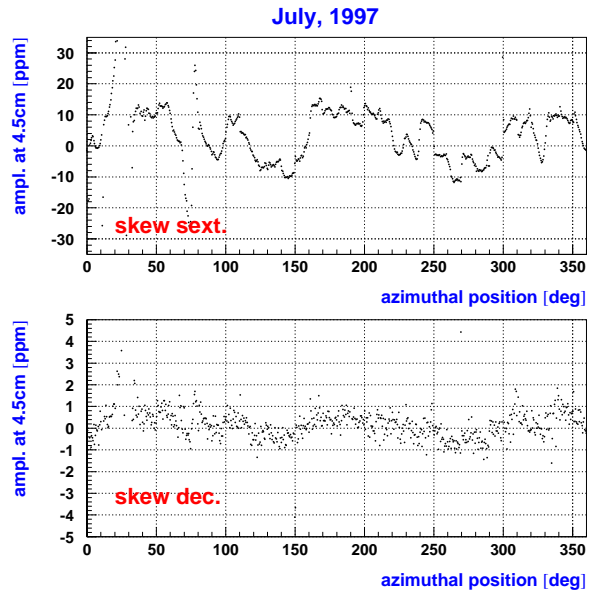


Figure 21: Skew sextupole and decupole.

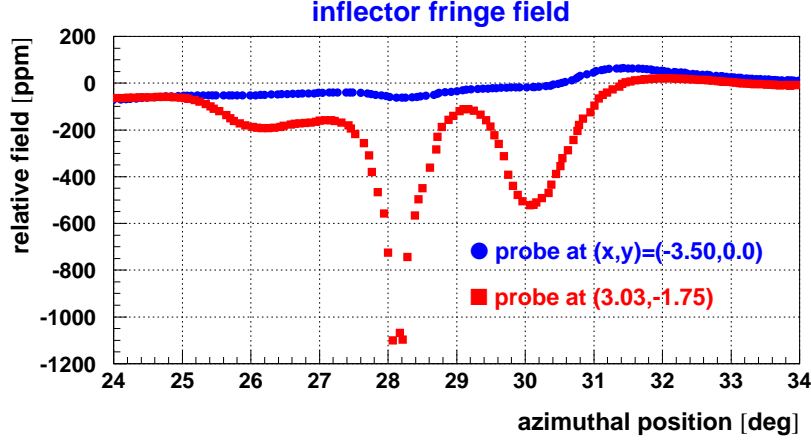


Figure 22: Field measurement in the inflector region at $x = -3.5$ cm, $y = 0.0$ cm (circles) and $x = 3.03$ cm, $y = -1.75$ cm (squares).

Table 1: Multipole coefficients, averaged in azimuth, in *ppm* at $r = 4.5$ cm.

<i>Date</i>	<i>norm1</i>	<i>norm2</i>	<i>norm3</i>	<i>norm4</i>	<i>skew1</i>	<i>skew2</i>	<i>skew3</i>	<i>skew4</i>
June 1996	-169.12	112.03	-34.16	23.71	27.06	5.82	3.12	0.46
November 1996	5.52	3.19	-1.11	1.95	9.13	5.32	0.85	0.45
July 1997	5.26	2.94	-1.03	1.45	12.26	2.78	0.36	0.25
August 08, 1998	7.73	-5.29	-2.79	0.38	-2.07	-0.02	-0.25	0.71
August 22, 1998	-2.54	-1.25	-2.70	0.34	-2.39	-0.18	-0.28	0.42

directly couple to the mean radius and elevation of the stored beam, which have uncertainties of 1-2 mm. The average values of the quadrupole coefficients have to be reduced to less than 1 *ppm* at $r = 4.5$ cm in future runs in order not to limit the accuracy in the knowledge of the average field. A new inflector magnet has recently been installed and a significant reduction in the fringe field leaking into the storage region is expected. This together with timely calibration measurements should allow us to control the quadrupole moments, by adjusting the surface coil currents, to the required accuracy.

VI. Measurement of the radial field component

As mentioned in section IV, the NMR frequency does not yield the vertical field component but rather the absolute value of the magnetic field. To ensure that this feature did not compromise the accuracy in the knowledge of the vertical field, we had to verify that the contribution of the minor field components to the absolute field were indeed negligible. In addition, the radial field component has a significant effect on the dynamics of the stored muon beam. A mean radial field value of 50 *ppm* changes the mean vertical position of the beam by about 3mm, and higher harmonics in $B_r \equiv B_x$ perturb the vertical betatron oscillations. Therefore

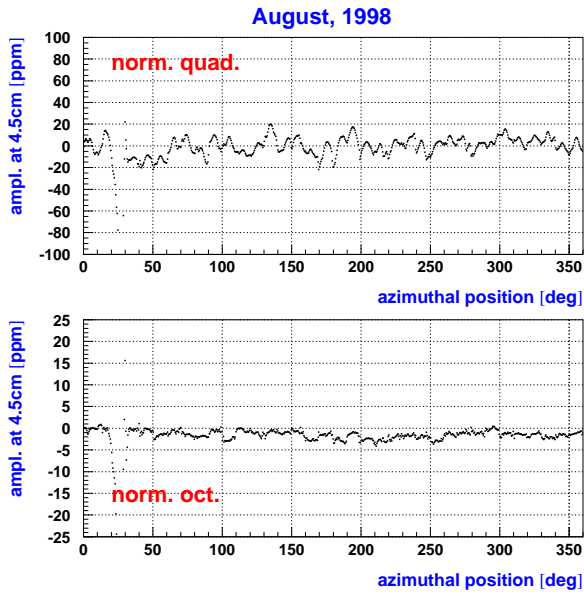


Figure 23: Normal quadrupole and octupole, in ppm at 4.5cm radius, as a function of azimuth (August 1998).

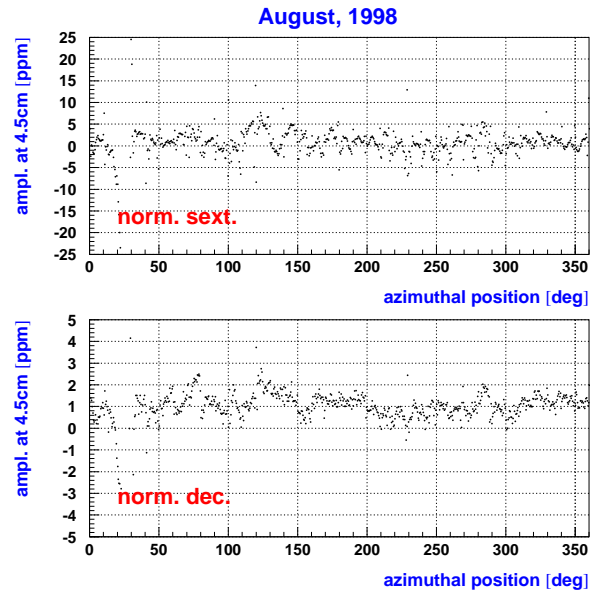


Figure 24: Normal sextupole and decupole.

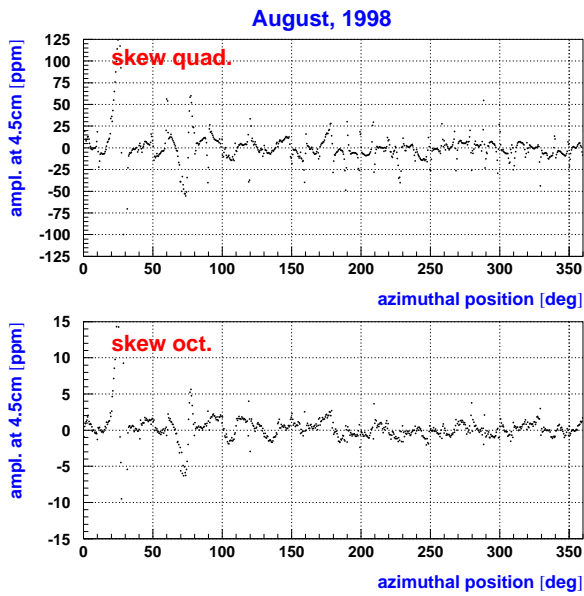


Figure 25: Skew quadrupole and octupole.

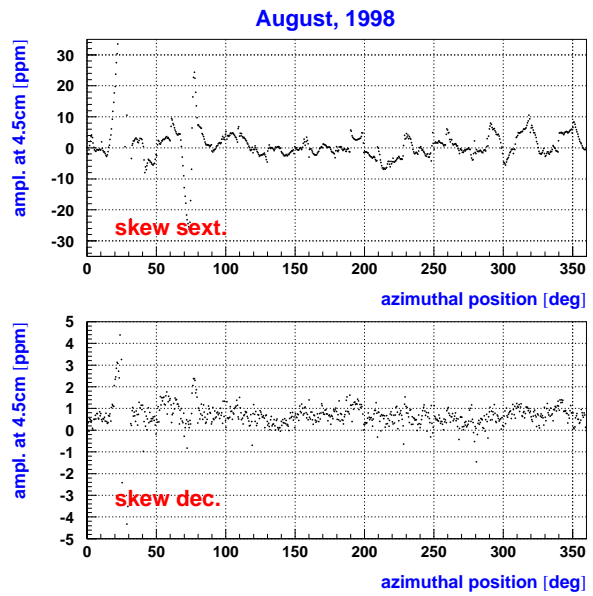


Figure 26: Skew sextupole and decupole.

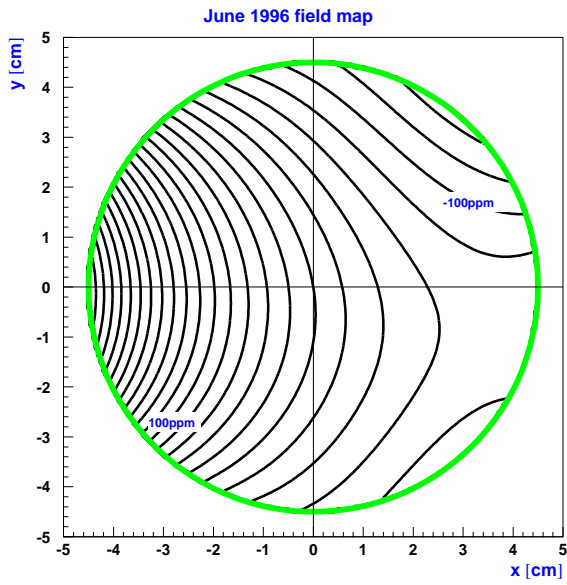


Figure 27: 20 ppm contour plot, June 1996.

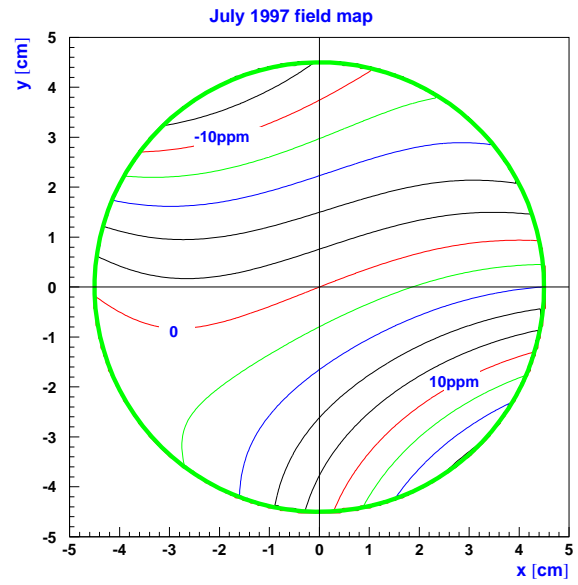


Figure 28: 2 ppm contour plot, July 1997.

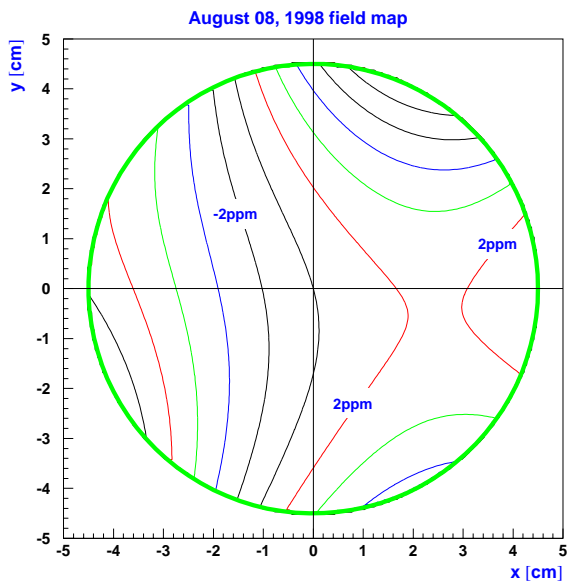


Figure 29: 2 ppm contour plot, August 08, 1998.

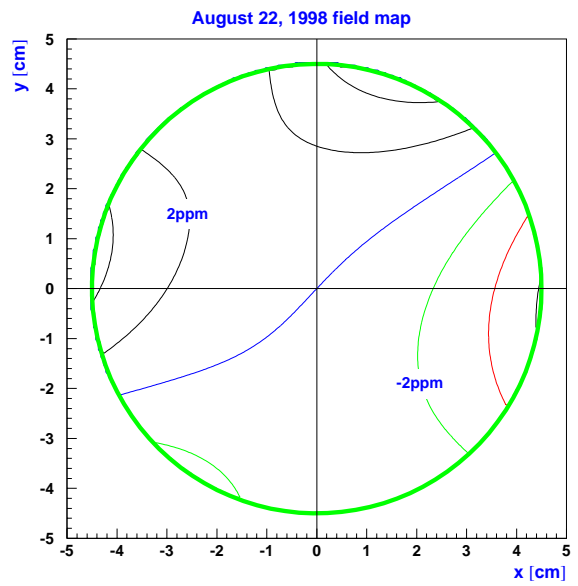


Figure 30: 2 ppm contour plot, August 22, 1998.

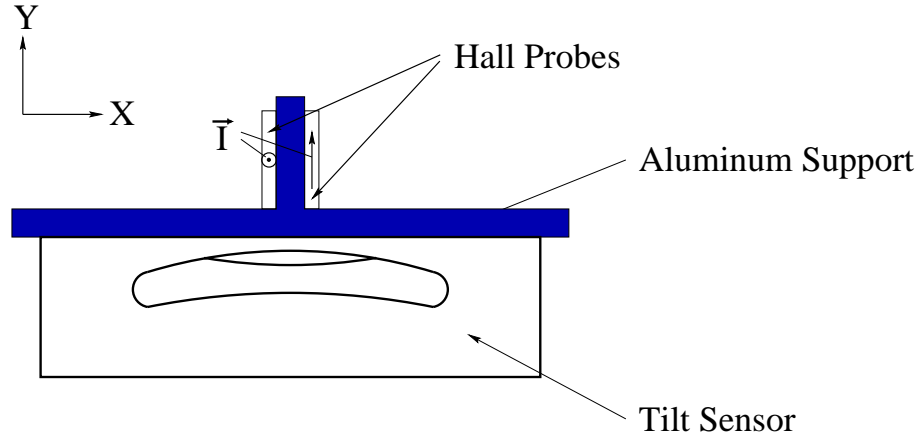


Figure 31: Schematic setup for radial field measurements.

we aimed to measure the radial field component as a function of azimuth to about 10 *ppm* accuracy. We chose to do this with Hall probes. For measurements of minor components in a strong magnetic field, the planar Hall effect and probe tilts are major concerns. The former problem was greatly reduced by use of two Hall probes (BH-206, F.W. Bell) with about the same planar Hall coefficients, but with Hall currents flowing in the z -direction for one probe and in the y -direction for the other, see Fig. 31. In the sum voltage, the contribution of the planar Hall effect is then $\Delta U_{Hall} = k_2 \cdot B_{\parallel}^2 \cdot I_{Hall} \cdot [\sin(2\alpha) + \sin(2(\alpha + 90^\circ))] = 0$, where k_2 is the planar Hall coefficient, $B_{\parallel} \approx B_y$ the field component in the y,z -plane in which the Hall current I_{Hall} flows, and α an arbitrary angle in the y,z -plane.

The Hall probe support structure was aligned with respect to gravity with an electrolytic tilt sensor (RG33A, Spectron Systems Technology, Inc.). The error from a possible tilt of the Hall probes with respect to the support structure was eliminated by flipping the whole setup by 180 degree about the vertical axis and subtracting the Hall voltages for the two configurations from each other. Details of the setup and measurement procedure can be found in [7, 8]. A single measurement took about 10 minutes, dominated by the electrolytic tilt sensor which needs several minutes to stabilize. Typically we restricted ourselves to one measurement every 10 degree.

The quality of the radial field measurements can be deduced from plots like those shown in Fig. 32 . In the 2-D approximation, the multipole coefficients for the vertical and radial field are the same, see Eqs. 1 and 2, and all terms in the radial field multipole expansion, except for the dipole term, can be calculated from the NMR measurements. The smooth curves in Fig. 32 are the result of these calculations. Since the dipole term cannot be derived from the absolute field measurements, the vertical position of the curves was adjusted to make the average deviation zero for each of the two cases, all edge shims installed vs. two of the four missing. The small scatter of the direct measurements with respect to the curves shows that the relative accuracy

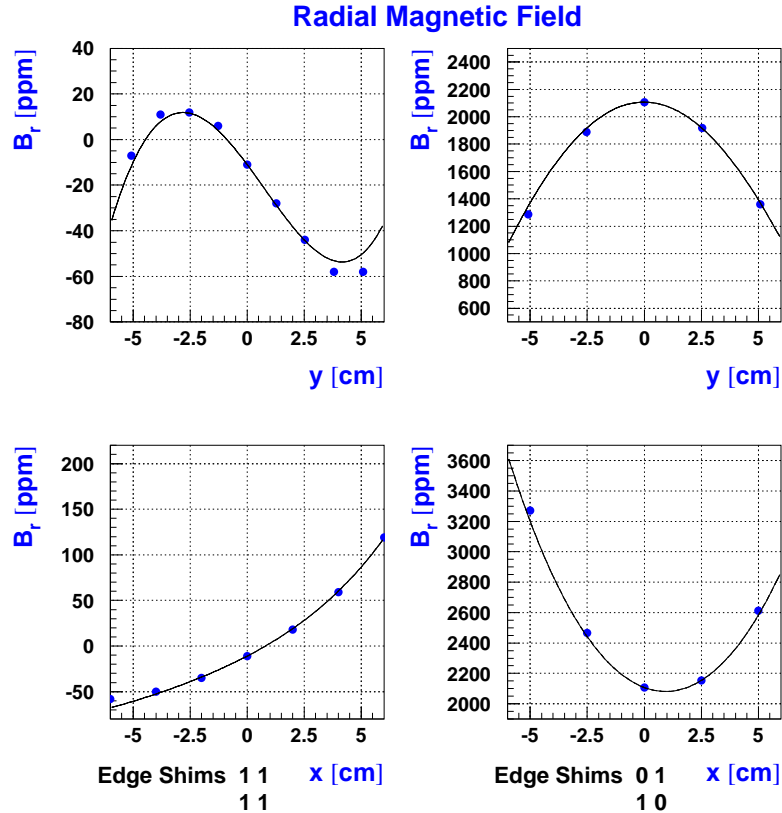


Figure 32: Radial field measurement as a function of x (bottom) and y (top), with all edge shims installed (left) and the inner upper and outer lower shims removed (right). The solid lines represent the field variation expected from the multipole coefficients calculated from the absolute field measurements.

of the radial field measurement is better than 10 ppm . The deviations at large values of x and y can be attributed to the truncation of the multipole expansion after the decupole term, and the fact that the NMR measurements were done out to a radius of 4.5 cm only.

Fig. 33 shows the radial field measurement as a function of azimuth superimposed on a measurement of the average tilt of the top and bottom pole pieces. The tilt was measured with an electrolytic tilt sensor, the same model as the one used in the radial field measurement. The average tilt dominates the radial field variation. There are various other effects that contribute to the radial field such as differences in the radial positions of the top and bottom poles or nonlinear curvatures of the pole surfaces. An imbalance in the thickness of the edge shims can also result in a radial magnetic field, see Fig. 32.

The average radial field calculated from measurements at the end of the shimming period was about 20 ppm . In the August 1998 run, we adjusted the average radial field using the surface correction coils. The beam can be centered vertically by maximizing the number of stored particles as a function of the average radial field. The required correction was about $10 - 15 \text{ ppm}$ in good agreement with the direct measurements. During the second physics run

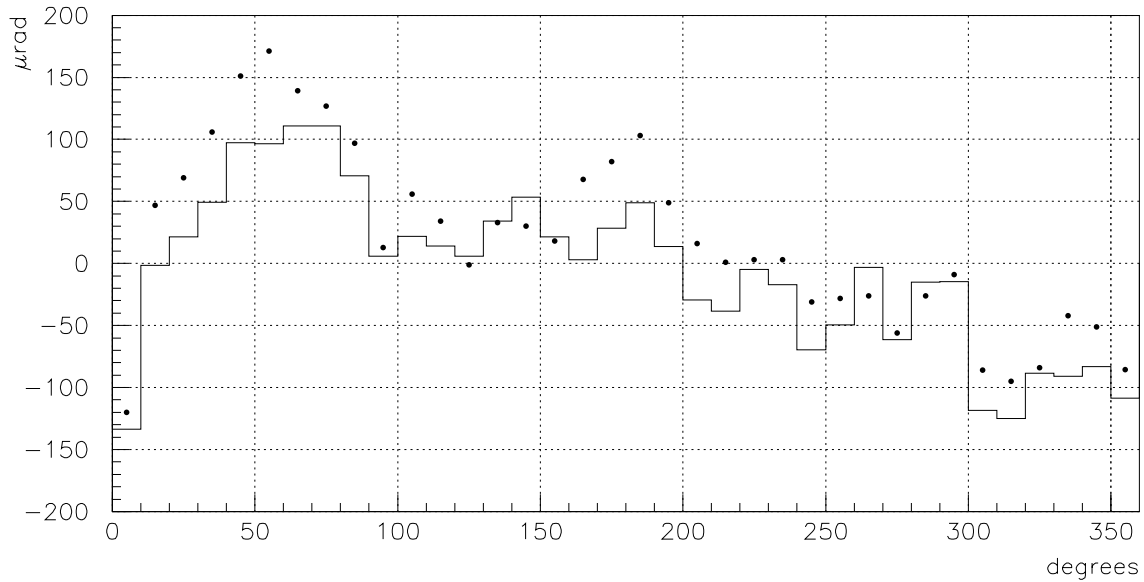


Figure 33: Radial field measurement (dots) superimposed on measurement of the average pole tilt (line) as a function of the azimuthal position.

in January 1999 we repeated the scan of the average radial field and found it to be close to 20 *ppm*, another confirmation of the direct radial field measurements as well as the excellent mechanical stability of the magnet.

References

- [1] R.M. Carey et al., Phys. Rev. Lett., Vol. 82 (1999) 1632.
- [2] G.T. Danby et al, to be published.
- [3] G.T. Danby and J.W. Jackson, IEEE Trans. Appl. Supercond. 5 (1995) 662.
- [4] G.T. Danby and J.W. Jackson, 'Shimming techniques for the ultra-precise muon g-2 storage ring at the AGS', MT-13, Canada 1993.
- [5] R. Prigl et al., Nucl. Instr. Meth. A., Vol. 374, No. 1, pp. 118-126, 1996.
- [6] A. Grossmann, PhD thesis, Heidelberg University, July 1998.
- [7] S.I. Redin, PhD thesis, YALE University, May 1999.
- [8] S.I. Redin, to be published.

Field map of the LEP spectrometer with a moving carbon fiber arm (Didier Cornuet / Cern)

September 21-24, 1999 at Brookhaven

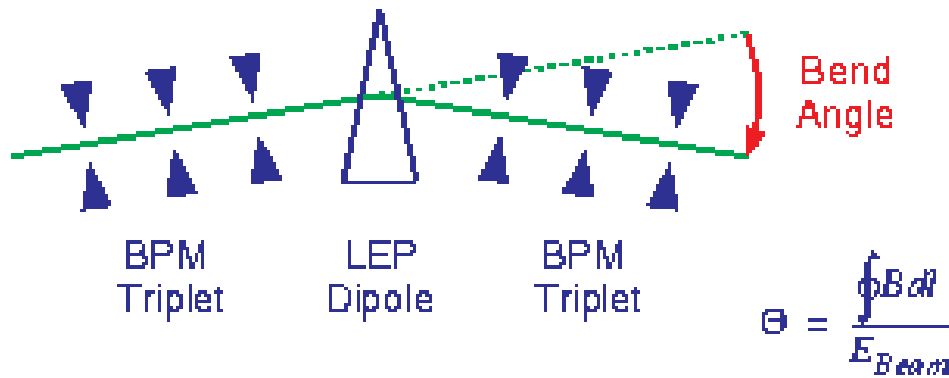
1. The LEP spectrometer
2. Field mapping bench
3. Data acquisition system
4. Results of the first campaign
5. Future improvements for next campaign

IMMW-11

(Didier Cornuet / Cern)

LEP Spectrometer Project

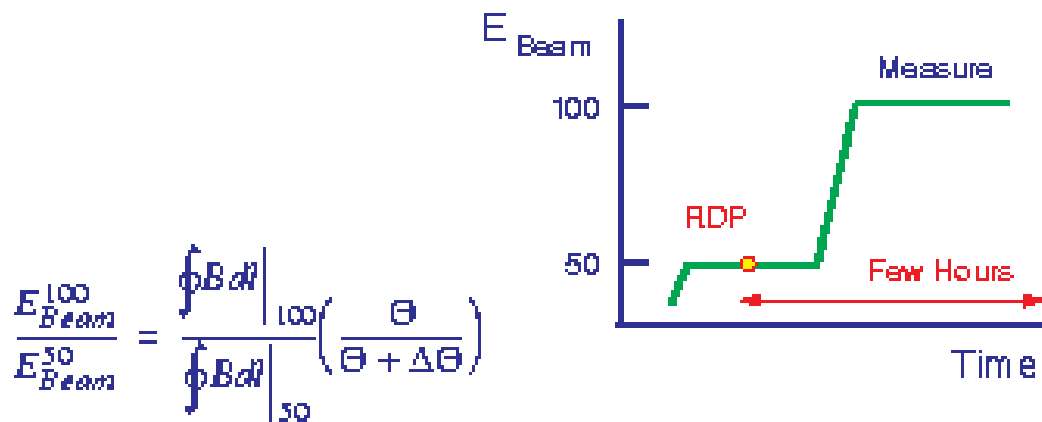
Inline Spectrometer Concept



- Use dipole which ramps with LEP
- BPM Triplets measure bend angle Θ
- $\int B dl$ from Local NMR and precision Field Map

Relative Energy Measurement

- Calibrate Spectrometer using RDP
- Ramp immediately to Physics Energy
- Direct Measurement of E_{Beam} in ratio



1. The LEP spectrometer

- a) The parameters
- b) Environment
- c) Magnetic stabilization

IMMW11

(Didier Cornuet)

a) The parameters

Gap	100	mm
Central field	0.225	T
Magnetic length	5.85	m
Nominal current	500	A
Power dissipation	18.6	kW
Water flow	13.4	l/min
Pressure drop	2.3	bar
Core length	5.75	m
Lamination Thickness	1.5	mm
Core weight	8.5	t
Girder weight	1.5	t
Total weight	10.3	t

- Design of injection magnets (MBI) with modified pole profile
- Coils and yoke manufactured by industry
- Assembly at CERN

IMMW11

(Didier Cornuet)

b) Environment

- Stable temperature in ISR tunnel
- Ambient temperature and humidity permanently registered
- 24 Pt100 probes in the yoke
- 10 Pt100 probes on the coils
- Yoke and coils wrapped up with aluminized glass fiber tissue
- Temperature control of the coils with a dedicated cooling station
- Connection end is cooled with fans.
- Fluxgates monitor the ambient end fields
- Mumetal sheets cut the end fields @ 50.0 cm each side



c) Magnetic stabilization

- Magnetization cycles ("Degaussing")

Ramps between 5 A and 500 A

(For LEP between 25 A and 500 A)

Ramp speeds ± 50 A/s

Flat-top duration 5 s

Flat-bottom dur. 5 s

Number of cycles 5

- Bending modulations

Modulation $I \in [I_{meas}, I_{meas} + 0.03\%]$

Modul. speeds ± 2.3 A/s

(For LEP ± 0.6 A/s)

Flat-top duration 2 s

Flat-bottom dur. 2 s

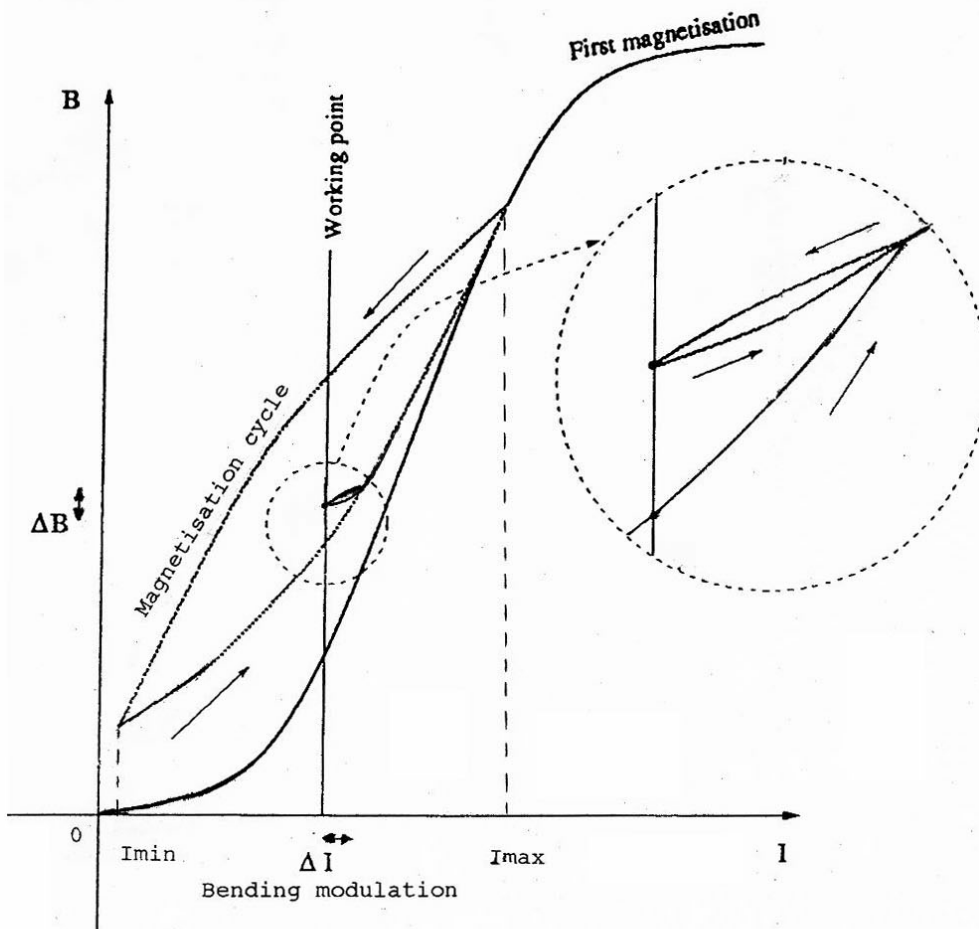
Number of cycles 7



1. The LEP spectrometer



c) Magnetic stabilization (cont.)



c) Magnetic stabilization (cont.)

- Measurement cycle

Magnetization cycles

Rest current I_{rest} 5 A

Ramp speeds ± 2.3 A/s

(For LEP ± 0.6 A/s)

Intermediate flat-top 22 Gev

Intermediate duration 5 min

Ramp to I_1 + bend. mod.

1st flat-top for mapping Energy 1

Maps ~ 40 min/map

Ramp to I_2 + bend. mod.

2nd flat-top for mapping Energy 2

Maps ~ 40 min/map

.....

.....

Ramping down to I_{rest}

NO OVERTSHOOT, NO UNDERSHOOT

IMMW11

(Didier Cornuet)

2. Field mapping bench

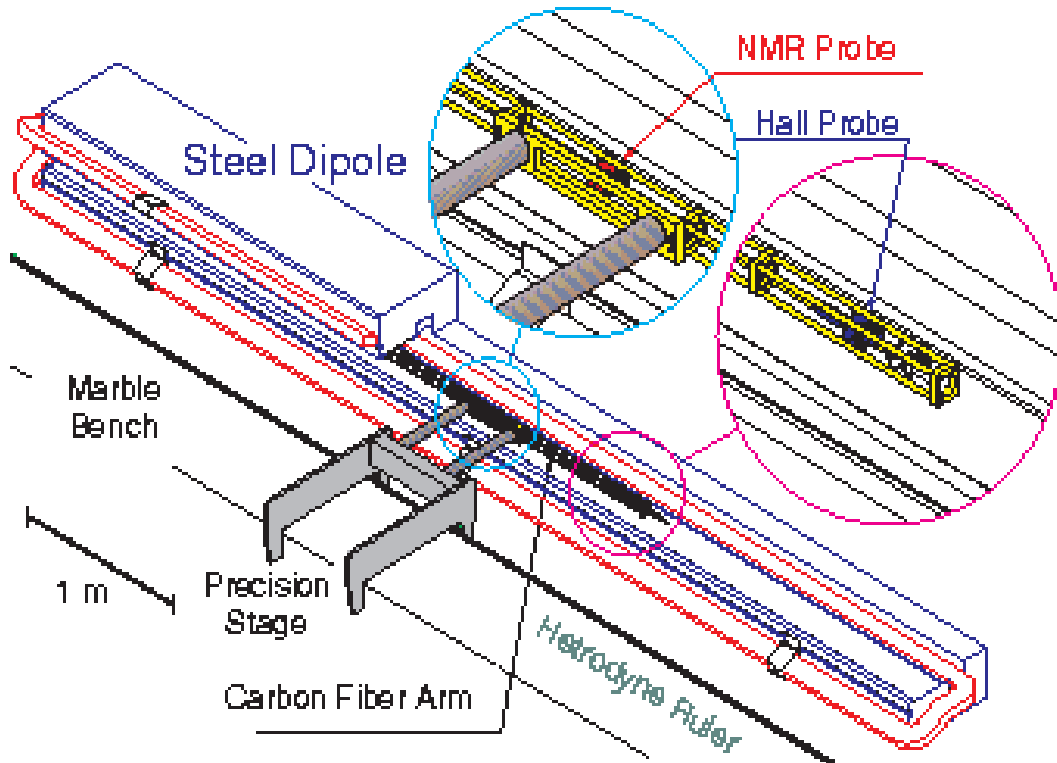
Part of previous LEP magnet measuring stand

- a) The marble
- b) The carriage
- c) The carbon fiber arm (new)
- d) Alignment

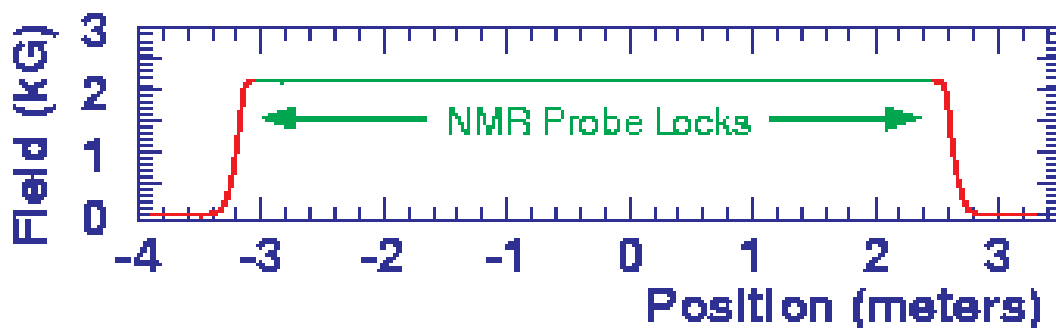
IMMW11

(Didier Cornuet)

Magnet Mapping



Need $\oint B \cdot dl$ as $f(B_{Ref})$



NMR Probe: $\delta B/B \sim 10^{-6}$ over 90%

Hall Probe: $\delta B/B \sim 10^{-4}$ over 10%

⇒ Independent *In Situ* measurements also made!

a) The marble

- 6200 mm × 600 mm × 600 mm
- Reference faces : top and lateral
- High thermal inertia (6000 kg)
- Cog-rail 6180 mm long for carriage
- Declutching rails + block stops
- **New steel measuring band fixed on the marble** at each end to measure longitudinal displacement (Z)

Type LIDA 105 C (Heidenhain)

Length 6140 mm

Period 40 μm

Accuracy $\pm 5\mu/\text{m}$

Optical head positioning is delicate :
help of a signal analyser (from the
manufacturer)

Thermal **coefficient** is **that of the
marble**: $\simeq 8 \times 10^{-6}/^{\circ}\text{C}$

b) The carriage

- 2 identical DC moto-reducers for X and Z
 ± 24 V/10 A ($I_{cc}=6$ A)
3000 rpm/80.9 rpm
Rotastop (^R BBC) for fixed pos. @ $V_{ref} = 0$
- 2 stainless steel rods for transverse (X)
One master rod driven by DC moto-reductor
One slave rod adjustable for align. of the arm
- Incremental ruler (transverse)

Type	LS 803 (Heidenhain)
Length	520 mm
Period	40 μ m
Accuracy	$\pm 10 \mu$ /m
Thermal coefficient	$\simeq 5 \times 10^{-6} / ^\circ\text{C}$
- Torque limiter (spring) on Z axis only
- Mechanical and optical end switches

c) The carbon fiber arm

- 4 carbon fiber tubes (10mm×8mm)

Length 2000 mm

High rigidity

Low weight (reduced vibrations)

Thermal coefficient $\simeq -0.5 \times 10^{-6} / ^\circ\text{C}$

- Epoxy/Fiber glass support (ME 730)

- Central NMR probe

Type Miniature N°2 (Metrolab)

Range 0.09 to 0.26 T

- 2 Hall probes, 850 mm apart

Type SBV 579 (Siemens)

Current regul. (Cern) 100 mA \pm 10 μ A

Temp. control (Cern) 40 $^\circ\text{C}$ \pm 0.02 $^\circ\text{C}$

Sensitivity 130 mV/T

Thermal coefficient $\simeq -400 \times 10^{-6} / ^\circ\text{C}$

HOLDERS in polyurethane foam boxes

Regular calibrations in situ

IMMW11

(Didier Cornuet)

d) Alignment

- Mobile support of micrometers
- Precisely machined plates screwed on reference faces of the dipole (dove tails)
- 3 jacks under the girder
- Parallelism Spectrometer/Marble
 - ± 0.1 mm vertically
 - ± 0.1 mm laterally
- Mobile target at the ends of the arm
- Telescope insensitive to magnetic field
- Parallelism Spectrometer/Arm
 - ± 0.5 mm vertically
 - ± 1 mm laterally

3. Data acquisition system

- a) The PC
- b) Control and acquisition of the current
- c) Control and acquisition of the position
- d) Acquisition of inductions
- e) Acquisition of temperatures of the arm

a) The PC

- PC Pentium 90 (Olivetti)
 - 16 Mbytes RAM
 - 811 Mbytes hard disk
 - RS 232 port
 - Ethernet connection
- GPIB card
 - Type PCIIA (National Instruments)
- Visual Basic language
 - Version 5.0 downloaded
 - Programs run in standalone mode
 - Results stored on hard disk and transferred to the network after mapping

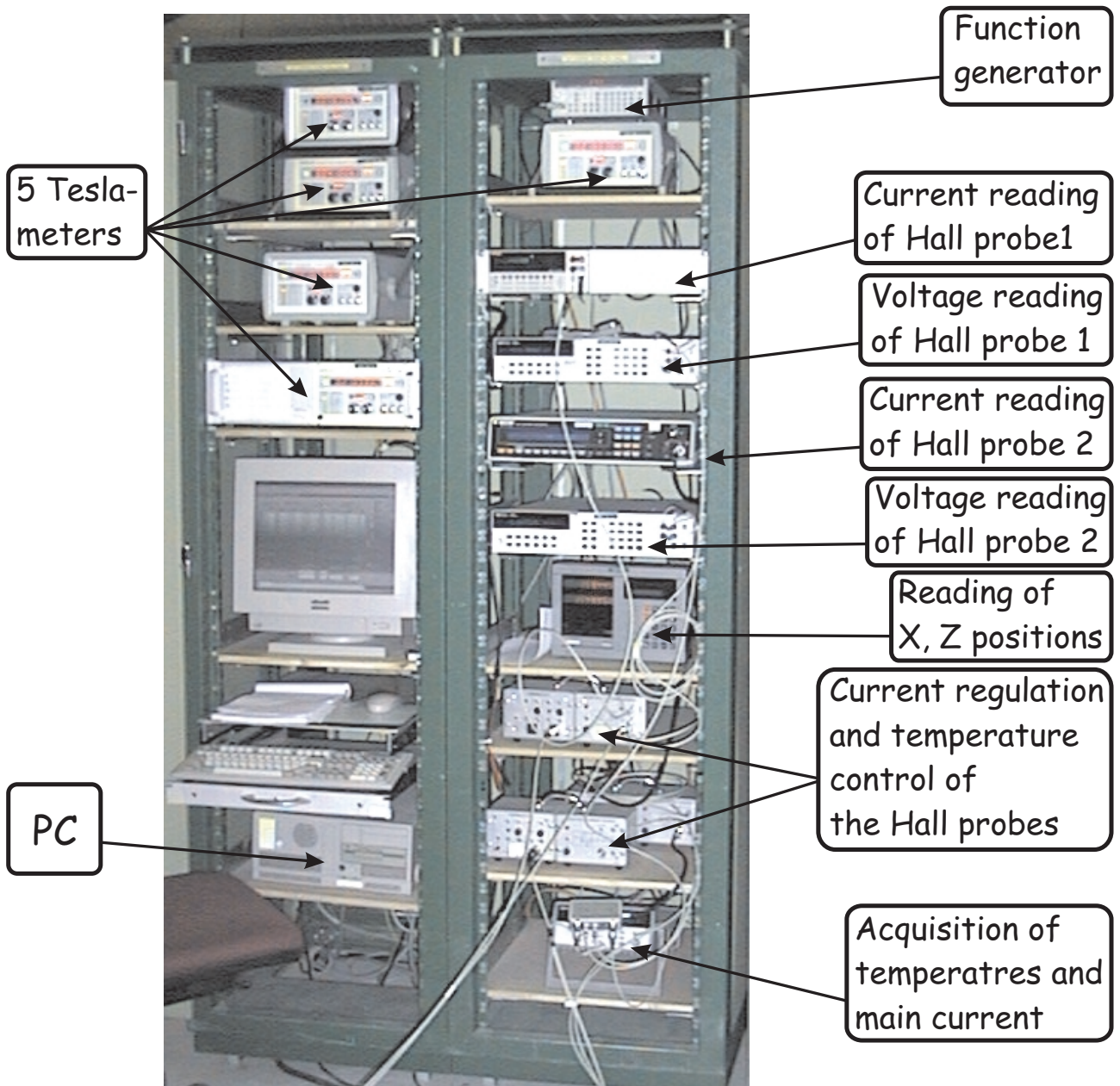
b) Control and acquis. of the current

- Unipolar power supply (Houvenhagel)
100 V / 600 A
ON / OFF local
- Reference
16 bit DAC
CERN made GPIB interface
- DCCT (Direct Current Current Transformer)
 ± 10 V / ± 1000 A (Hazemeyer)
Accuracy 10^{-4}
- Multimeter HP34970A
Multiplexer module HP34901A
Resolution 5 1/2 digits (50ms readout time)

c) Control and acquis. of the position

- Analog signals to control X&Z displacements
Function generator for Z movement:
 - type DS 345 (Standford Research System)
 - bipolar ± 10 V , 12 bits
 - GPIB interface
 - succession of pulses (amplitude function of the error with respect to final position)
- Steps
 - 10 mm ± 0.01 mm
 - Number 536/map
- Two axis display
 - Type ND 920 (Heidenhain)
 - Resolution $1\mu\text{m}$
 - RS 232C interface

Data acquisition system



d) Acquisition of inductions

- 4 fixed reference NMR probes
 - 2 subminiature type 1 (0.043 - 0.13 T)
 - 2 subminiature type 2 (0.090 - 0.26 T)Location close to the lower pole
Difficulty to find "flat zones"
for good locking (laminated magnet)
- 1 mobile NMR probe (type 2)
- 5 teslameters
 - Type PT2025 (Metrolab)
 - Resolution 10^{-7} T
 - Permanent locking (No mobile phones !)
- No multiplexer (too long for relocking)
- Not all teslameters in use altogether (interferences)

d) Acquisition of inductions (cont.)

- 2 mobile Hall probes (SBV 579)

Two Hall currents measured via shunts with two 7061 voltmeters (Solartron)

Range 1 V

Resolution $5\frac{1}{2}$ digit (100 ms read out time)

Two Hall voltages measured with two HP 3458A voltmeters (Hewlett Packard)

Range 100 mV

Resolution $7\frac{1}{2}$ digit (100 ms read out)

Polynomial approx. of the transfer function

Renormalization of each end fields

by comparison with the mobile NMR probe

e) Acquis. of temperatures of the arm

- 5 thermistors

Type UUT51J1 (Fenwal)

Resistance 100 k Ω @ 25 °C

Thermal coefficient $\simeq -4.8$ %/°C

High resolution

Small size ($\phi < 2.5$ mm)

Accuracy ± 0.2 °C

Polynomial approx. of the transfer function

- 2 (heat sinks of each Hall probe)
- 3 for ambient temperatures (ends and middle)
- Multimeter HP34970A
Multiplexer module HP34901A
GPIB interface

4. First results

- a) Magnetization curves, homogeneity
- b) Perturbations
- c) Relative accuracy achieved

a) Magnetization curve, homogeneity

$$B = f(Z)$$

$$\int B dz = f(I)$$

$$Leq = f(I)$$

$$Bnmr_i = f(B_{center})$$

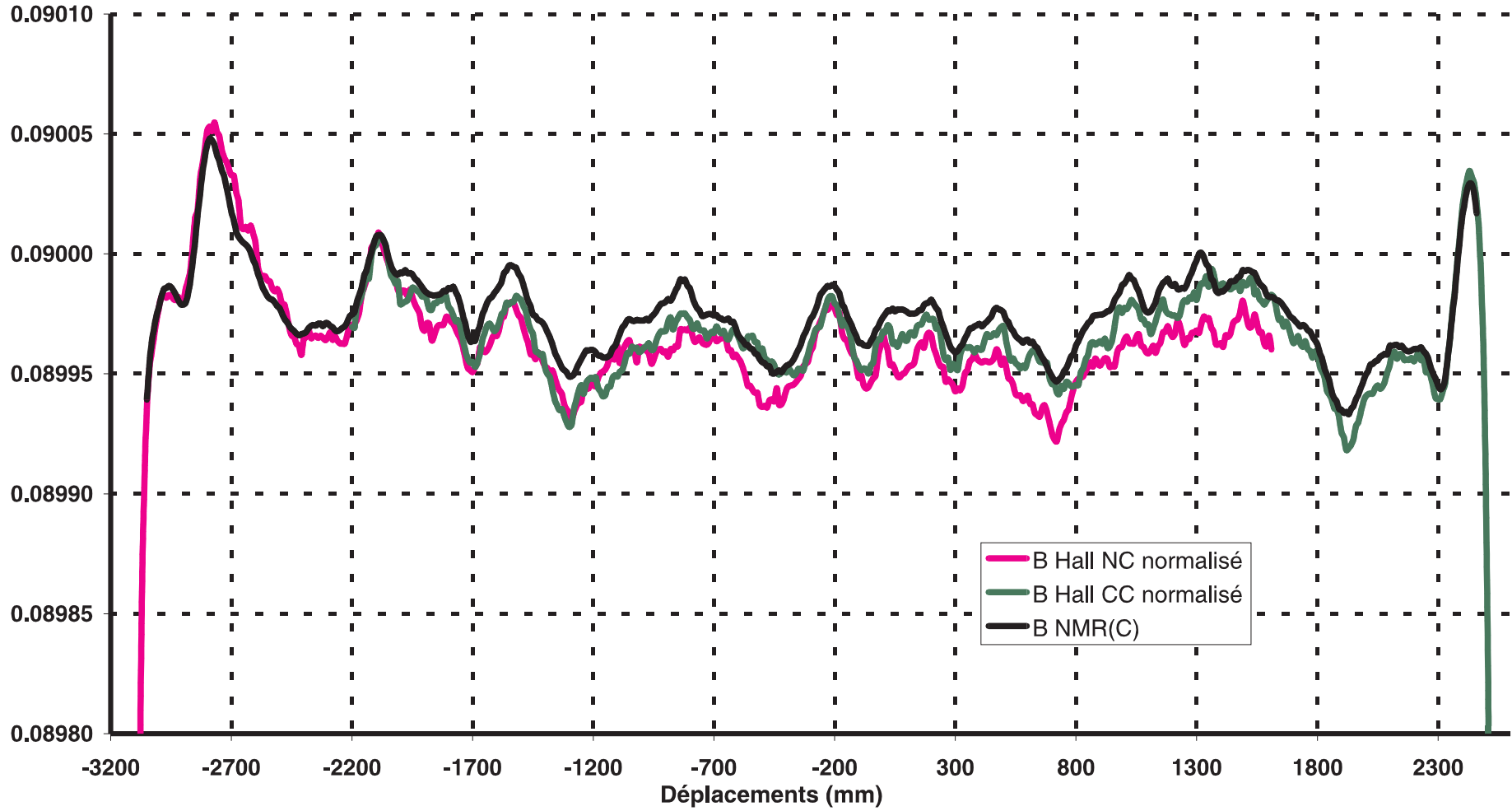
$$\int B dz = f(Bnmr_i)$$

$$\int B dz = f(X)$$

Homogeneity better than 10^{-5} for
 $-7.5 \text{ mm} \leq X \leq +7.5 \text{ mm}$: end fields partially
compensate the small gradient inside the yoke.

Induction (T)

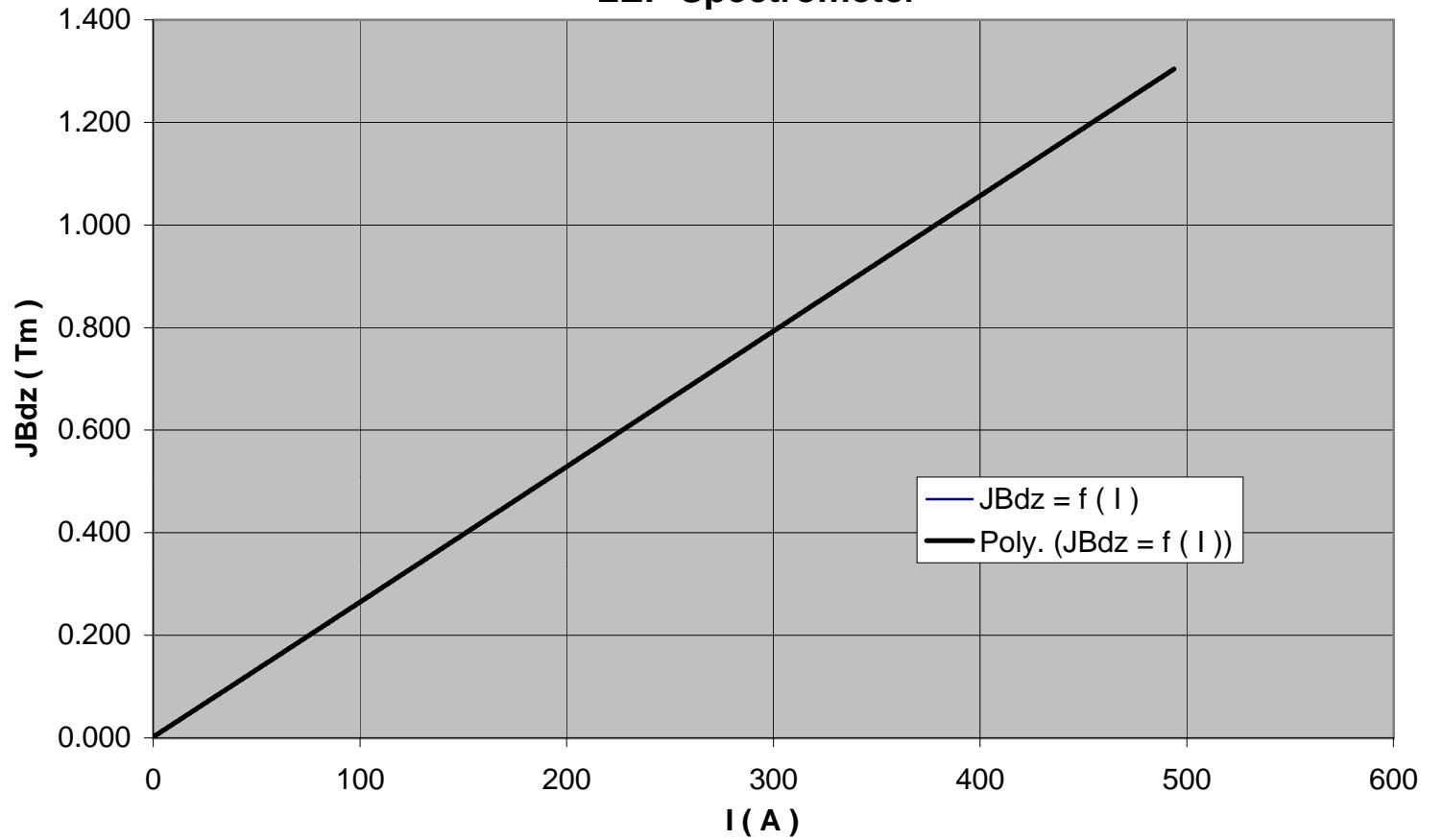
Mesure du spectromètre à 41.6 Gev



LEP Spectrometer

I(A)	JBdz = f (I)	p(GeV/c)
0	0.00192	
199.416	0.52716	41.63730
211.046	0.55790	44.06540
239.675	0.63358	50.04240
263.686	0.69701	55.05290
287.624	0.76023	60.04610
335.571	0.88680	70.04300
383.520	1.01328	80.03340
431.458	1.13968	90.01690
455.428	1.20285	95.00610
480.382	1.26857	100.1970
493.781	1.30385	102.9840

p for a = 3.7956E-3 radian



$$SBdz = 2.102155E-13 I^4 - 2.974767E-10 I^3 + 1.351049E-07 I^2 + 2.617194E-03 I + 1.920431E-03$$

LEP Spectrometer

I(A)	JBdz (Tm)	Bc (T)	Leq (m)
0	0.001921	0.0003280	5.858941*
199.416	0.527160	0.0899753	5.858941
211.046	0.557902	0.0952222	5.858949
239.675	0.633575	0.1081387	5.858911
263.686	0.697011	0.1189656	5.858929
287.624	0.760229	0.1297591	5.858772
335.571	0.886797	0.1513654	5.858651
383.520	1.013284	0.1729560	5.858623
431.458	1.139682	0.1945394	5.858361
455.428	1.202849	0.2053233	5.858317
480.382	1.268573	0.2165447	5.858251
493.781	1.303851	0.2225684	5.858202

*Estimated value

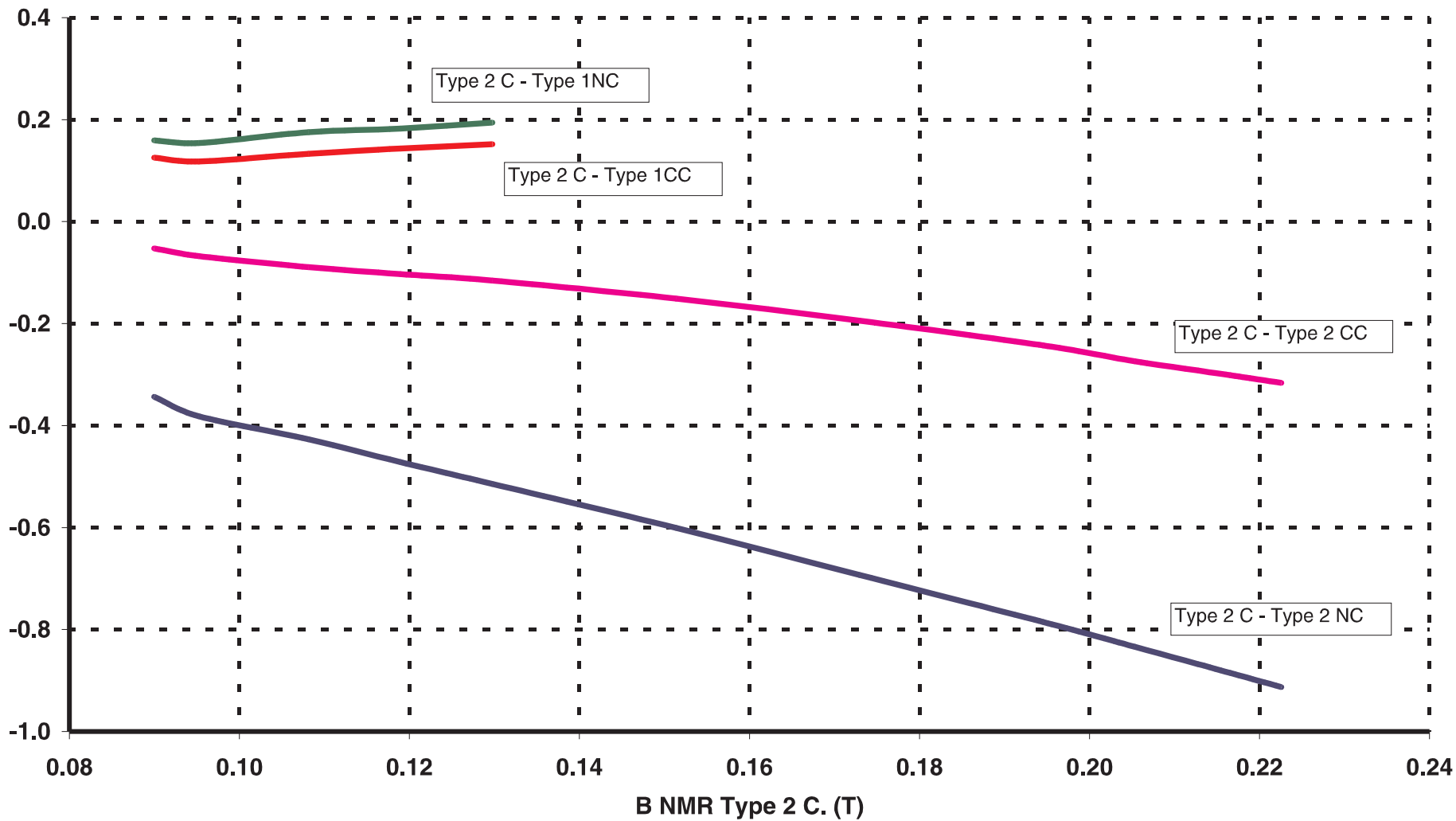
Equivalent length : $Leq = (JBdz) / Bc$

$\Delta Leq / Leq < 1.4 \text{ E-4}$ for $0 < I < 500 \text{ A}$

Ecart. (G)

Ecart entre sondes NMR.

25/02/99



Linear fit with respect to the 4 reference NMR probes :

$$J Bdz (Tm) = P_i . Bnmri + R_i$$

**Approximation $10 \cdot E^{-5}$ in the following domain of validity ,
 $0.527 (Tm) < JBdz < 0.761 (Tm)$**

NMR type 1 / connection side P1 = 5.858952 (m) R1 = 0.66817 E-4 (Tm)

NMR type 1 / non connection side P3 = 5.859020 (m) R3 = 0.85190 E-4 (Tm)

**Approximation $10 \cdot E^{-5}$ in the following domain of validity ,
 $0.761 (Tm) < JBdz < 1.304 (Tm)$**

NMR type 2 / connection side P2 = 5.856001 (m) R2 = 3.09169 E-4 (Tm)

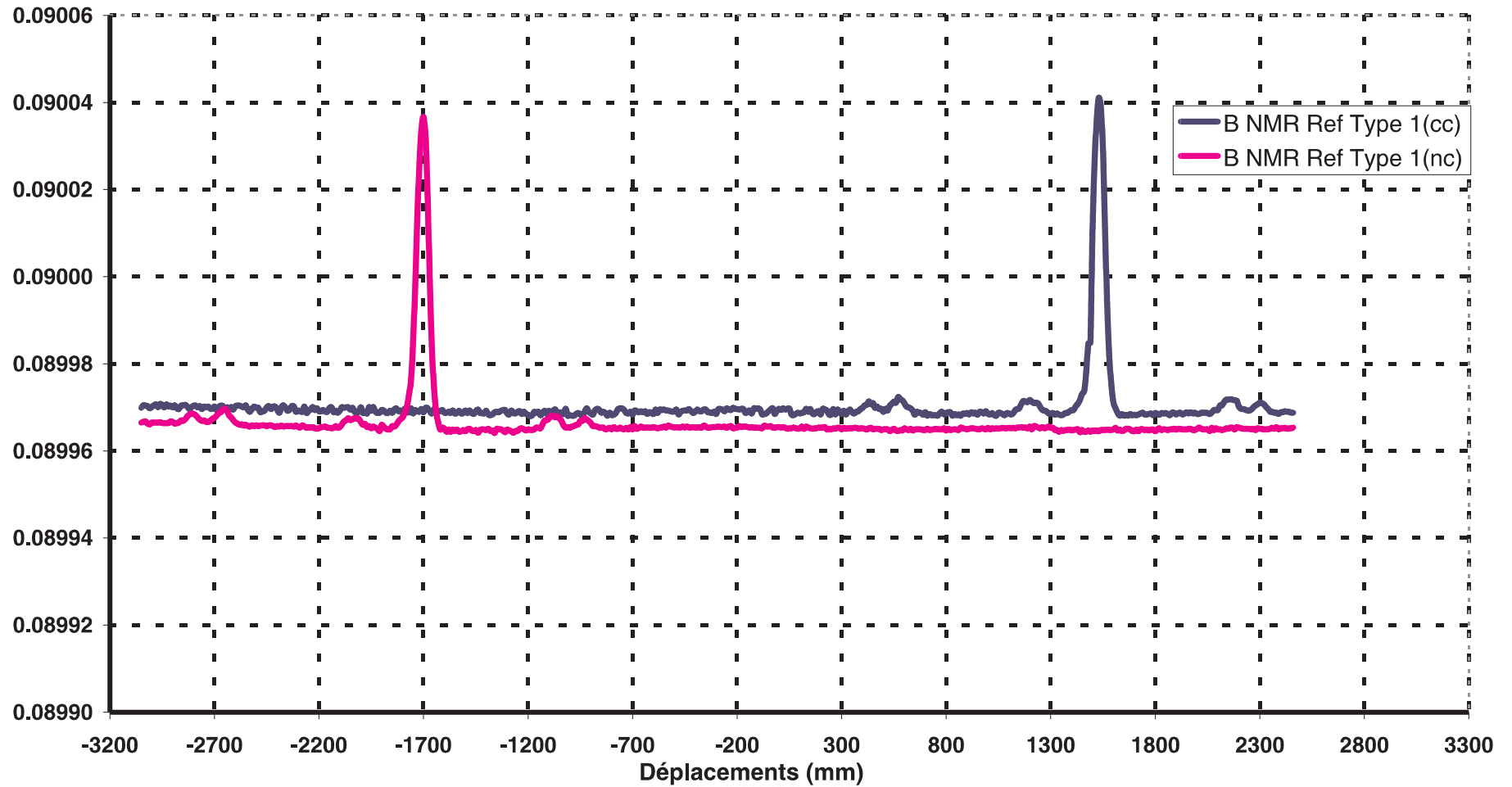
NMR type 2 / non connection side P4 = 5.854698 (m) R4 = 2.44711 E-4 (Tm)

b) Perturbations

- Unstability of Hall probes
 - Up to $2.5 \mu\text{V}$ @ random low frequency
- Displacement step
 - 3% of B / step (10 mm) in the end fields
- Stainless steel pieces
- Temperature
 - Temperature control of the magnet
 - Temperature control of the vacuum chamber supporting the mumetal shields in the tunnel
- Current steps
 - No significant differences according to the number of current steps
 - Expected 2 hours between different energies
- Unstability of the power supply
 - Maps for which the current fluctuations exceed 5×10^{-5} are eliminated

Induction (T)

Influence du déplacement du chariot sur les NMR de référence



c) Errors for ratio between integrals

$$k(2, 1) = \frac{(\int B dz)_{E2}}{(\int B dz)_{E1}}$$
$$\frac{dk(2,1)}{k(2,1)} = \frac{d(\int B dz)_{E2}}{(\int B dz)_{E2}} - \frac{d(\int B dz)_{E1}}{(\int B dz)_{E1}}$$

- Systematic errors cancel

Alignment of the marble / magnet

Distances of the Hall plates / central NMR

Non linearity of the steel measuring band

Sagitta of particle trajectory, etc...

- Random errors add up quadratically

Hall probes @ low currents 2×10^{-5}

Hall probes @ high currents 10^{-5}

NMR probes @ lower range 10^{-5}

Magnet (hysteresis) 10^{-5}

Temperature 10^{-5}

Arm positions 0.2×10^{-5}

$$\frac{\Delta k(2, 1)}{k(2, 1)} \leq 3 \times 10^{-5} \quad (\approx 600 \text{ maps})$$

5. Future improvements

- 2 stainless steel rods replaced Al alloy rods
- 4 stainless steel bearings replaced by ^RTeflon reinforced with carbon

- 2 new Hall probes

Type	KSY 44 (Siemens)
Current regul. (Cern)	5 mA $\pm 2\mu\text{A}$
Temp. control (Cern)	40 °C $\pm 0.02^\circ\text{C}$
Sensitivity	1000 mV / T
Thermal coefficient	$\simeq -300 \times 10^{-6} / ^\circ\text{C}$
Signal/noise ratio	2 \times that of SBV 579

- Ceramic felt for heatsink insulation
- Smaller measurement steps (5 mm) in end fields
- Normalization of each point to reference NMR
- **Goal** : 2×10^{-5} precision for ratio between integrals.

Analytic Form for Fitting Hysteretic Magnet Strength

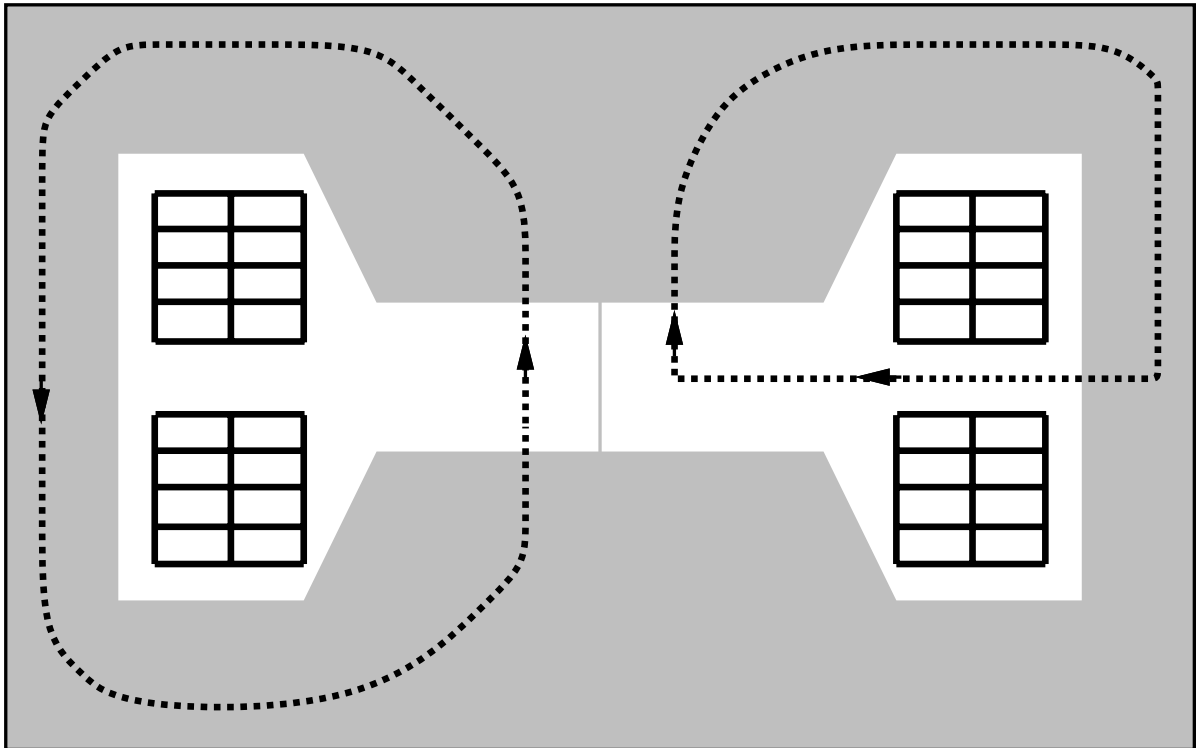
Bruce C. Brown
IMMW XI at Brookhaven
21-September-1999

21-Sep-1999 IMMW
Hysteresis Fits
Bruce C. Brown

At IMMW X at Fermilab, I presented a strategy for studying hysteresis effects in accelerator and beam line magnets. I would like to update that with a report on my progress at finding an analytic form which will fit this data to a precision of 3×10^{-4} or so.

A status report on this work was presented at PAC99 and can be found on my WWW site:
<http://www-ap.fnal.gov/bcbrown/Docs/p-Conf-99-096.ps>

21-Sep-1999 IMMW
Hysteresis Fits
Bruce C. Brown



To predict magnetic fields we employ Ampere's Law:

$$\int_g \frac{1}{\mu_0} \vec{B}_g \cdot d\vec{\ell} + \int_{\mathcal{L}} \vec{H} \cdot d\vec{\ell} = N_g I, \quad (1)$$

where g represents the path in the air gap and \mathcal{L} represents the path through the steel. We will use N_g turns per gap as for loop on left.

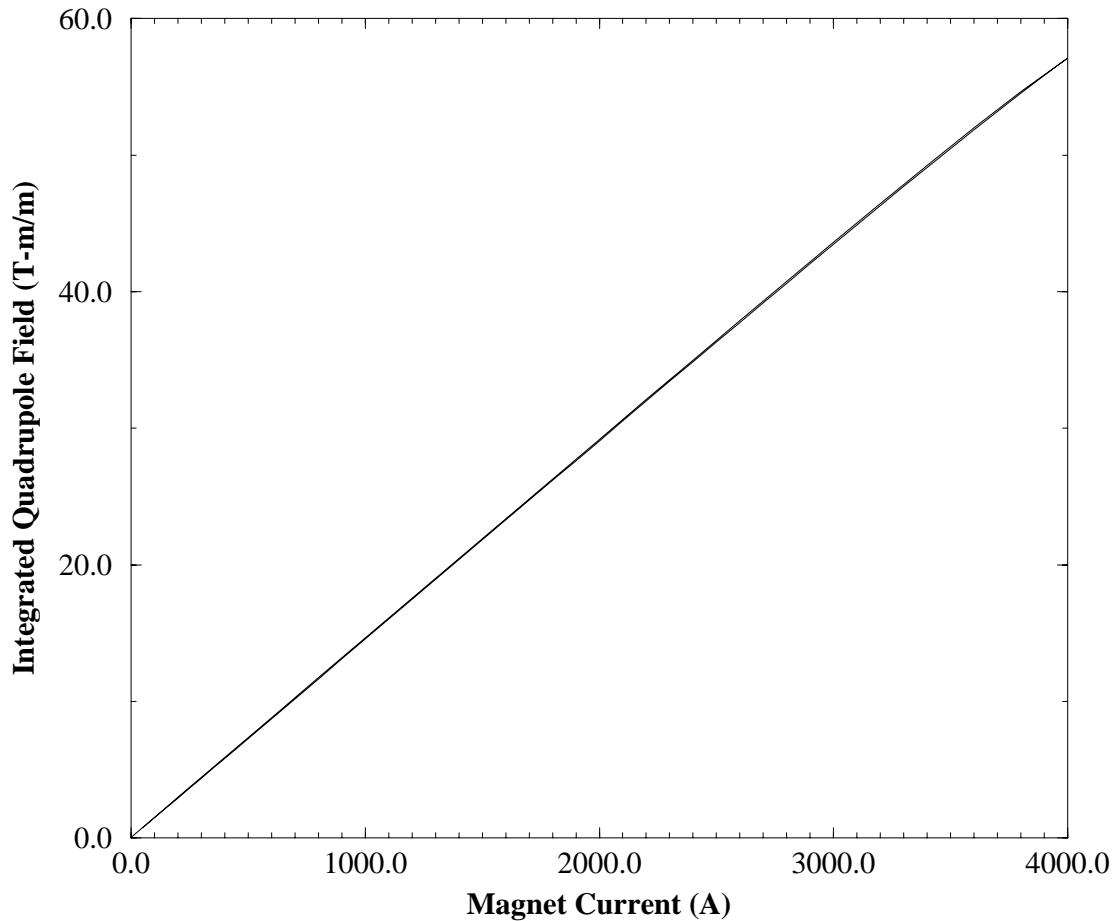
In a well designed multipole magnet (dipole, quadrupole....) the the field in the gap is well represented by the dominant multipole component. We integrate along a field line in the gap (to pole radius A). To be ready to fit integrated field measurements, we integrate along the beam path by multiplying our body field strength by an effective length, L_{eff} . For the integral over the path in steel we choose a typical path along a flux line.

$$B_N L_{eff} = \frac{\mu_0 N N_g L_{eff} I}{2A^N} - \frac{N \mathcal{L} L_{eff}}{2A^N} \mu_0 \langle H_{steel} \rangle . \quad (2)$$

where N is the harmonic number (1 for dipole), N_g is the number of turns per gap in the coil, A the pole tip radius ($g/2$ for a dipole), \mathcal{L} is the length of a flux line in iron with average H along the path of $\langle H_{steel} \rangle$. I is the current through the coil. We note that the first term is proportional to I and it represents the field created in idealized iron by the magnet current. The second term describes the field lost in driving the iron. All saturation and hysteretic terms due to iron remanence are described by $\langle H_{steel} \rangle$.

Quadrupole Field Strength

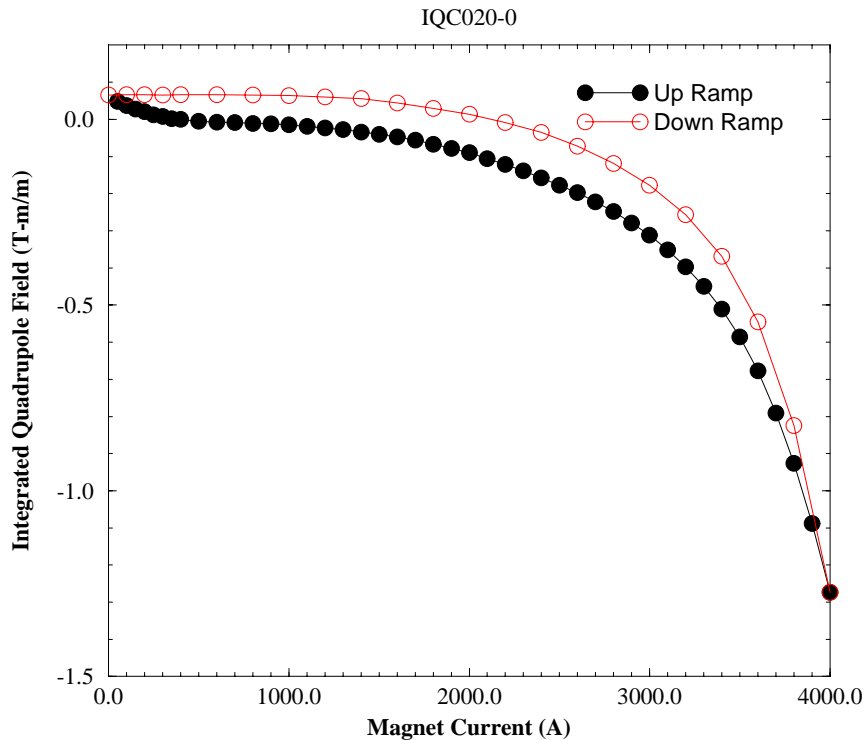
IQC020-0



Let us look at some typical data for magnet strength. Note that there is both an up ramp and a down ramp measurement on this plot.

21-Sep-1999 IMMV
Hysteresis Fits
Bruce C. Brown

Non-linear Portion of Quadrupole Field Strength

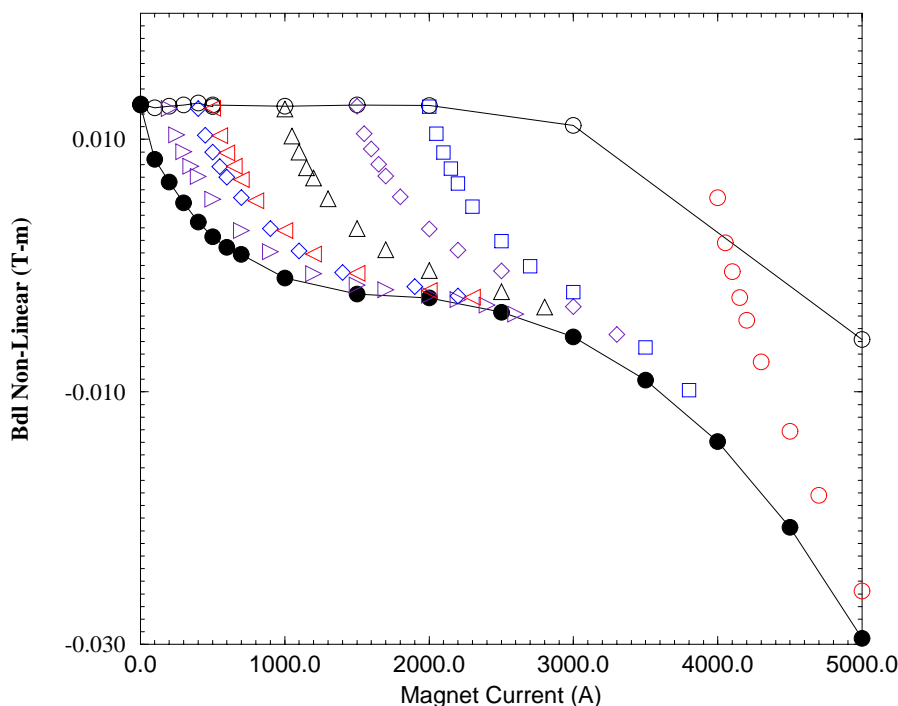


To see the effects of $\langle H_{steel} \rangle$, we subtract a term linear in current. It can be from fitting the previous plot or by calculation from pole geometry and the number of turns. We see two sorts of contributions in this plot. The upramp strength is less than the downramp strength (hysteresis) and there is a sharp change at high field (saturation).

21-Sep-1999 IMMW
Hysteresis Fits
Bruce C. Brown

Downramp Transition Study

IDA114-0

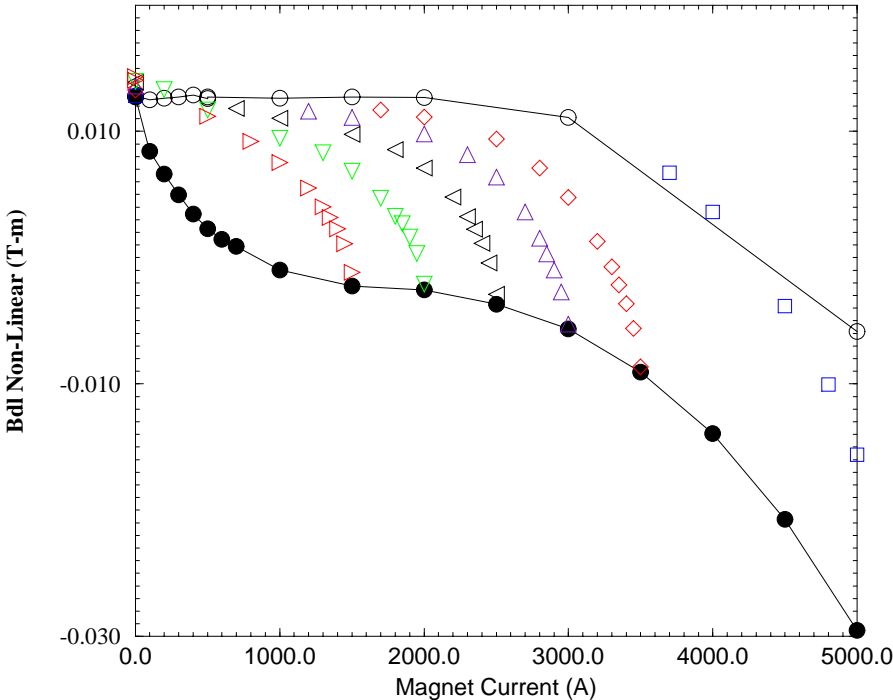


Before selecting an analytic fitting form, we need to examine additional measurements which will guide our choices. If we perform measurements with a series of different minimum (re-set) fields we find a family of similar curves for the non-linear field.

21-Sep-1999 IMMW
Hysteresis Fits
Bruce C. Brown

Downramp Transition Study

IDA114-0



The results for measurements with various peak excitations again have an obvious pattern with shapes very suggestive of the same form.

21-Sep-1999 IMMW
Hysteresis Fits
Bruce C. Brown

Our analytic form will need two types of terms. We have chosen to call the form reached well after current changes as the 'hysteresis curve'. There is an upramp hysteresis curve and a downramp hysteresis curve. We initially note that it has some obvious similarity to a hyperbola which has been suitably rotated and offset.

$$H(I, D) = -\sqrt{h_2x} - \sqrt{h_2x^2 + h_0}$$

The curves which transitions the strength between the upramp curve and the downramp curve we call Interjacent curves. The exponential character of these is apparent to the most casual observer.

$$J(I, I_r, I_p, D) = A(I_r, I_p, D) e^{-\left(\frac{I-I_r}{I_{C,D}}\right)}$$

Adding a parabola to provide a little freedom for fitting, we applied this to the data and achieved a fit precision of about 0.3% (30×10^{-4}). We are using this prescription, however inadequate, for Main Injector operation at this time.

To fit the data more precisely, we had to overcome a number of problems:

- The remanent field has a weak dependence on the peak of the last ramp. This is likely to be unimportant for ramps of operational interest, but in trying to get sufficient range of data to constrain the fit parameters, we get enough differences to make this significant.
- The hyperbola is not sufficiently 'rich' to represent the hysteresis curves.
- A single exponential falls too quickly to represent the data.
- The current control was very good (a 10 kA system operating at 500 A gave an RMS magnet strength deviation consistent with less than 20 mA RMS current deviation) but the current readback was about one order of magnitude worse. We 'calibrate' the the control current to get information for fitting.

21-Sep-1999 IMMW
Hysteresis Fits
Bruce C. Brown

We consider the magnet strength M ($\int B_1 dl$, $\int B_2 dl$ or $\int B_3 dl$) to be comprised of four terms, L (linear), R (remanent), H (hysteretic) and J (interjacent) . We continue to explore suitable expressions for these contributions but find useful fits with the following functional relations:

$$M(I, I_r, I_p, D) = L(I) + R(I_p, D) + H(I, D) + J(I, I_r, I_p, D)$$

where I is the magnet current during the measurement, I_r is the reset current (current at last sign change in dI/dt), I_p is the preset current (reset current of last ramp), and D is the ramp direction with $+1$ for upramps and -1 for downramps. We express the relations with normalized variables to provide consistency of representation among magnets. Use I_{scale} as a maximum current of interest (rounded) and I_S as a characteristic current for saturation.

$$x = \frac{I - I_S}{I_{scale}} \quad x_0 = \frac{-I_S}{I_{scale}}$$

21-Sep-1999 IMMV
Hysteresis Fits
Bruce C. Brown

Expressions used for these terms are

$$L(I) = Slope * I$$

$$R(I_p, D) = RemStr_D + RemSlp_D * (I_p - I_{scale})$$

$$H(I, D) = C_1 * \frac{I}{I_{scale}} - \sqrt[4]{h_4 x} - \sqrt[4]{h_4 x^4 + h_3 x^3 + h_2 x^2 + h_1 x + h_0} + \sqrt[4]{h_4 x_0} + \sqrt[4]{h_4 x_0^4 + h_3 x_0^3 + h_2 x_0^2 + h_1 x_0 + h_0}.$$

Note that H is defined to have the value 0 at $I = 0$. Each parameter is distinct for the upramp or downramp curve and could be expressed as h_{iD} or C_{1D} .

Two forms have been used for fitting J :

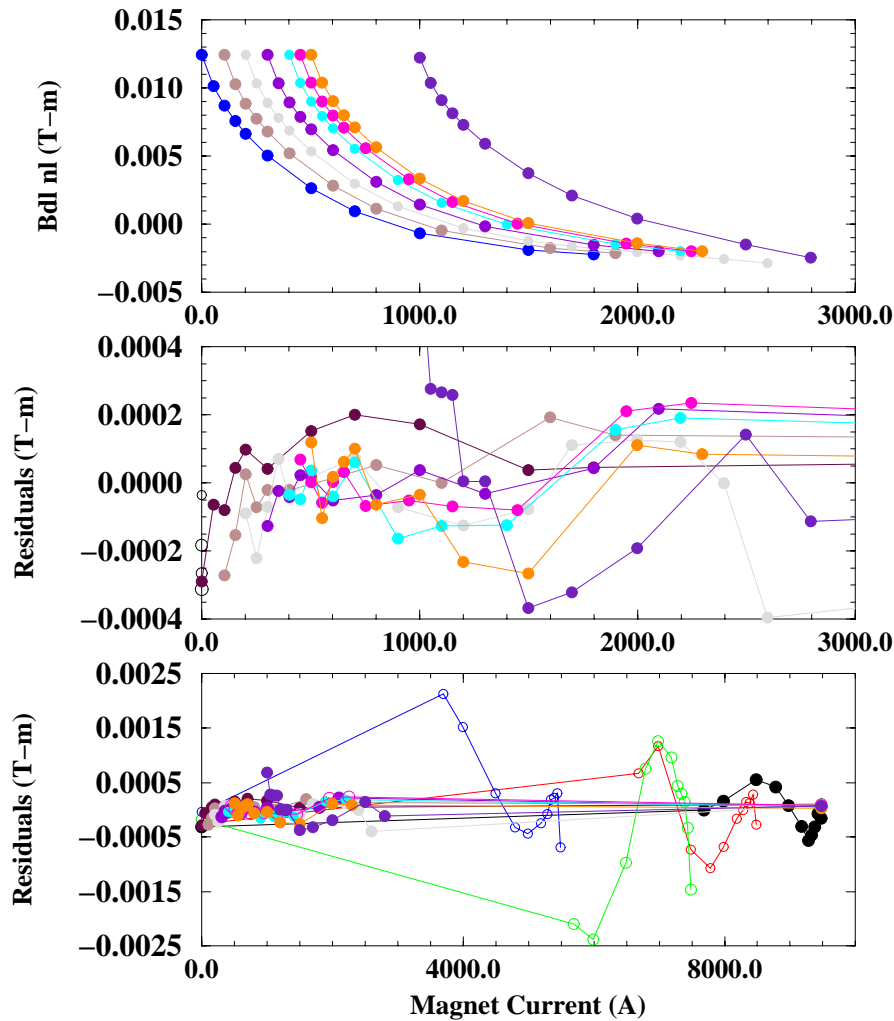
$$J(I, I_r, I_p, D) = A(I_r, I_p, D) \left(s e^{-\frac{I-I_r}{I_{C1,D}}} + (1-s) e^{-\frac{I-I_r}{I_{C2,D}}} \right)$$

$$J(I, I_r, I_p, D) = A(I_r, I_p, D) e^{-\left(\frac{I-I_r}{I_{C,D}}\right)^N}$$

where N is a real number, typically less than 1. The amplitude function A is the difference in hysteresis curves at the reset current.

$$A(I_r, I_p, D) =$$

$$H(I_r, -D) - H(I_r, D) + R(I_p, -D) - R(I_p, D).$$



Selected data from the IDA114-0 hysteresis study were fit with the interjacent curve described by 2 exponentials. Top plot shows fits to the selected upramp data. Center and lower plots show residuals (measured - fitted) on scales which emphasize the low field and high field results.

21-Sep-1999 IMMW
Hysteresis Fits
Bruce C. Brown

Summary

- Strength measurements of accelerator magnets, while dominated by the linear strength term have important field components which are not linear in excitation current. These non-linear terms have surprisingly simple regularities which permit analytic descriptions.
- To good accuracy, these non-linear terms exponentially approach a common hysteresis curve following a sign change in dI/dt . A small effect due to the reset (or preset) current may remain.
- The Interjacent curves which characterize the fashion in which the strength approaches the hysteresis curve is nearly exponential. Fits using two exponentials or a modified exponential are sufficient for present requirements.
- Analytic fitting functions have been found which describe these effects well enough to leave fitting residuals which are less than 5×10^{-4} relative to the magnet strength at each current.
- Data have been measured on six or more magnet designs. The same characteristics are apparent in all of them. Efforts to get a complete software system which will fit all of this measured data is continuing.

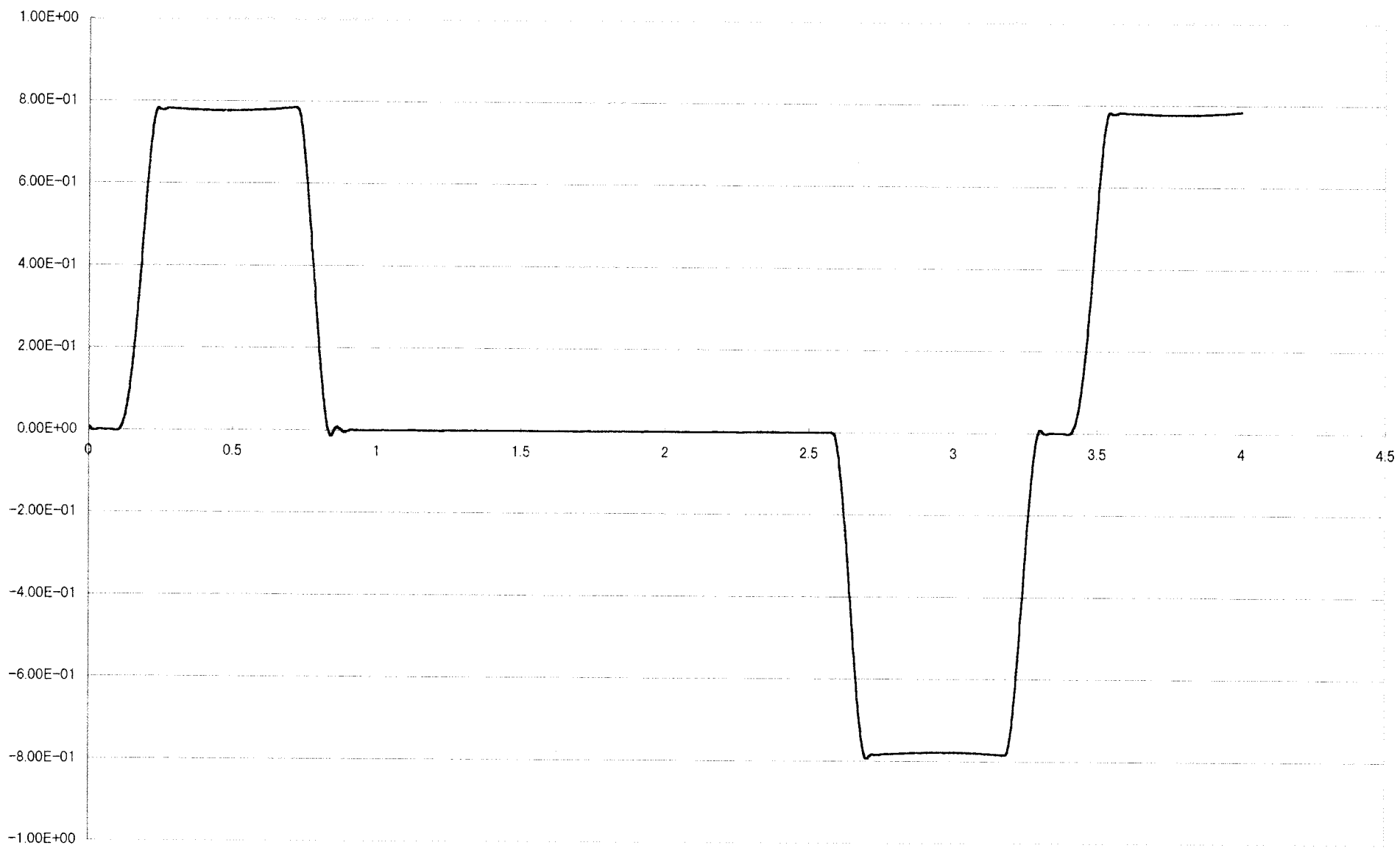
21-Sep-1999 IMMV
Hysteresis Fits
Bruce C. Brown

"Magnetic field measurement by Digital Integration of a repetitive magnetic field"

M.Kumada, K.Nishikigoori, T.Togasi and
Takashi Aoki
NIRS(National Institute of Radiological
Sciences) and AEC(Accelerator
Engineering Corporation)

Abstract

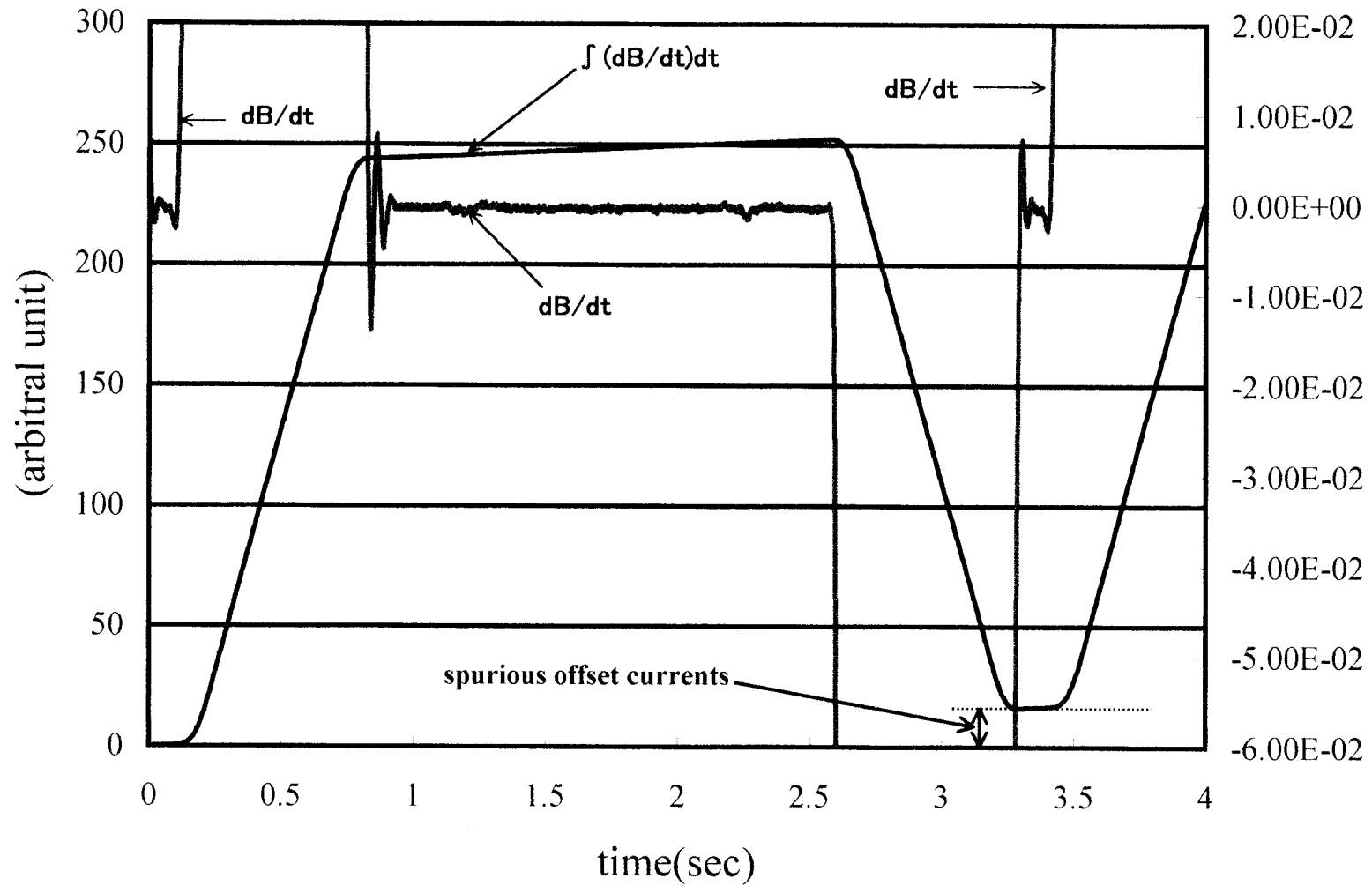
In order to monitor a cyclic magnetic field of synchrotron we have developed a digital integration technique instead of conventional hardware integration technique. This method provides us an easy and less costly but accurate real time magnetic monitoring.

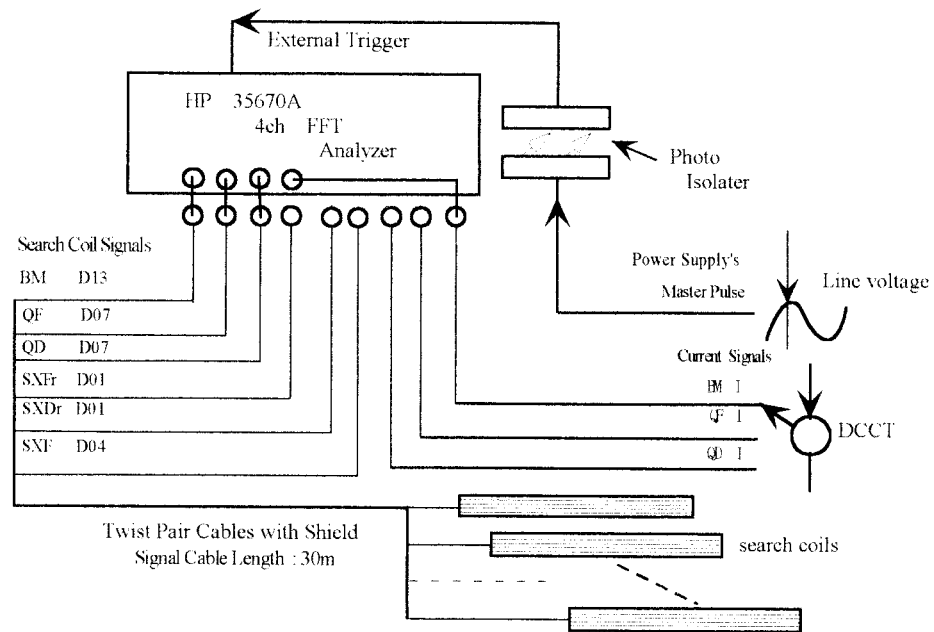


$\int (dB/dt)dt$

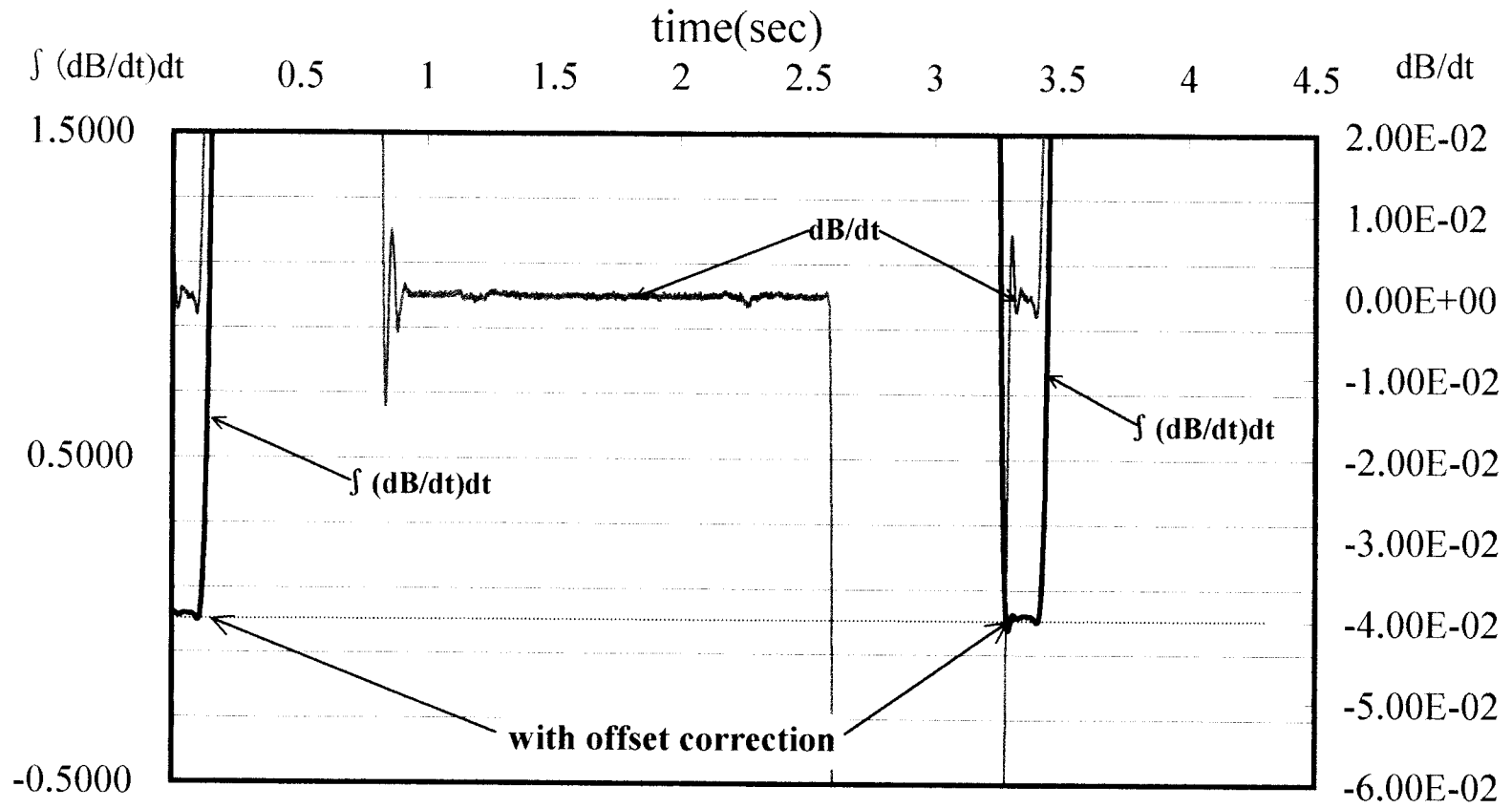
without offset correction

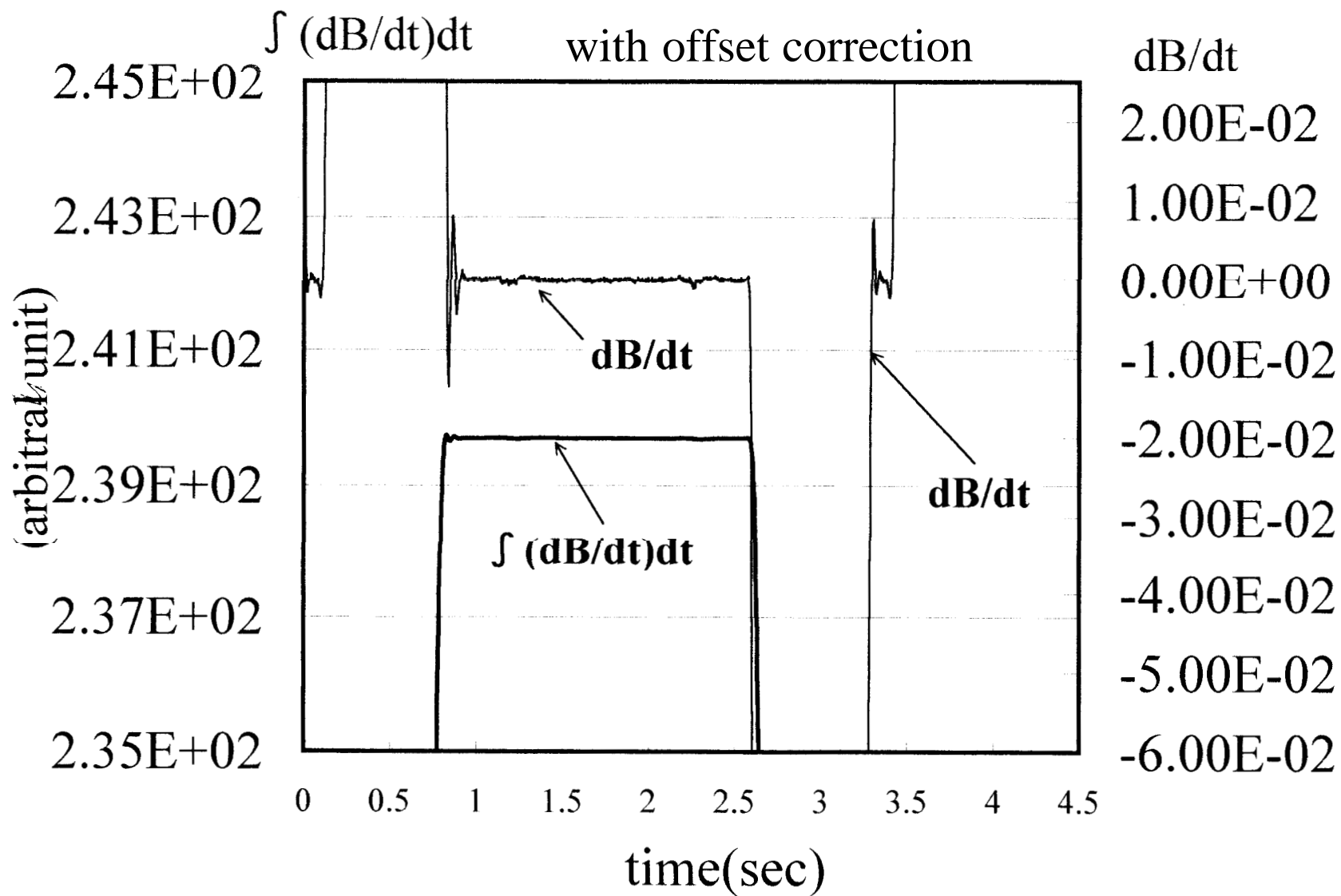
dB/dt

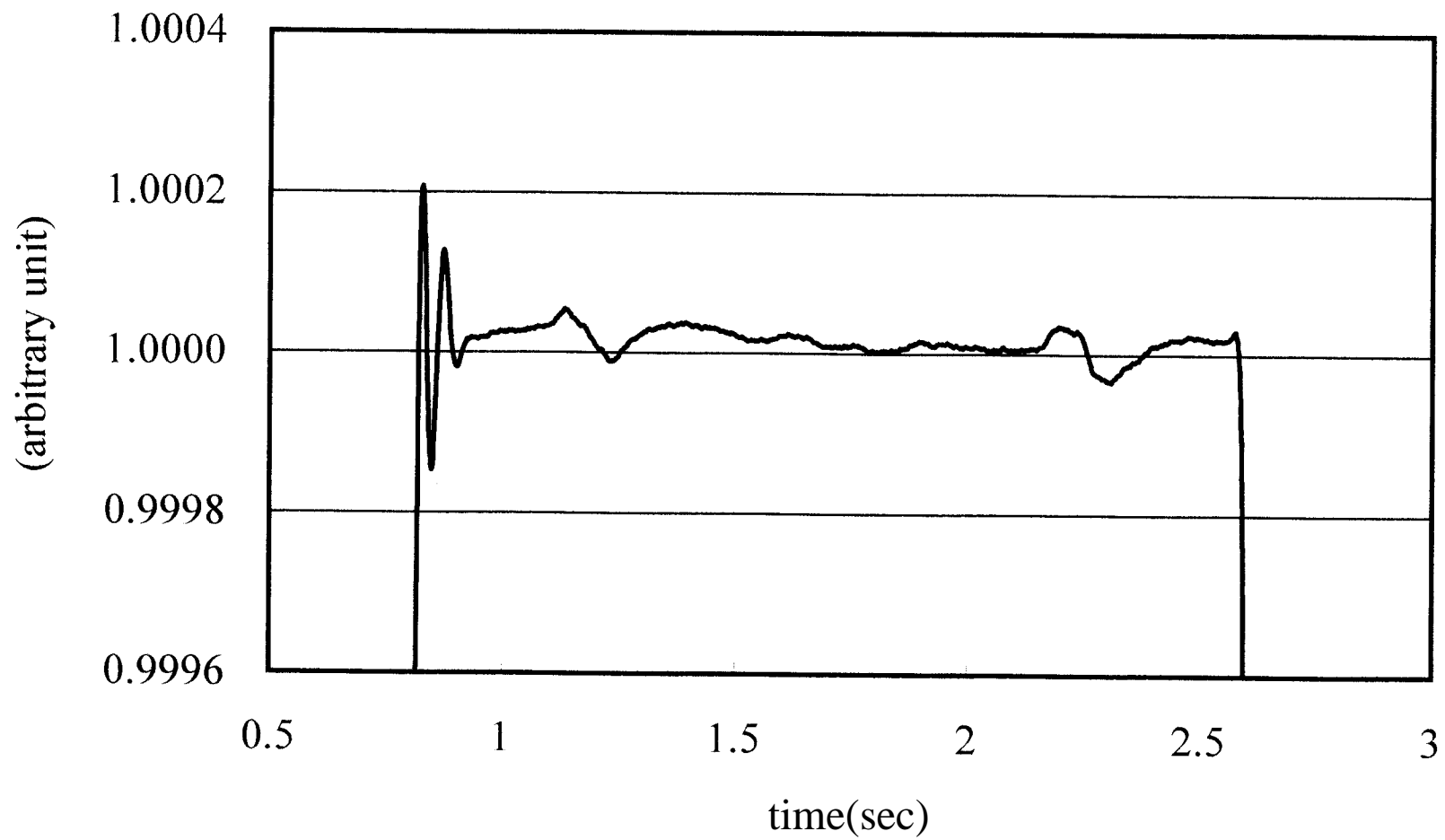




$$B(t) = A \int_0^t \{e(t) + e_k\} dt + \Delta B(t)$$

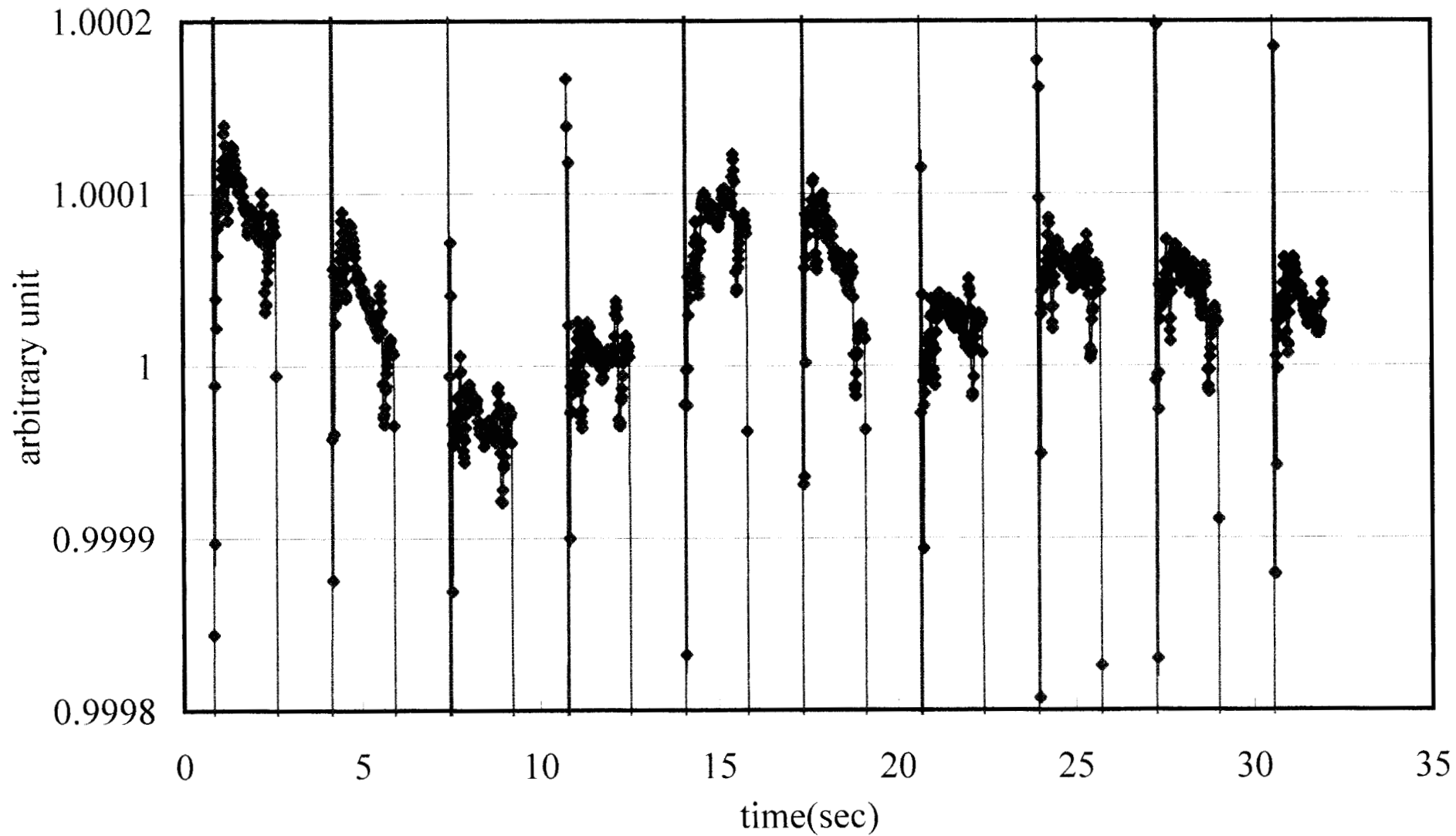




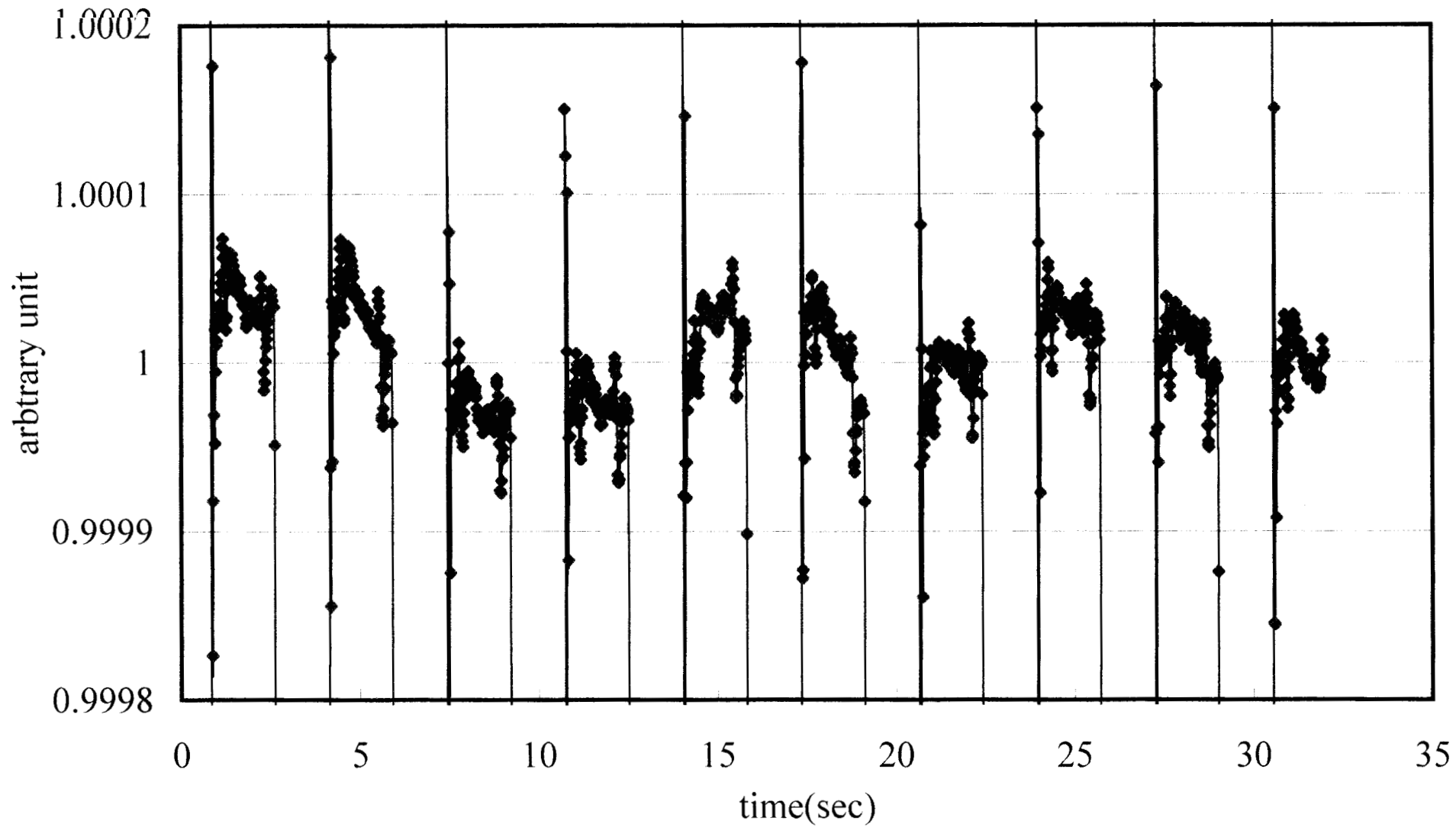


$$\Delta B(t) = a_0 \exp(-b_0 t) \cos(c_0 t + d_0) \\ + e_0 \exp(-f_0 t) \sin(g_0 t + h_0)$$

Long periodic fluctuations without noise cancellation



long periodic Fluctuation with cancellation



Summary

We have developed an accurate magnetic measurement system using search coil with digital integration device of wide dynamic range. This system leads to a finding of fine structure of the magnetic field at the flat top and the flat base. Those findings include a finding of a coupling between the power supplies and between the magnets in the synchrotron ring and correlation between a fine beam structure in the extracted beam line. This method could be further improved by implementing into the feedback system, which is also under study.



Power Loss Measurements of Superconducting Magnets

Richard Thomas
Brookhaven National Laboratory

INTRODUCTION

Two Methods:

- ① Electrical
- ② Thermal

Both are attempting to measure a small change in the measured parameters.

The thermal method requires knowing the thermal characteristics of the system well and the ability to hold the system in the loss and non-loss states for extended periods of time. Very good for measuring the electrical losses in a small system that can be thermally isolated at cryogenic temperatures.

Electrical Measurement Method

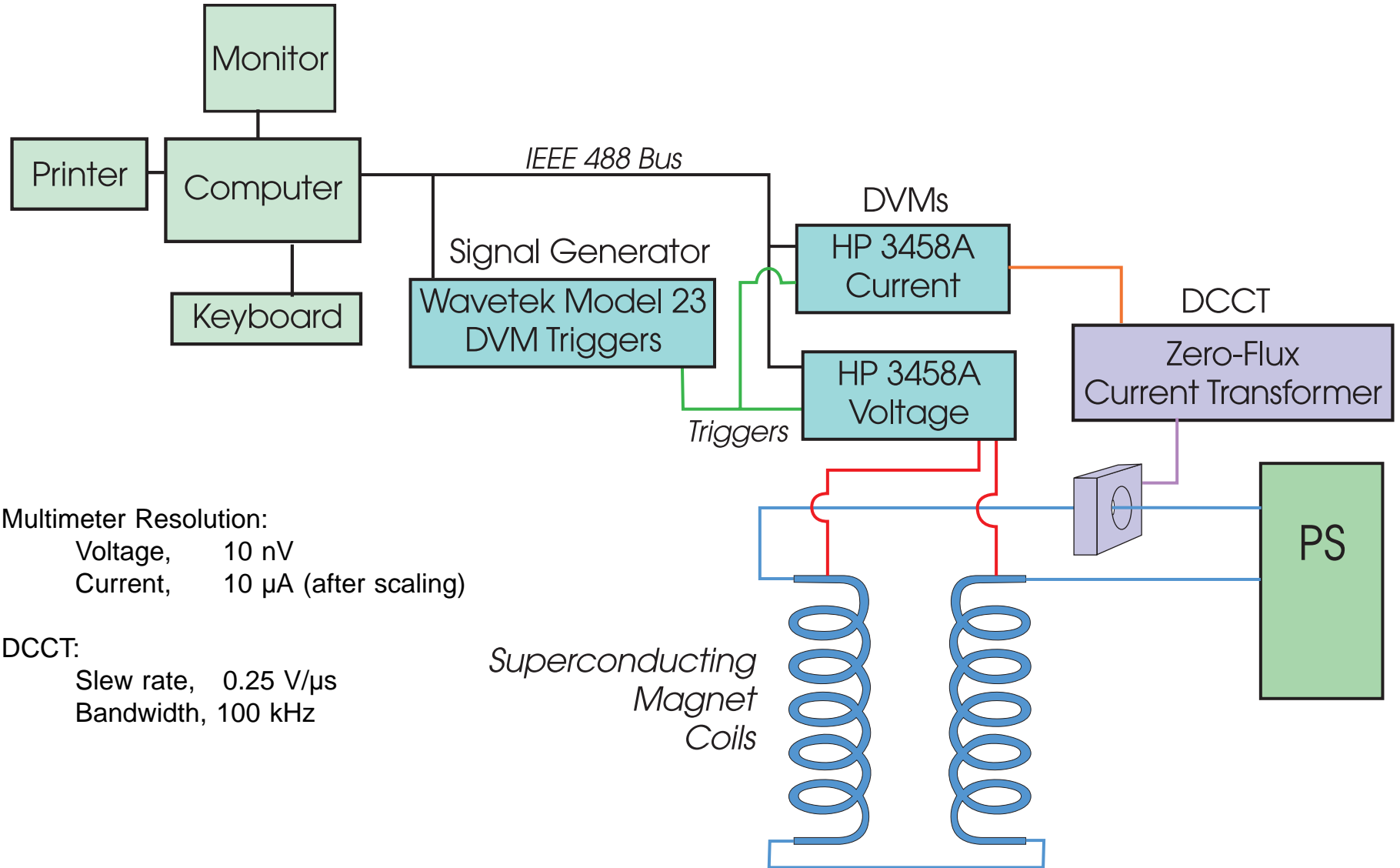
This method was used to measure the 60-Hz losses in a 100-m long, 4100 A, superconducting power transmission line (1984)

Also used to measure the hysteretic losses in small samples of magnet steel

Procedure for Superconducting Magnet:

- ★ Measure Current and Voltage across the magnet
- ★ Ramp the magnet current up then back down
- ★ Compute the Power at each point and the Energy Loss for the ramp cycle

*Note: This method measures **all** the losses that are 'powered' by the changing magnetic field.*



Multimeter Resolution:

- Voltage, 10 nV
- Current, 10 μ A (after scaling)

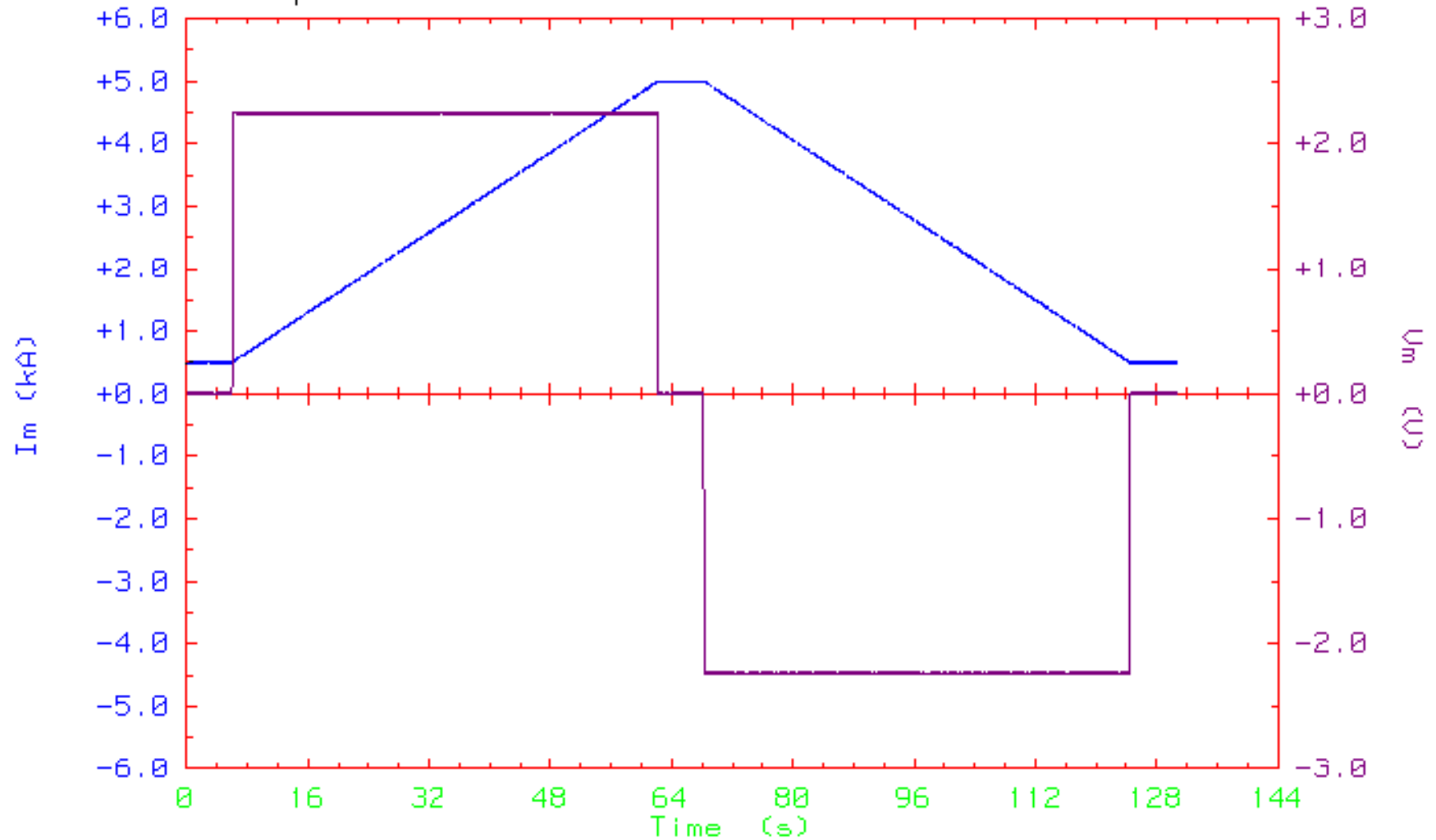
DCCT:

- Slew rate, 0.25 V/ μ s
- Bandwidth, 100 kHz

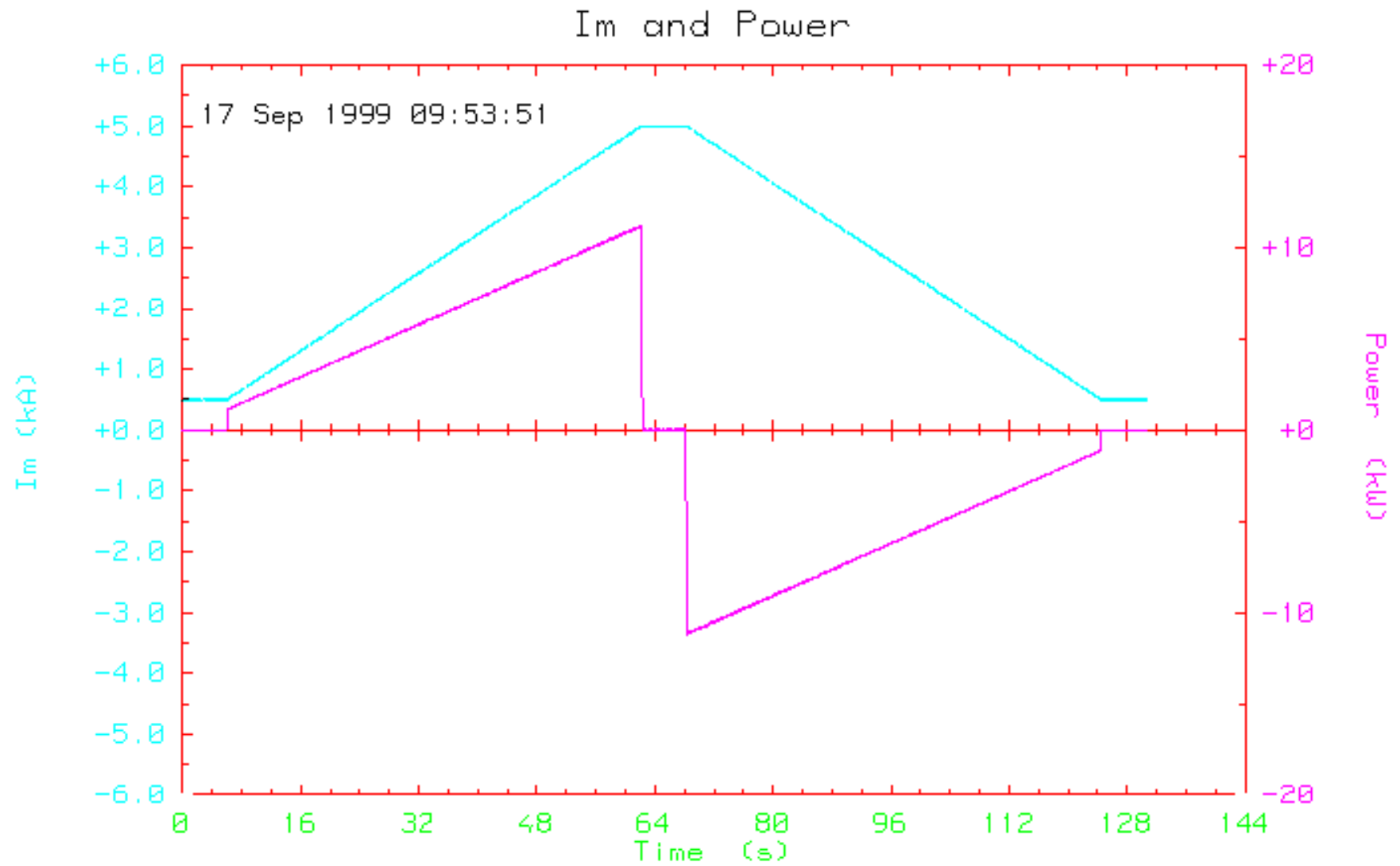
Superconducting
Magnet
Coils

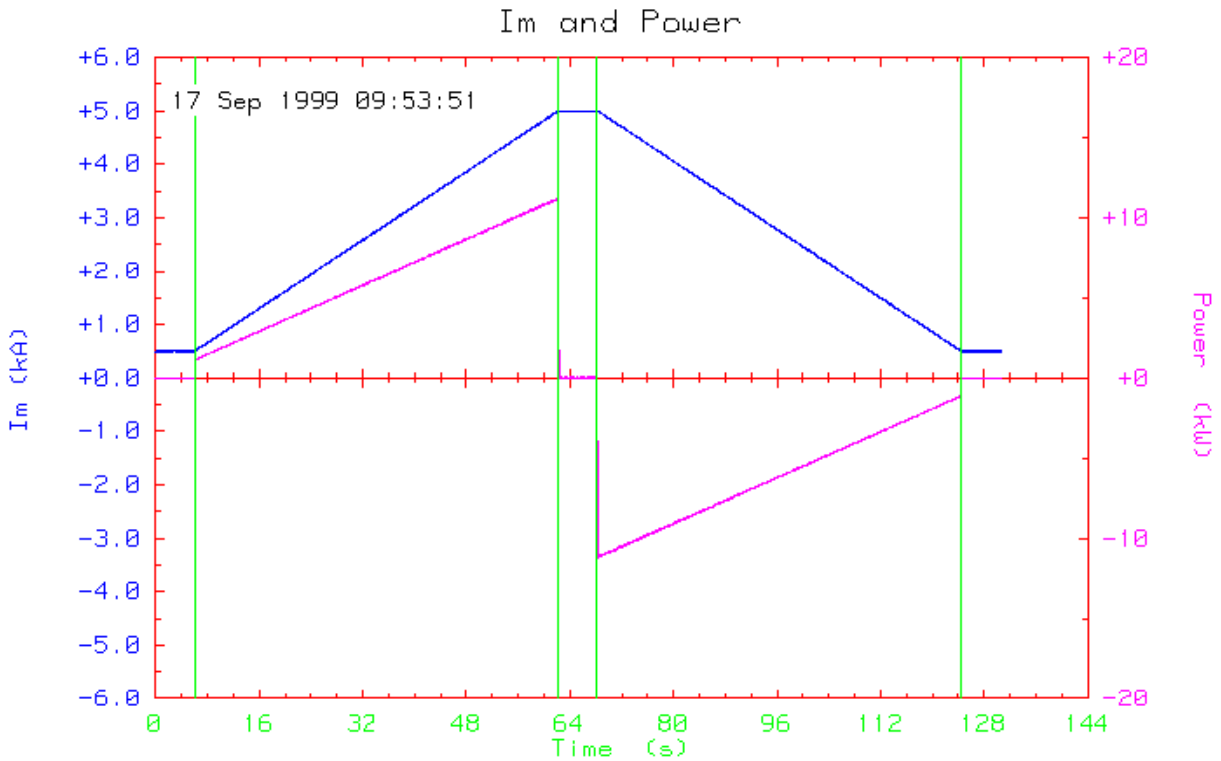
I_m and U_m

17 Sep 1999 09:28:49



Time per point: 40 ms





17 Sep 1999 14:25:58 Magnet Ac Loss Measurement (Simulation)
 Test. 10 mV voltage noise, 5 A current noise. 4.0 Watts
 Method: Unipolar
 3265 readings spaced 0.040 s apart, NPLC = 2, coverage = 83%
 Imax +5004.8, Imin +495.0
 Vmax +2.252, Vmin -2.248
 Ramp Pts 150 1555 1705 3113 Diffs: 1405 150 1408
 Im +498 +4993 +5001 +501
 Vm +2 +2 +0 -0
 1 149.506 5.997 s .14 A/s 499.05409 A
 2 1555.199 62.225 s 80.01 A/s
 3 1705.103 68.221 s .53 A/s 5001.29540 A
 4 3113.119 124.541 s -79.98 A/s
 5 3264.000 130.577 s .18 A/s 498.04587 A
 Sum of voltages over entire cycle: 4.886 V, Equiv. drift per point: 1497 uV

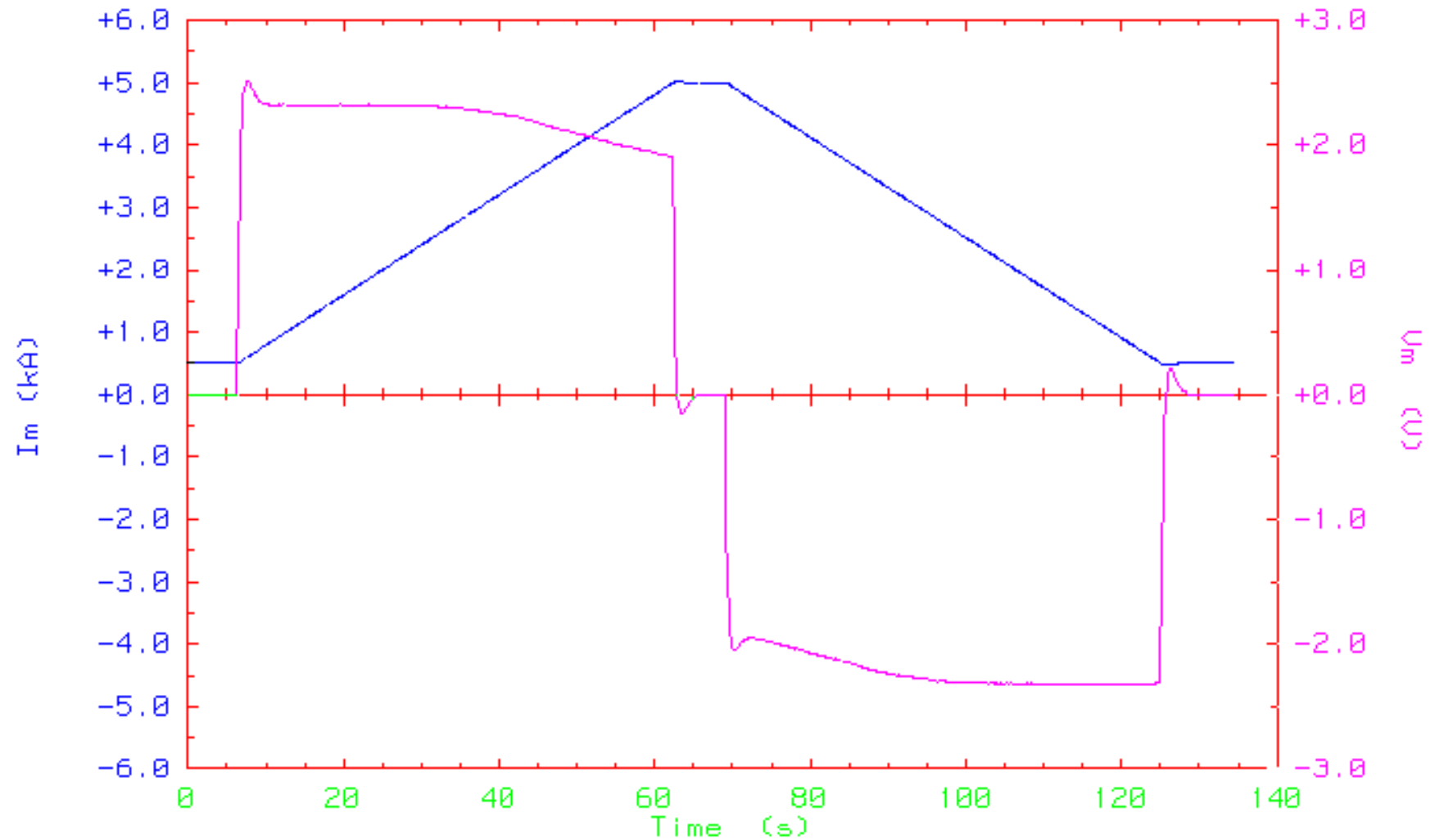
Ramp Rates: +80.009 A/s -79.981 A/s Avg. = 79.995 A/s
 Inductance: 28.02 mH 27.99 mH Avg. = 28.00 mH

The average power and energy over the entire measurement period were:
 4.063 W 530.6 J

Dwell		Ramp Up		Dwell		Ramp Down		Dwell	
W	J	W	kJ	W	J	W	kJ	W	J
-0.0	-0	+6157.1	+346.7	+1.1	+6	-6134.8	-346.2	+0.3	+2

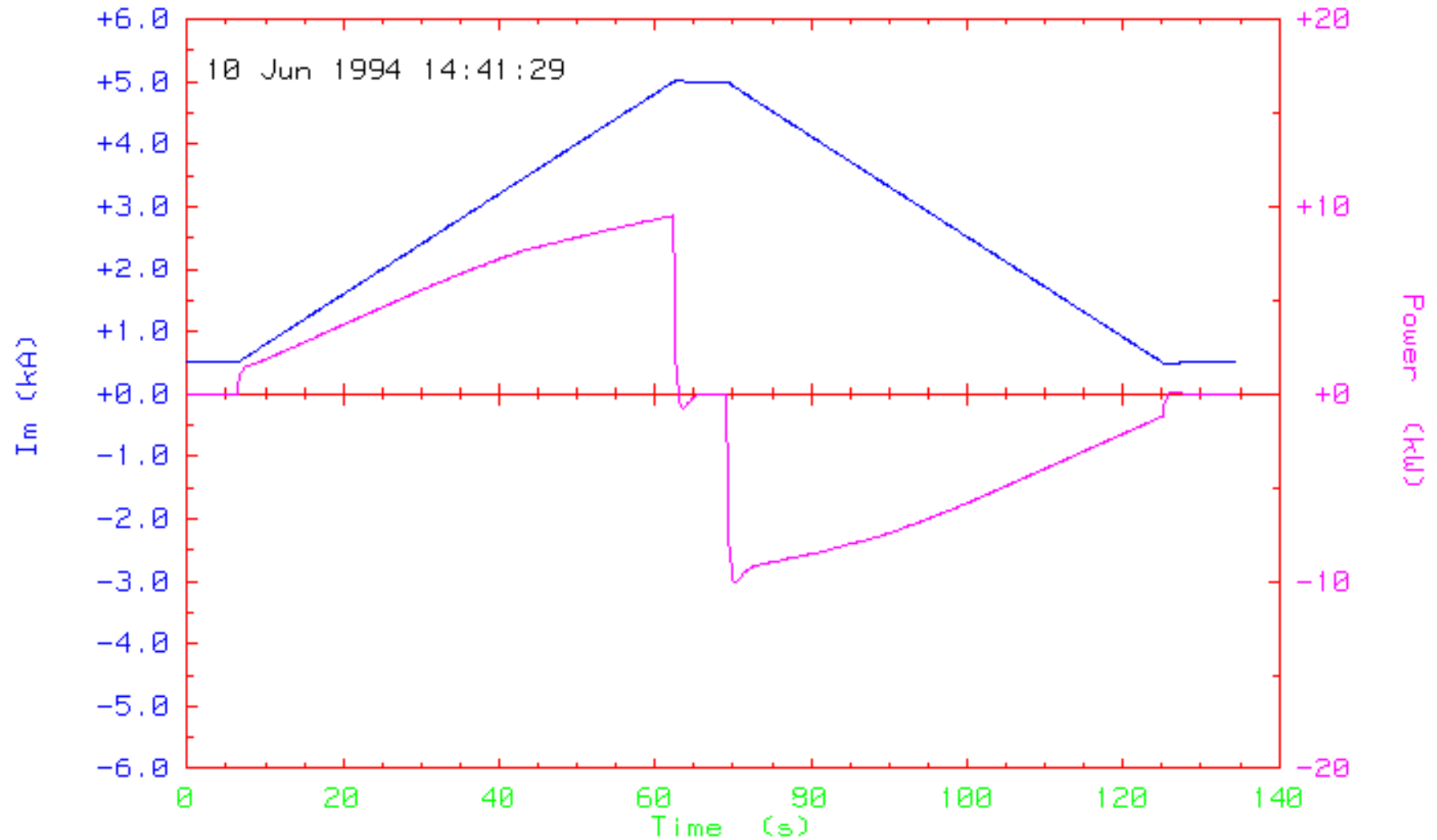
Im and Um

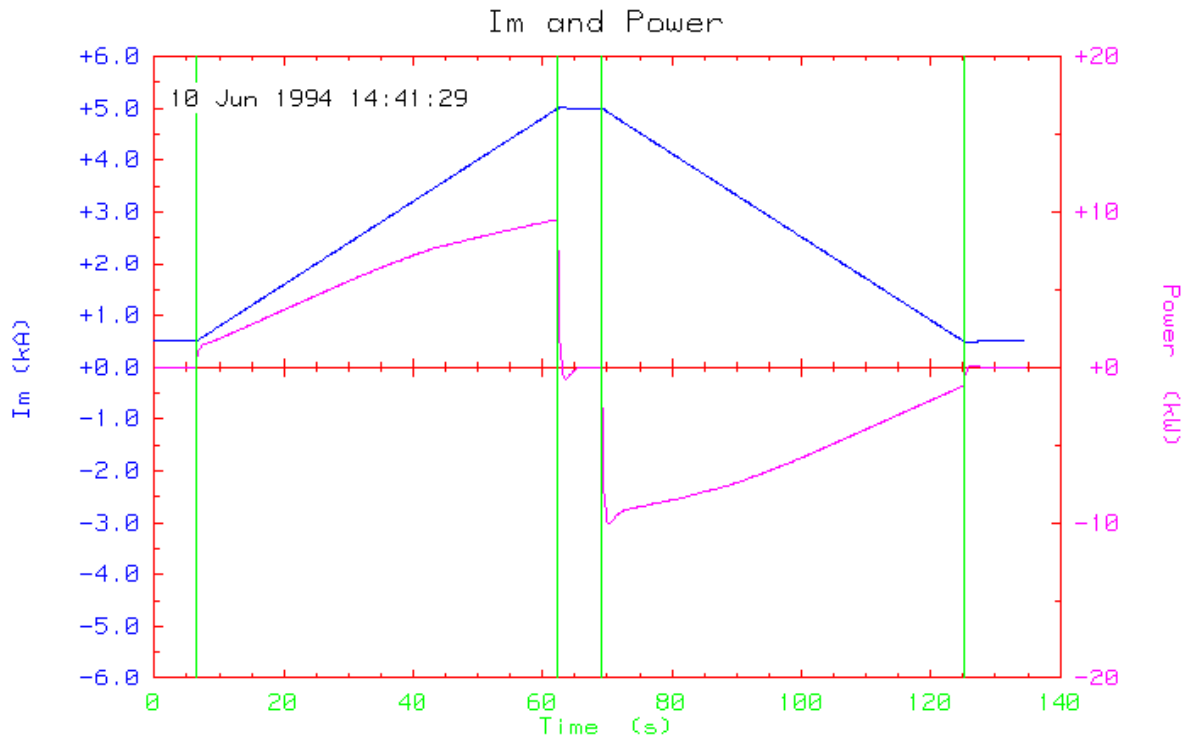
10 Jun 1994 14:41:29



Time per point: 169 ms

Im and Power





10 Jun 1994 14:41:29 Magnet Ac Loss Measurement DRG111

Data File: DRG111_v

Method: Unipolar

798 readings spaced 0.169 s apart, NPLC = 10, coverage = 99%

Imax +5008.8, Imin +489.4

Vmax +2.516, Vmin -2.325

Ramp Pts 38 370 410 742 Diffs: 332 40 332

Im +503 +5002 +4997 +498

Vm +1 +1 -1 -1

1 37.601 6.425 s -0.00 A/s 499.98805 A

2 369.906 62.474 s 80.33 A/s

3 409.633 69.175 s -.53 A/s 5000.48061 A

4 741.682 125.180 s -80.33 A/s

5 797.000 134.511 s 0.00 A/s 499.97751 A

Sum of voltages over entire cycle: .0491 V, Equiv. drift per point: 61.6 uV

Ramp Rates: +80.332 A/s -80.331 A/s Avg. = 80.332 A/s

Inductance: 27.51 mH 27.83 mH Avg. = 27.67 mH

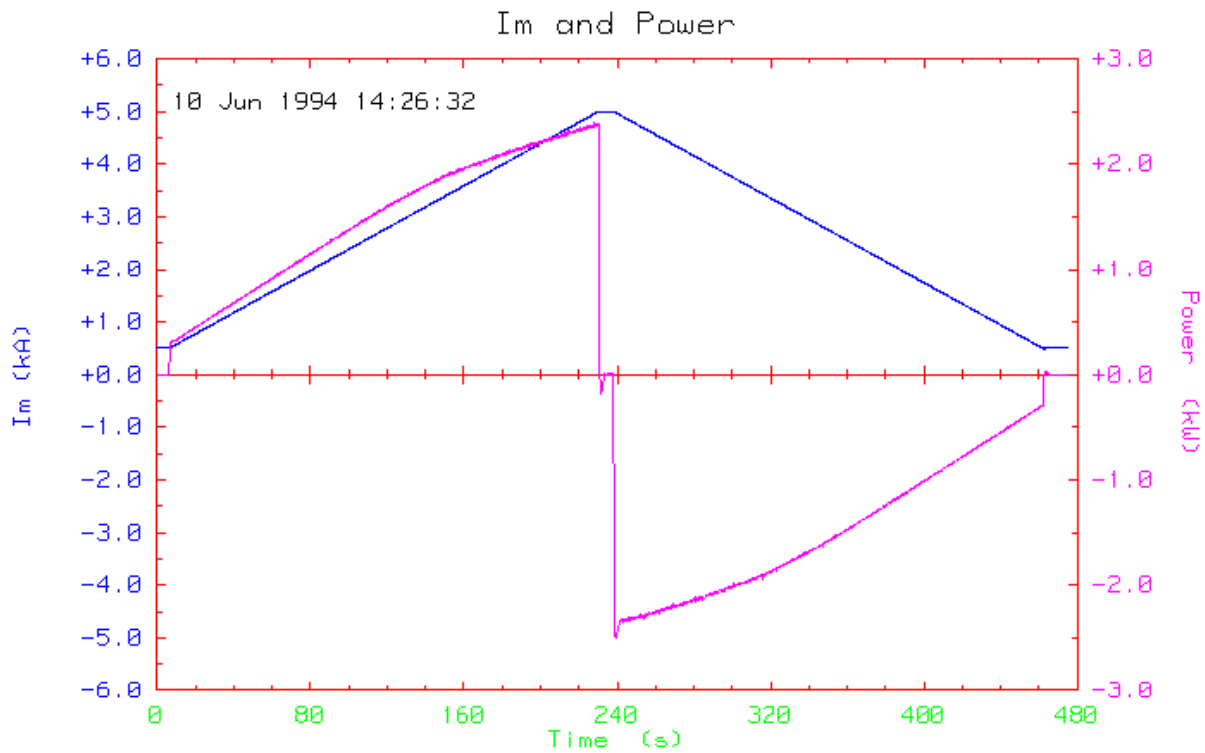
The average power and energy over the entire measurement period were:

3.232 W 435 J

Dwell		Ramp Up		Dwell		Ramp Down		Dwell	
W	J	W	kJ	W	J	W	kJ	W	J
-0.0	-0	+5905.8	+333.7	-134.5	-839	-5885.3	-332.5	+12.8	+117

Time for one cycle: 118.75 s (including dwell at top)

Actual Cycle: +489.4 A to +5008.8 A and return.



10 Jun 1994 14:26:32 Magnet Ac Loss Measurement DRG111

Data File: DRG111_t

Method: Unipolar

2817 readings spaced 0.169 s apart, NPLC = 10, coverage = 99%

Imax +5002.1, Imin +497.4

Vmax +.612, Vmin -.591

Ramp Pts 37 1366 1411 2740 Diffs: 1329 45 1329

Im +500 +5000 +5000 +500

Vm +0 +0 -0 -0

1	37.119	6.344 s	-0.00 A/s	499.98848 A
2	1365.795	230.447 s	20.08 A/s	
3	1411.390	238.138 s	-.10 A/s	4999.96426 A
4	2739.897	462.213 s	-20.08 A/s	
5	2816.000	475.049 s	.01 A/s	499.99331 A

Sum of voltages over entire cycle: -.01563 V, Equiv. drift per point: -5.55 uV

Ramp Rates: +20.082 A/s -20.081 A/s Avg. = 20.082 A/s

Inductance: 27.57 mH 27.64 mH Avg. = 27.61 mH

The average power and energy over the entire measurement period were:

0.6861 W 326 J

Dwell		Ramp Up		Dwell		Ramp Down		Dwell	
W	J	W	kJ	W	J	W	kJ	W	J
-0.0	-0	+1482.2	+333.0	-29.3	-208	-1480.0	-332.5	+2.1	+27

Time for one cycle: 455.87 s (including dwell at top)

Actual Cycle: +497.4 A to +5002.1 A and return.

Ramp Rate (A/s)	Loss (J/cycle)
20	374
20.079	326.0
20.080	352.3
20.081	355.0
30.529	359.8
30.530	368.1
30.541	358.4
40.164	395.0
40.169	385.6
40.170	392.3
50.864	395.4
50.881	393.6
50.895	389.3
61.059	407.3
61.075	403.7
61.076	403.9
69.258	397.5
69.268	419.7
69.283	421.3
80.362	435.0
80.363	432.0
80.363	421.2
80.364	433.0
80.364	435.3
101.791	453.2
101.792	456.3
101.794	462.6
101.798	464.2
101.799	458.6
101.800	464.4

Regression Statistics

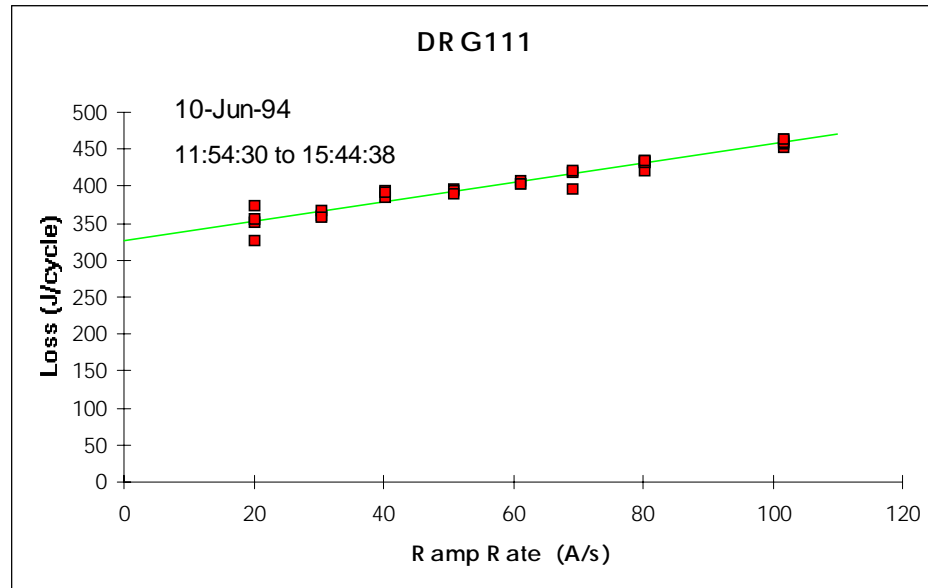
Multiple R	0.9703
R Square	0.9415
Adjusted R Square	0.9394
Standard Error	9.3004
Observations	30

AC Loss Measurements
DRG111

Analysis of Variance

	df	Sum of Squares	Mean Square	F	Significance F
Regression	1	38948.3725	38948.3725	450.29	8.53639E-19
Residual	28	2421.9155	86.496983		
Total	29	41370.2880			

	Coefficients	Standard Error	t Statistic	P-value	Lower 95%	Upper 95%	Lower 90 %	Upper 90 %
Intercept	327.2	4.1	79.1821	9.2E-35	318.7	335.6	320.2	334.2
Ramp Rate (A/s)	1.297	0.061	21.2203	2.8E-19	1.172	1.422	1.193	1.401



Ramp Rate (A/s)	Loss (kJ/cycle)
16.061	1.177
16.065	1.264
16.118	1.210
32.382	1.272
32.385	1.295
32.387	1.294
49.131	1.322
49.133	1.328
49.139	1.353
66.156	1.384
66.177	1.444
66.198	1.459
66.246	1.399
76.316	1.472
76.317	1.445
76.320	1.455
76.325	1.455
101.745	1.406
101.748	1.579
101.757	1.478
101.758	1.583
127.207	1.604
127.249	1.625
127.261	1.641
127.286	1.671
152.720	1.680
152.727	1.885
152.754	1.748
152.758	1.717
169.677	1.830
169.716	1.814
169.728	1.823
190.905	1.964
190.922	1.812
190.937	1.999
190.937	1.809
218.177	2.099
218.184	1.977
218.196	1.923
218.222	1.950

Regression Statistics

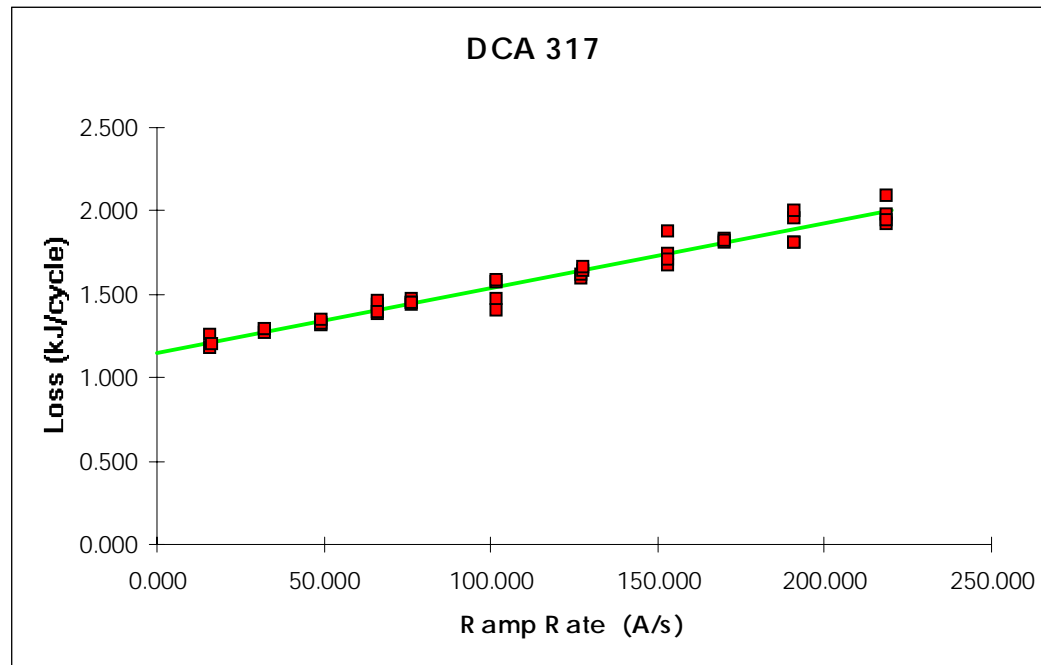
Multiple R	0.9769
R Square	0.9544
Adjusted R Square	0.9532
Standard Error	0.0547
Observations	40

Analysis of Variance

	df	Sum of Squares	Mean Square	F	Significance F
Regression	1	2.3778	2.3778	794.47	4.44299E-27
Residual	38	0.1137	0.002993		
Total	39	2.4916			

	Coefficients	Standard Error	t Statistic	P-value	Lower 95%	Upper 95%	Lower 90 %	Upper 90 %
Intercept	1.154	0.018	64.963	2.29E-41	1.118	1.190	1.124	1.184
Ramp Rate (A/s)	0.00386	0.00014	28.186	1.52E-27	0.00358	0.00413	0.00363	0.00409

AC Loss Measurements
DCA317



Confounding Factors

- ☆ Aperture (integration-time) and dead-time of the meters
- ☆ Noise
 - What is noise and what is signal?
- ☆ Phase shift in either the V or I signal, including any rate-dependent phase shift
- ☆ Start and End Current must be identical, (~ 74 J/A error for RHIC)
- ☆ Main Magnet Power Supply ramping characteristics
- ☆ Time-consuming to acquire data when ramping to full field at low ramp rates

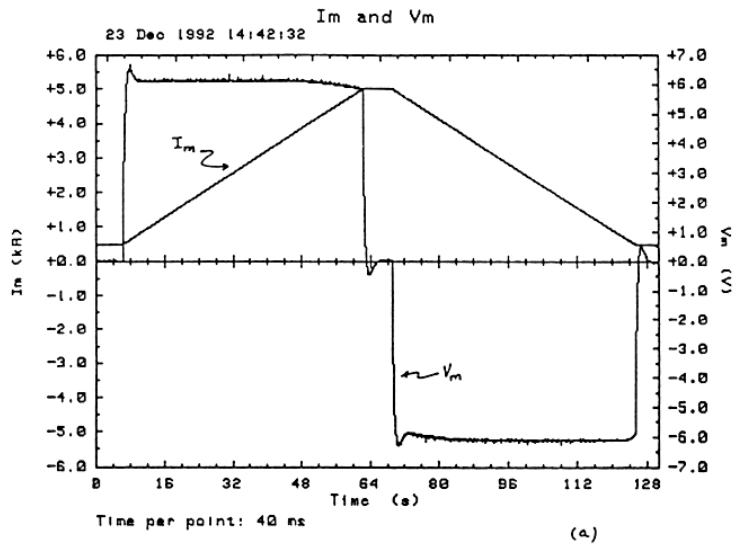


Figure 1. (a) I_m and V_m .
(b) I_m and instantaneous Power.

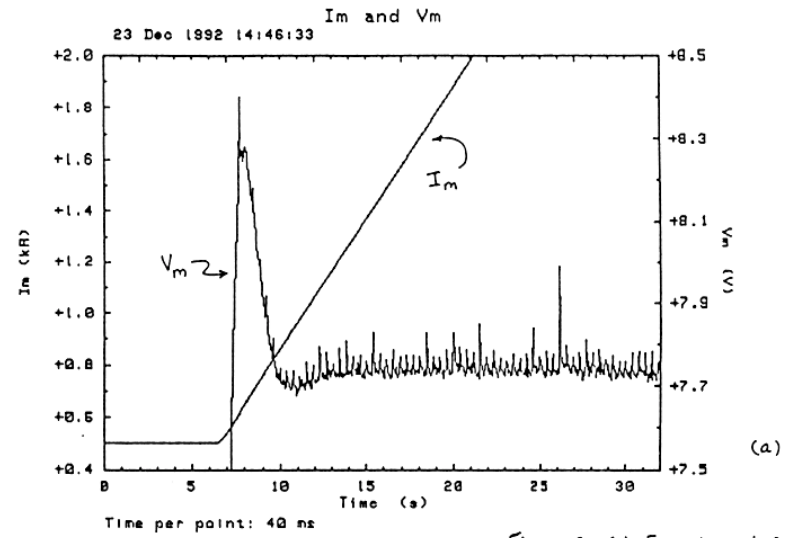
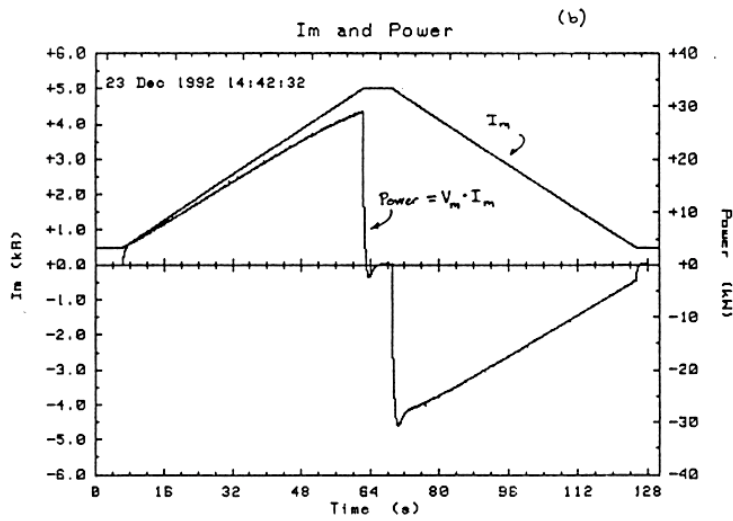
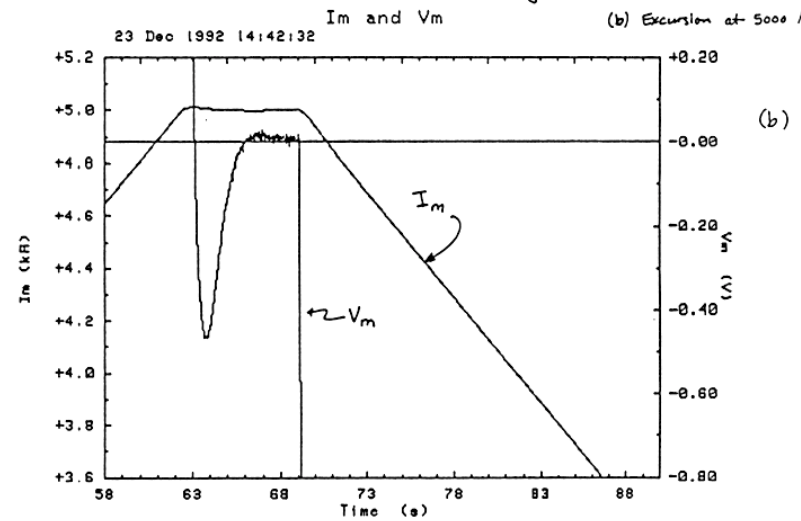
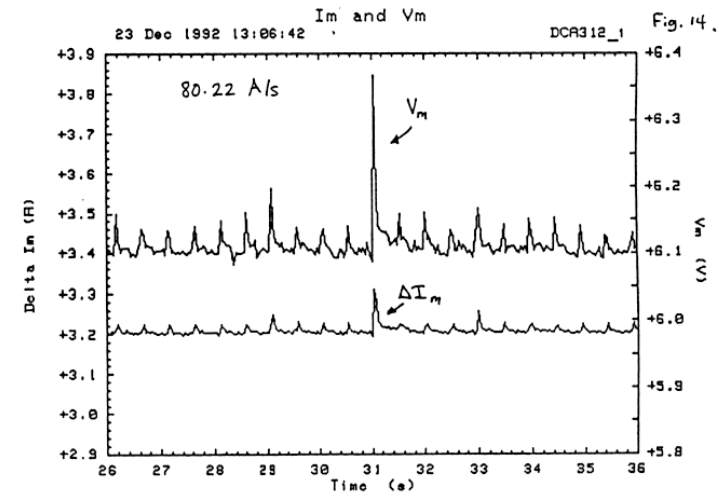
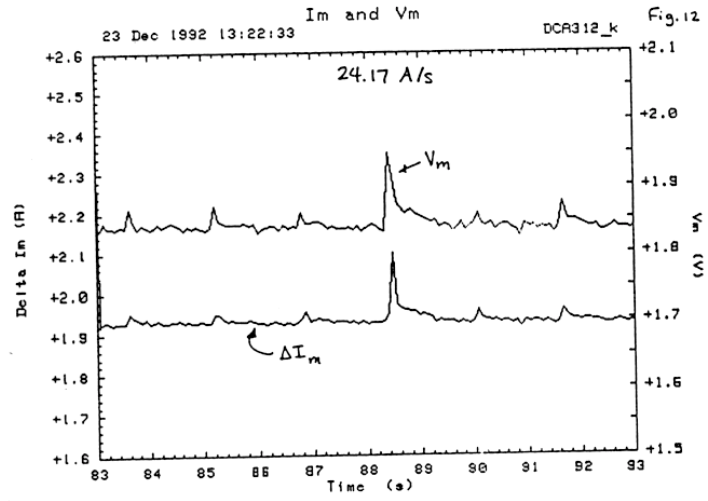
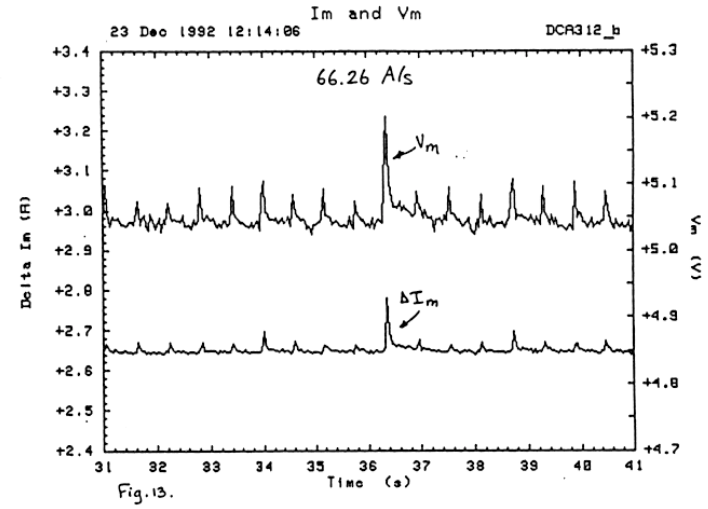
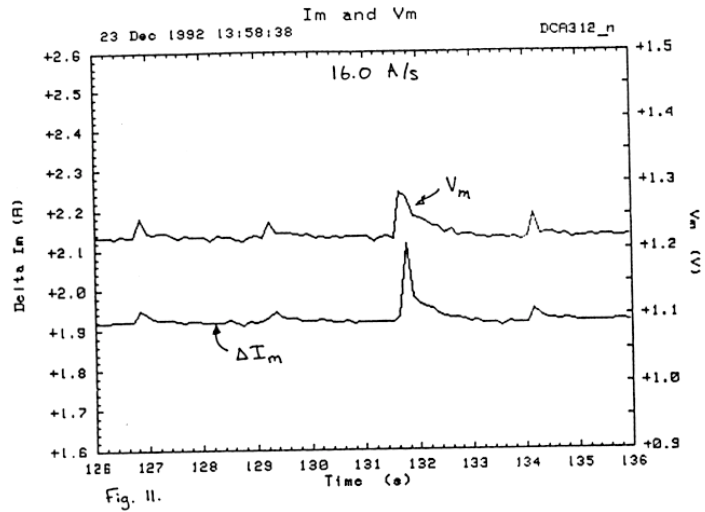
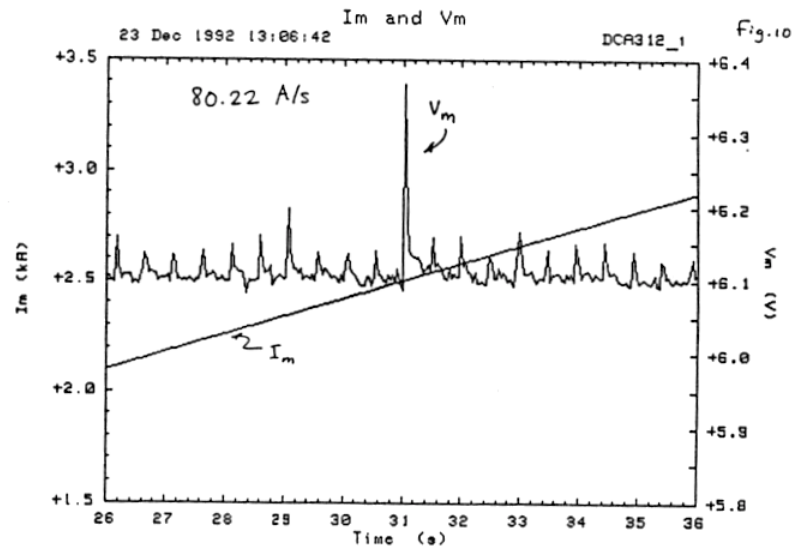
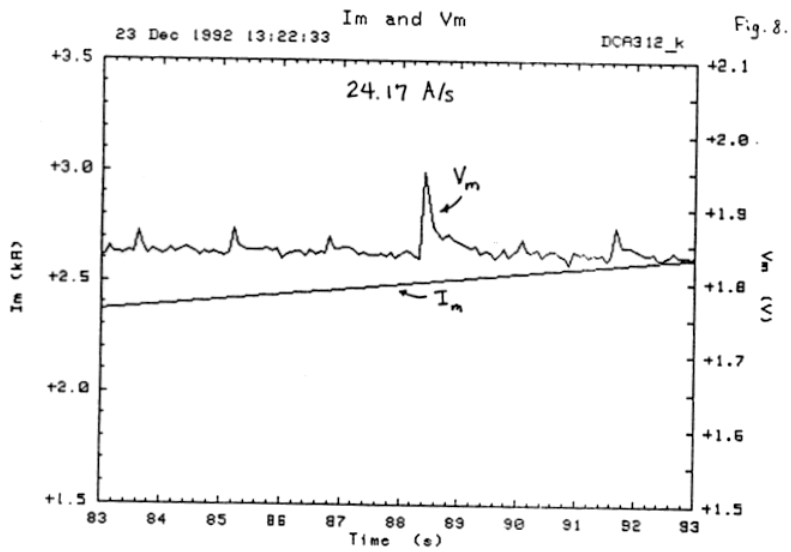
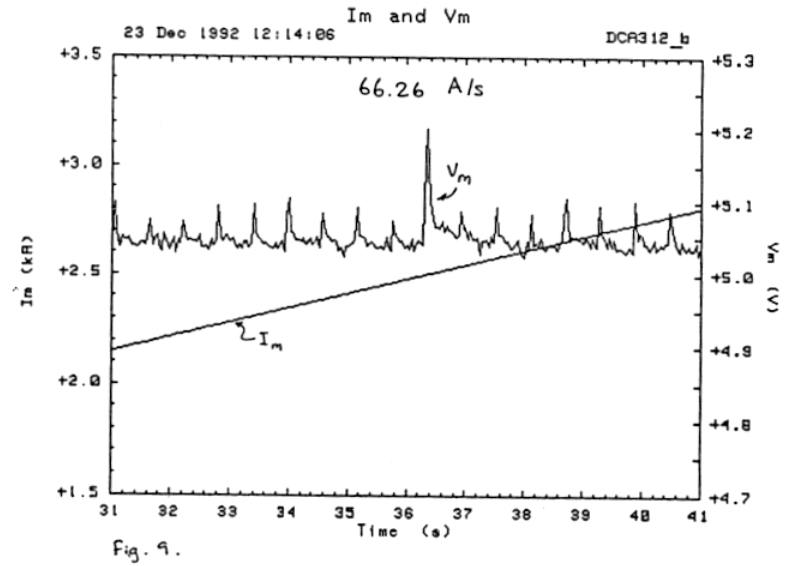
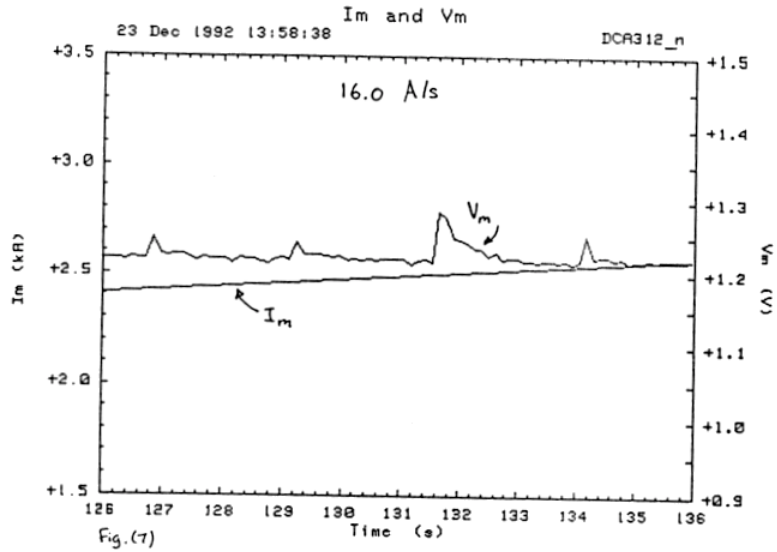


Figure 2. (a) Excursion at 500 A.
(b) Excursion at 5000 A.

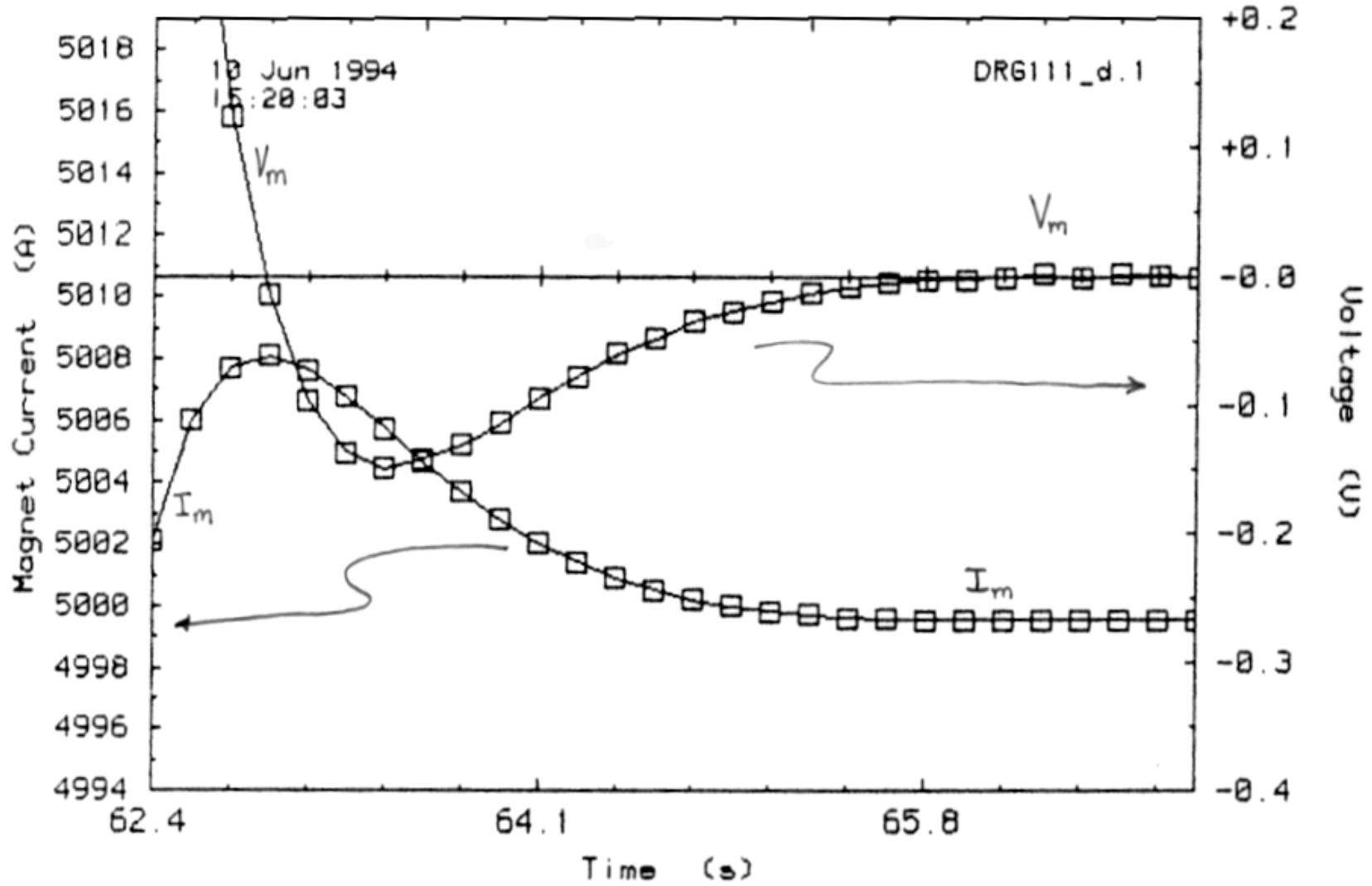


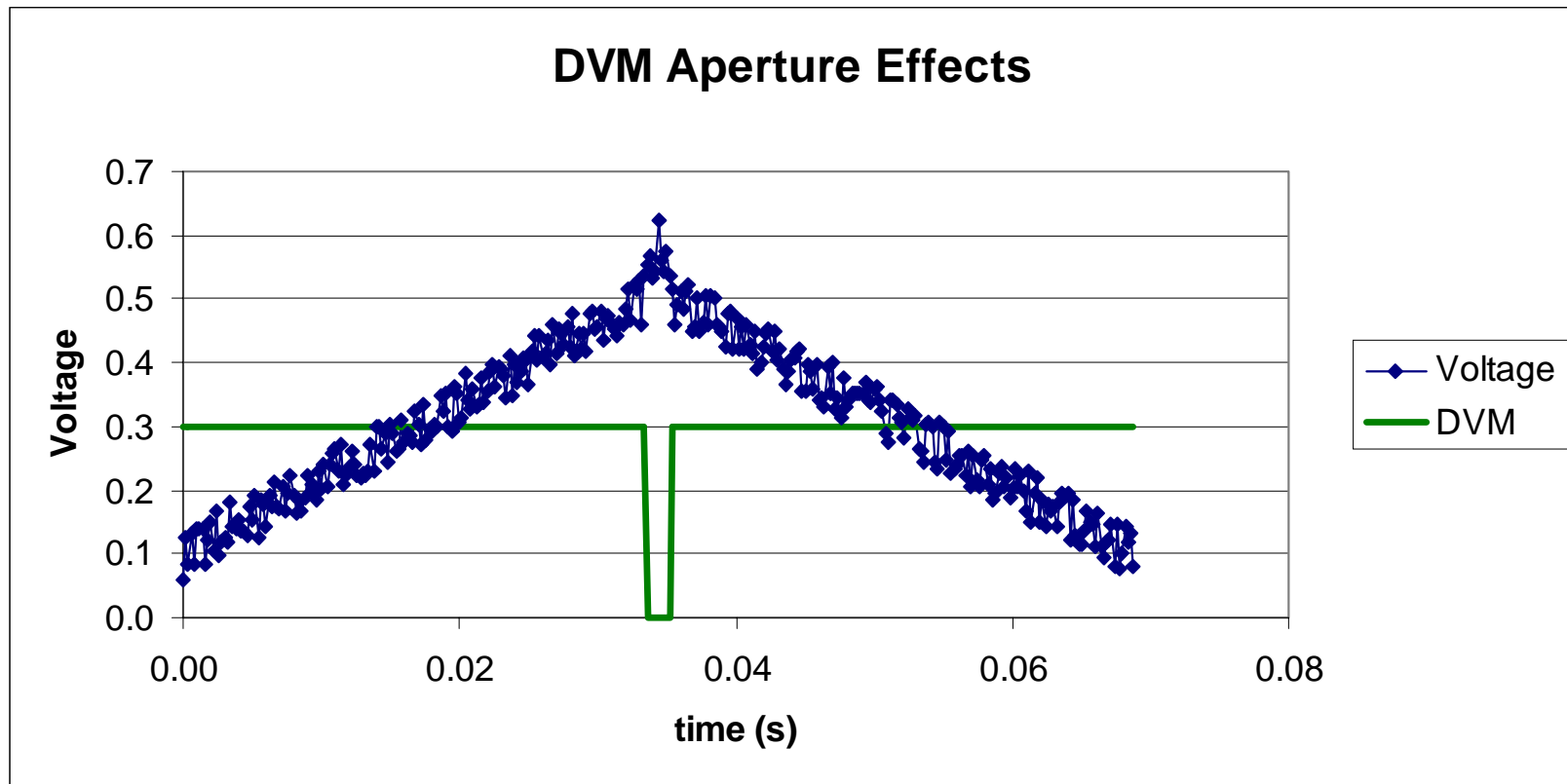


Old Power Supply DAC

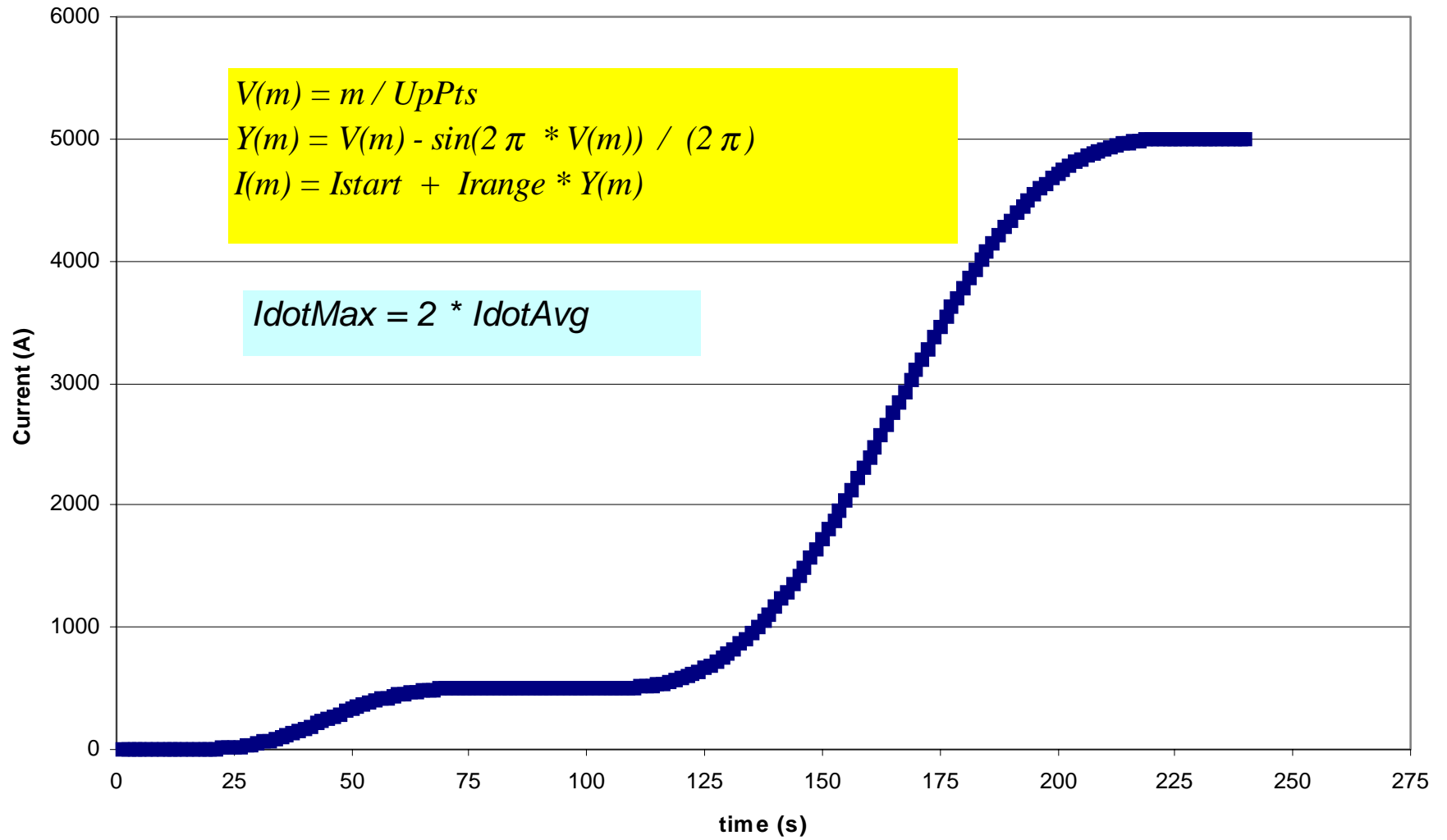


Im and Vm vs. Time





Current vs. Time



Calibration

Methods to check ability of $I \cdot V$ method to measure small losses

* **Eddy Currents**

$$P = \frac{\pi \dot{B}^2 l r_o^4}{4\rho}$$

For 2-inch radius brass rod as long as the magnet, the energy loss is ~200 J at 70 A/s.

$$E_{loss} = P \times 2 \frac{I_{end} - I_{start}}{\dot{I}}$$

- * **Coil** More attractive than eddy current method, but requires construction. Probably capable of producing larger losses than a brass tube, and the amount of added loss can be controlled by rotating the coil.

Conclusions

- ❑ If the energy loss per cycle is $> \sim 0.3\%$ of the field energy, the $V \cdot I$ electrical technique should be capable of measuring the loss.
- ❑ “Smooth” ramps are desirable to avoid the effects of power supply overshoot and undershoot.
- ❑ A calibration device is needed to verify that the method works.

NMR PROBE AS
A FIELD MARKER
IN A QUADRUPOLE

(D. Cornuet, F. Caspers)
(Cern)

September 21-24, 1999
at Brookhaven
IMMW-11

1. NMR magnetic markers

- A B-train generation is necessary for synchronization of the equipment of an accelerator. This is obtained by electronic integration of the signal of a pick-up coil in a reference magnet.
- Magnetic markers improve the B-train accuracy and reproducibility by taking into account the remanent field and by correcting the gain drift and offset drift of the electronics.

- NMR (nuclear magnetic resonance) markers are used on the flat-bottom and flat-top in a reference dipole of the CERN-SPS since late 80's. Implemented in normal mode which requires 0.3 second and stable value of the field.
- The standard range of operation for miniature NMR probes starts around 0.04 Tesla and extends beyond 13 Tesla. Bigger custom probes may operate down to 0.011 Tesla.

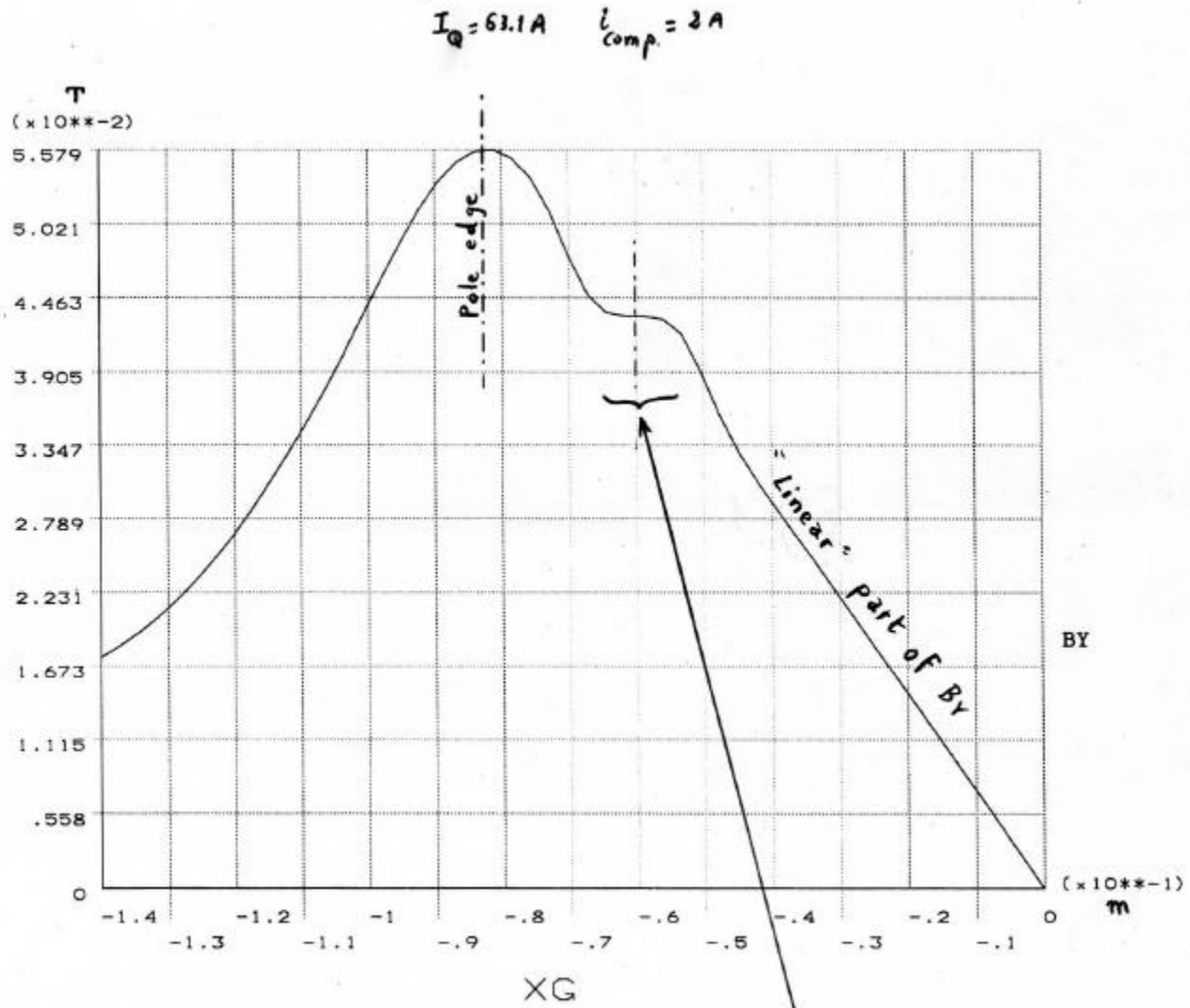
- Certain NMR instruments can operate in a ramp mode and deliver a bip when the field crosses a predefined value. For the CERN PS Booster NMR probes in a reference dipole are used in both (normal and ramp) modes since 1997 to generate the B-train.
- For the CERN AD (Antiproton Decelerator) a dipole of the machine itself is equipped with pick-up coils and NMR probes outside the vacuum chamber. Gradient compensation coils correct non homogeneity of the field and a copper shield eliminates noise > 600 Hz.

- For the CERN SPS (super proton synchrotron), in the framework of the LHC era, a better reproducibility (10^{-4}) of the focusing lenses (quadrupoles) is required. A study of a NMR marker in a reference quadrupole is undertaken in the view of the creation of a "G-train".

2. G-train for quadrupoles

- a) NMR probe in “linear” part of the quadrupolar field.
- b) NMR probe in the zero gradient region
 - . With homogenizing plates
 - . With compensation coils

1



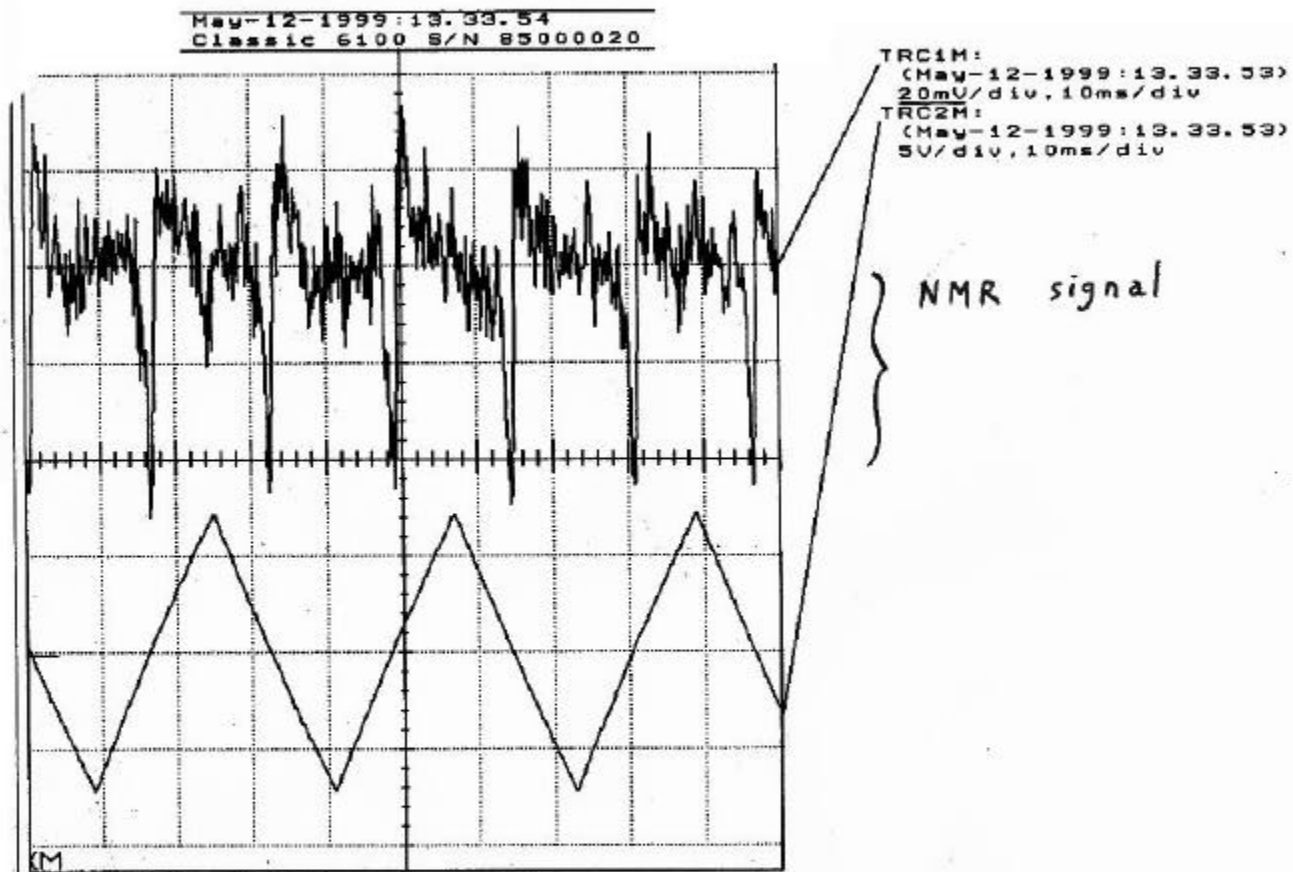
Magnetic Analysis SPS Quadrupole QP + Compensation Coils

Plot 1

a) NMR probe in “linear” part of the field (plot 1)

- Difficulty for locking (see plot 2) with gradient compensation coils (homogeneity of 200 ppm/cm required).
- Drawbacks:
 - First order of the gradient of the quadrupole has to be compensated, the cumulated unstabilities of the main power supply and the compensation power supply should be better than 10^{-4}

plot 2

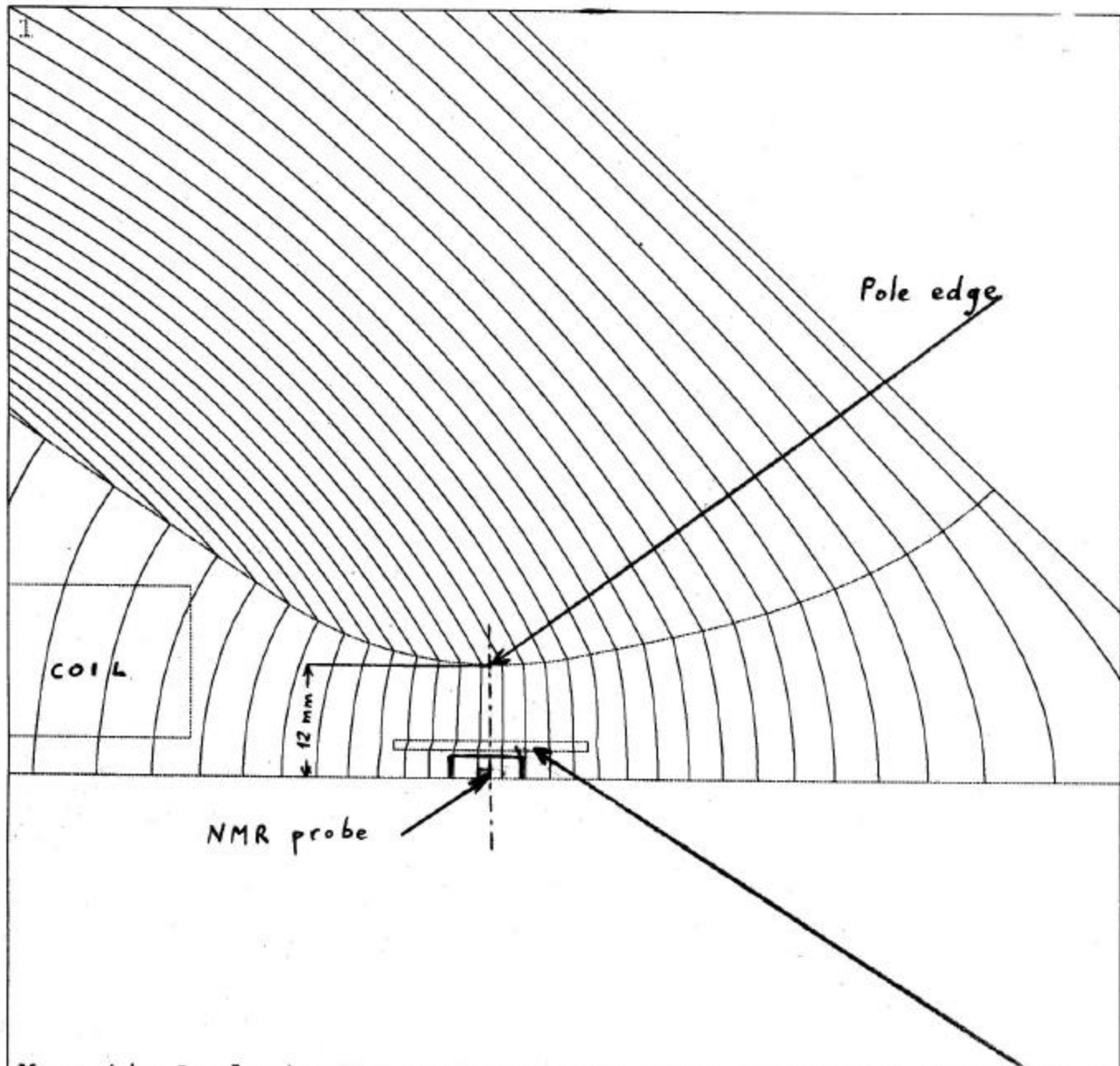


SPS Quadrupole QP + Compensation Coils

- The mechanical stability is crucial (< 6 micron for a position 60 mm from the center) and should be guaranteed with time and temperature.
- Any tiny inhomogeneity of the gradient or noise of the power supply prevents locking of the NMR probe.
- To avoid too much heating up, the compensation current should be kept reasonably low (approx. 3 A), but in the lower range of the probe the useful signal amplitude is reduced (< 90 mV @ 0.06 T).

b) NMR probe in zero gradient region (plot 1)

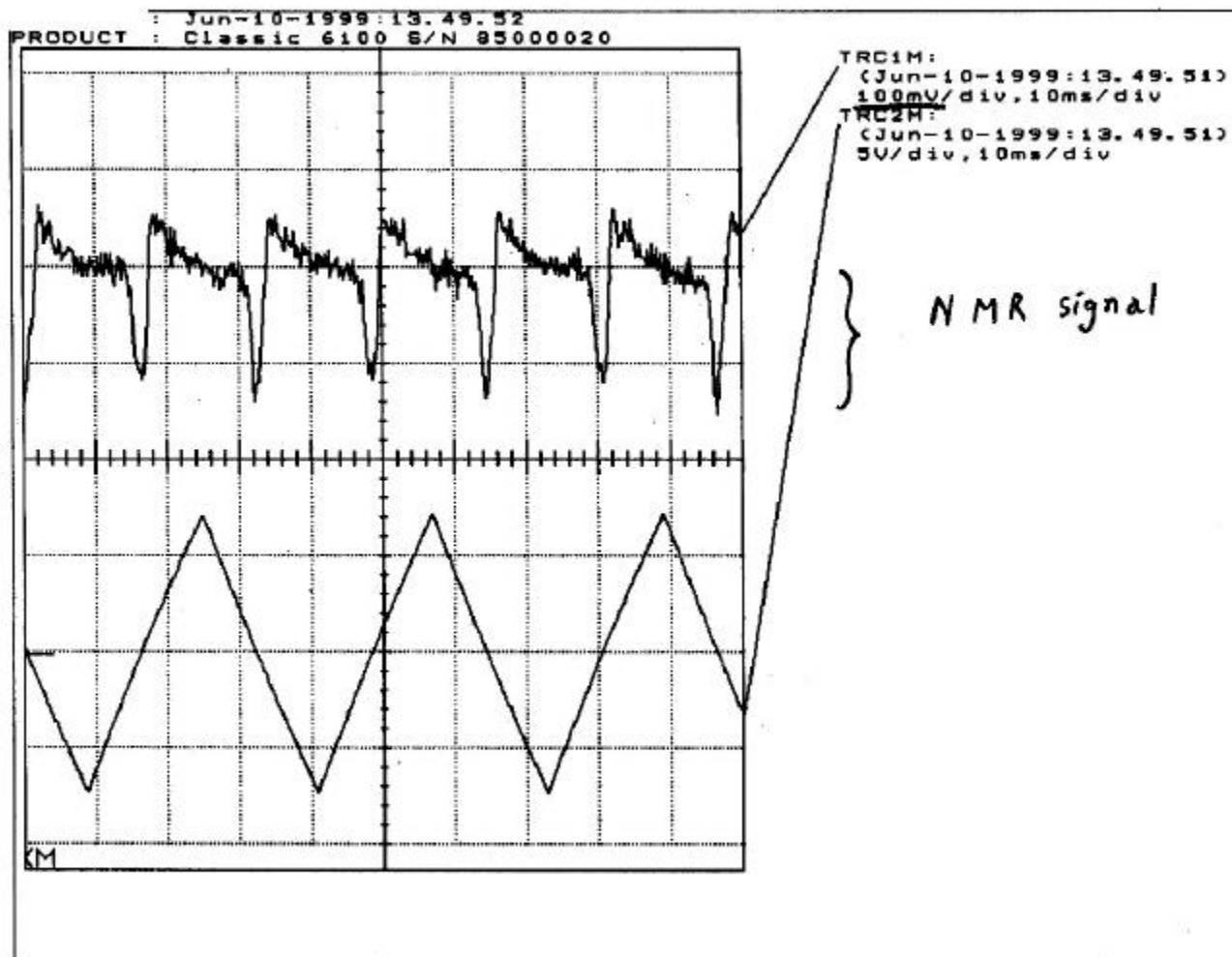
- With homogenizing plates (plot 3) :
 - No problem for locking (see plot 4) ,
 - No compensation coils ,
 - No severe tolerances needed .



Magnetic Analysis SPS Quadrupole QP with Additional Homogenizer

plot 3

plot 4



SPS Quadrupole QP with Additional Homogenizer

– Drawbacks :

- Despite the lack of space, the mechanical stability of the magnetic homogenizing plates must be guaranteed (high electromagnetic forces when the quadrupole is pulsed to the maximum current) ,
- Magnetic properties of the plates might drift in time and distort the field locally, then give a wrong image of the behaviour of the quadrupole magnet; but studies to replace steel plates by ferrites are under way.

- **With compensation coils**
 - Gradient coils + Sextupolar coils
(see plot 1)
 - Many parameters to adjust :
 - the expected level of field for locking,
 - the current of the sextupolar coils,
 - the current of the gradient coils.
 - Tests will begin soon.

3. Conclusion

- Preliminary tests of the feasibility of a “G-train” for the Cern-SPS machine has been undertaken.
- Several methods have been evaluated: with and without gradient compensation coils.
- The set-up where NMR probes are placed under the pole edges seems promising for a reproducibility of the focusing elements of the machine better than $10E-4$.

Overview Of Magnetic Measurements At SLAC

Z. Wolf, SLAC

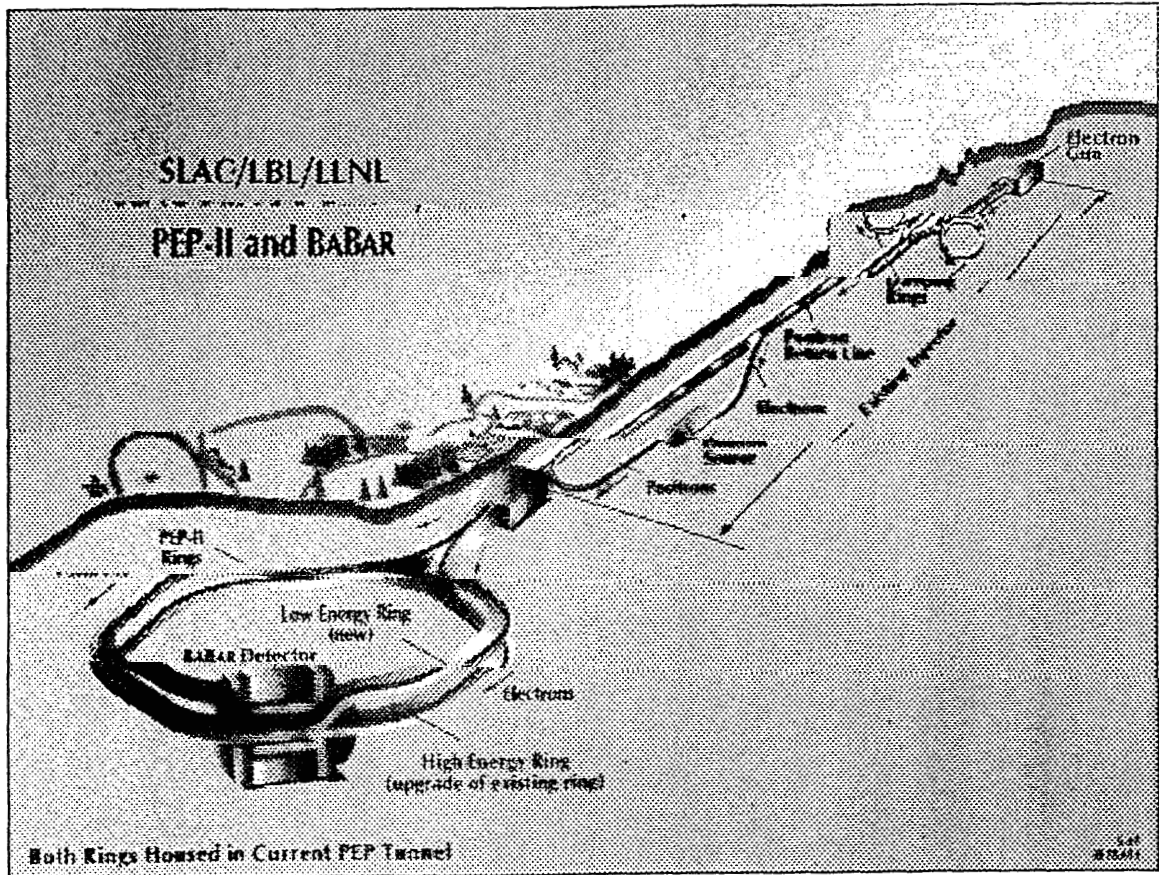
- 1) PEP II (asymmetric B factory) is running
5 year magnetic measurement effort

- 2) Next project is SPEAR III
Light source
Combined function magnets
Performing initial design study measurements

- 3) On the horizon is LCLS
Linac Coherent Light Source
Initial studies are underway

- 4) Over the horizon is NLC

PEP II

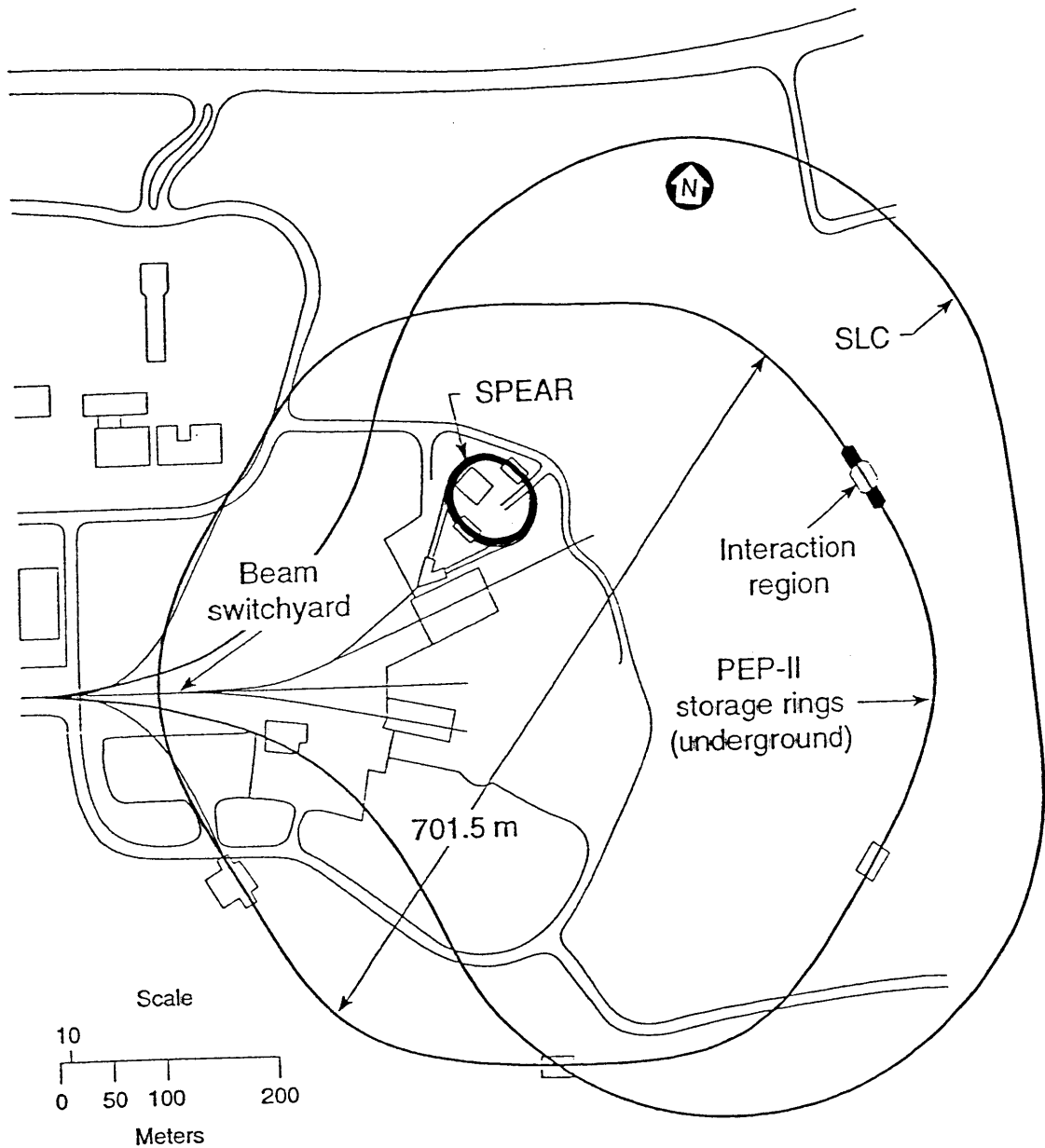


Asymmetric B Factory

$$E_{e^-} = 9 \text{ GeV}$$

$$E_{e^+} = 3.1 \text{ GeV}$$

SPEAR III



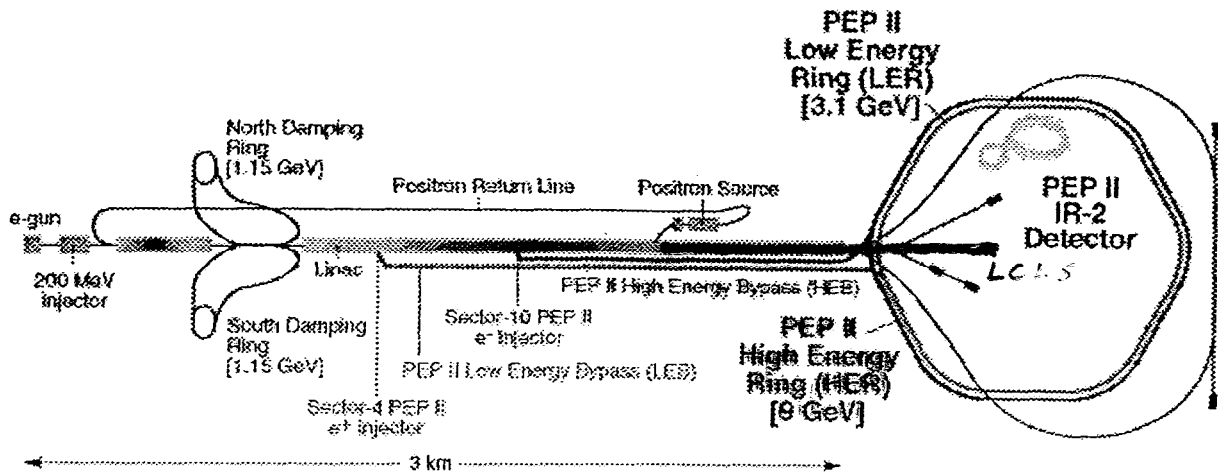
Light source

SPEAR III

30	<i>Gradient Dipoles</i>
102	<i>Quadrupoles</i>
76	<i>Sextupoles</i>
72	<i>Correctors</i>

The magnets are being designed now. They will be built in China. Field quality measurements will be made in China. Other measurements will be made at SLAC.

LCLS



*The SLC is no longer running.
The last 1/3 of the linac
is available to build a
free electron laser.*

*Experiments are underway now
(e.g. VISA) in preparation for
this project.*

Magnet Alignment of the RHIC Magnets and Operational Experience

Dejan Trbojevic, BNL

ABSTRACT

No abstract was received for this talk.

The contents of this talk were not available for inclusion in the proceedings.



Automated Polarity Checking for RHIC Magnet Assemblies

Richard Thomas, Wing Louie,
George Ganetis, Animesh Jain,
and Peter Wanderer

RHIC Project
Brookhaven National Laboratory

INTRODUCTION

Collider magnet assemblies have numerous variations relating to the power connections

Needed a quick method to check that the polarity of magnetic elements agreed with the database specification before the assembly was delivered to the tunnel

RHIC Magnet Assemblies, Definitions

Sextant → Sextant 1 = 12 — 2 o'clock,
Sextant 2 = 2 — 4 o'clock, etc.

HS → Half Sextant, Half sextants 1 & 2 are in Sextant 1,
HS 11 & 12 in Sextant 6.

Yellow, Blue Rings →

Yellow Ring: Beam circulates in the ring counterclockwise (CCW)

Blue Ring: Beam circulates in the ring clockwise (CW)

Inner, Outer → The rings cross.

Yellow Ring is the Outer Ring in Sextants 1, 3, and 5.

YO = Half Sextants 1,2,5,6, 9,10

YI = Half Sextants 3,4,7,8,11,12

Blue Ring is the Outer Ring in Sextants 2, 4, and 6.

BO = Half Sextants 3,4,7,8,11,12

BI = Half Sextants 1,2,5,6, 9,10

CW, CCW = The lead-end of the assembly points in this direction.

Focus, Defocus → What the quad does in the *horizontal* plane. It does the opposite in the vertical plane.

Lead-End → The end of the CQx Assembly where the corrector magnet is located, opposite the end where the BPM is located. (*Exceptions: CQ3's have correctors at both ends, CQ1's have no correctors, and CQ2's have correctors at their non-lead ends and no BPMs.*)

CQS → Corrector, Quad, Sextupole (Corrector is at the Lead-End)

CQT → Corrector, Quad, Quad Trim

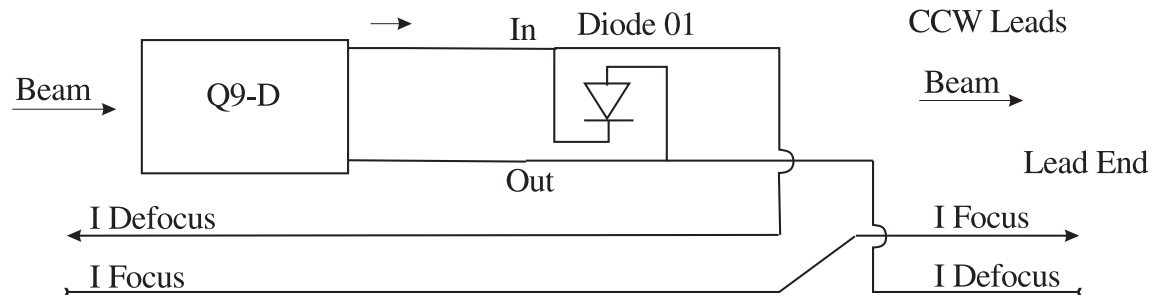
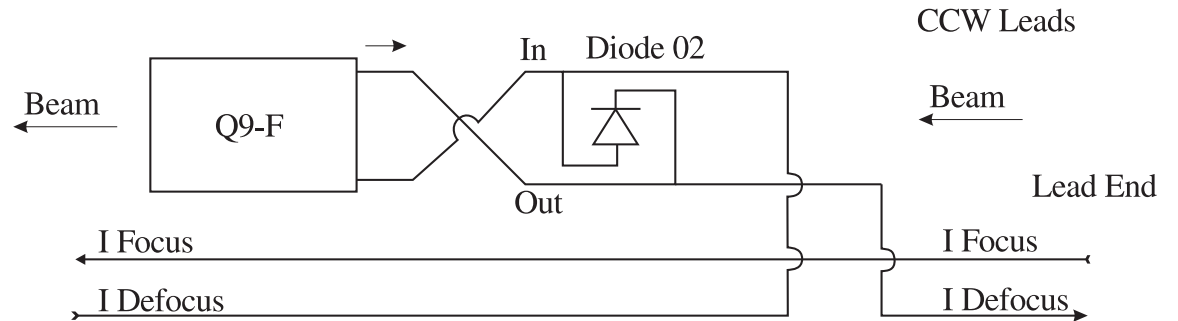
CQB → Corrector, Quad, Blank. A blank has the iron, but no powered coils.

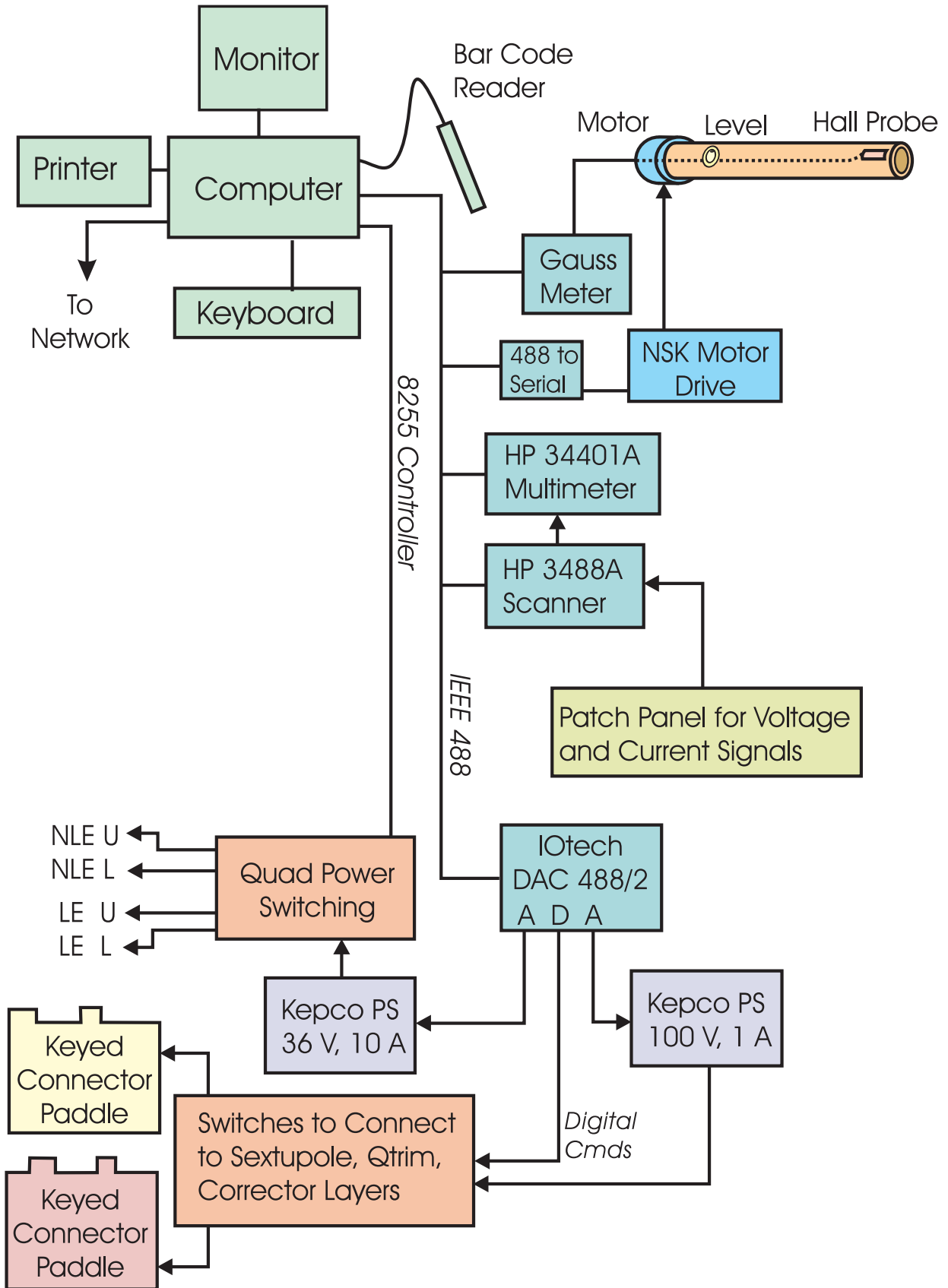
CQn → ($n \geq 4$), A short quadrupole assembly (not even a blank at the BPM end).

94 Quad Magnet Assembly Models with 8-cm bore (420 assemblies)

24 Quad Magnet Assembly Models with 13-cm bore (72 assemblies)

For all models except the CQ3 models, quadrupoles with Diode Type 01 all have a North magnetic pole on the upper right as seen from the lead end and quadrupoles with Diode Type 02 all have a South pole there *unless there is a Boxswitch to reverse the current in the quadrupole*. For the CQ3's, the opposite is the case.





Place rotating Hall Probe in one end of assembly.

Enter Assembly Name (or swipe bar code with bar code reader)



Program uses the Assembly Name entered to retrieve information regarding this combined element magnet assembly from the network database.

Operator is asked which element is being measured (Lead-end, non-lead end, or main quad [center element]).

Program applies current to appropriate magnetic element(s).

obtains B at 32 angles for +I

obtain B at 32 angles for -I

does FFT on Bdiff (the difference signal)

determines whether the result is the expected result

plots results, informs operator of results

After measuring all the magnetic elements at each location of the assembly, the operator replays the results and the program prepares a summary file which is stored on the network.

Replay of Run CQS192.P01

1 Sep 1995 CQS192.P01
Points/Revolution: 32

Assembly: CQS192 Type: CQS Diode Polarity: 01
Elements: CRB QRG SRE
Style: B
Layers: b0 b1 b3 b4 b1 b2

Record: 1 12:57:40

Z = 0.00 I- = -0.200 I+ = +0.200 Hall temp = 25.6

Element: 1 Layer: 1

Element: CRB Normal Dipole Layer R = 390 ohms

The field seen by the Hall Probe is primarily a dipole field.

0	1	21.361	+0.782	<<<<<
1	2	0.136	-84.095	
2	3	0.106	-19.572	
3	4	0.053	-21.082	
4	5	0.086	+35.756	
5	6	0.026	-13.427	
6	7	0.032	-6.019	
7	8	0.017	-4.008	
8	9	0.014	-1.650	

Normal Dipole Field

Record: 2 13:00:32

Z = 0.00 I- = -0.200 I+ = +0.200 Hall temp = 25.6

Element: 1 Layer: 2

Element: CRB Normal Quadrupole Layer R = 120 ohms

The field seen by the Hall Probe is primarily a quadrupole field.

0	1	0.100	+113.659	
1	2	3.310	-1.871	<<<<<
2	3	0.027	+48.977	
3	4	0.011	-31.863	
4	5	0.008	-15.690	
5	6	0.016	+28.465	
6	7	0.004	-11.139	
7	8	0.004	-4.503	
8	9	0.003	-6.693	

Normal Quadrupole Field

Record: 5 14:52:57
 Z = 0.00 I- = -0.250 I+ = +0.250 Hall temp = 25.6
 Element: 3 Layer: 1
 Element: SRE Normal Sextupole R = 218 ohms
 The field seen by the Hall Probe is primarily a sextupole field.

0	1	0.167	+66.860	
1	2	1.092	+31.976	
2	3	24.813	+2.173	<<<<<
3	4	0.110	+5.908	
4	5	0.097	+28.681	
5	6	0.028	-18.002	
6	7	0.018	-22.183	
7	8	0.145	-11.081	
8	9	0.627	-16.782	

Normal Sextupole Field

Record: 6 14:57:53
 Z = 0.00 I- = -1.005 I+ = +1.005 Hall temp = 25.6
 Element: 2 Layer: 1
 Element: QRG Normal Quadrupole R = 0.54 ohms

Diode Polarity check:

Forward Bias Voltage: 1.493
 Reverse Bias Voltage: 2.725
 Diode Polarity Test PASSED

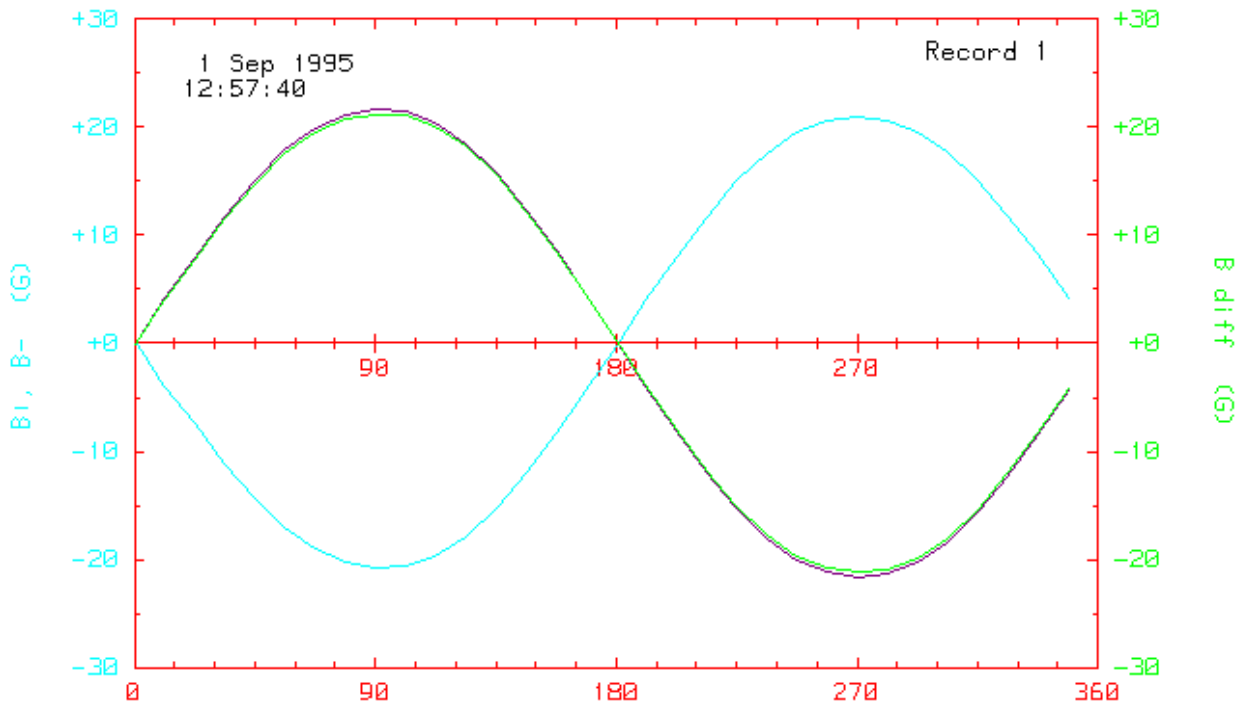
The field seen by the Hall Probe is primarily a quadrupole field.

0	1	0.265	-104.624	
1	2	4.543	+1.438	<<<<<
2	3	0.025	+4.839	
3	4	0.019	+31.344	
4	5	0.005	-23.337	
5	6	0.009	+27.947	
6	7	0.006	-19.127	
7	8	0.002	+4.609	
8	9	0.004	+18.165	

Normal Quadrupole Field

Normal (non-inverted) field result is correct.
 A non-inverted field is expected for non-CQ3 quadrupole magnets with diode polarity 01, no boxswitch, and to which the power leads have been properly connected.

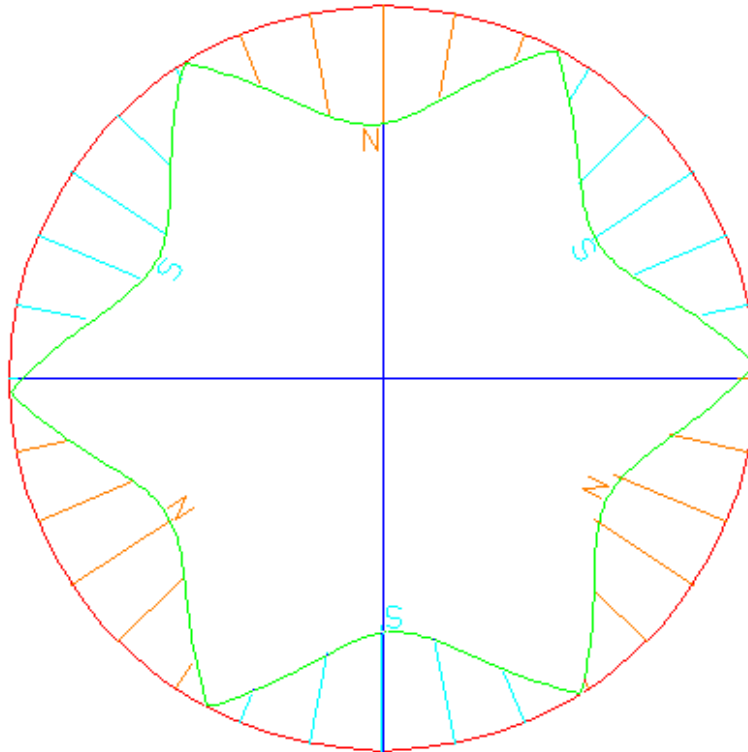
Hall Field Measurements
+I, -I, and Difference
CQS192.P01 Corrector Normal Dipole Layer



Normal Sextupole Field
CQS192.P01

1 Sep 1995
14:52:57

CQS Assembly
Element: SRE
Normal Sextupole



Pass/Fail for CQS179, written on 26 May 1995 at 14:16:56
Using data file of 26 May 1995 at 13:38:59
Operator Life Number: Unknown

Program: Polarity.Ck V 3.0 15 May 95 9:30
Assembly: CQS179 Type: CQS Diode Polarity: 01
Elements: CRB QRG SRE
Style: B
Layers: b0 b1 b3 b4 b1 b2

Element: CRB	Normal Dipole Layer	PASSED	R = 388 ohms
Element: CRB	Normal Quadrupole Layer	PASSED	R = 119 ohms
Element: CRB	Normal Octupole Layer	PASSED	R = 101 ohms
Element: CRB	Normal Decapole Layer	PASSED	R = 88 ohms
Element: SRE	Normal Sextupole	PASSED	R = 216 ohms
Element: QRG	Normal Quadrupole	PASSED	R = 0.54 ohms
Diode Polarity Test		PASSED	

Example of the Summary File written to the Network File Server

Pass/Fail for CQS142, written on 15 May 1995 at 09:33:44
 Using data file of 15 May 1995 at 08:58:16
 Operator Life Number: Unknown

```

Program: Polarity.Ck V 3.0 15 May 95 9:30
Assembly: CQS142 Type: CQS Diode Polarity: 02
Elements: CRD QRG SRE
Style: D
Layers: b0 b1 b2
Element: CRD Normal Dipole Layer PASSED R = 390 ohms
No layer 2
No layer 3
No layer 4
Element: SRE Normal Sextupole PASSED R = 216 ohms
Element: QRG Normal Quadrupole PASSED R = 0.54 ohms
Diode Polarity Test PASSED
  
```

Conclusions

Clarify Definitions (Example: Does “Lead End” mean the “Lead End” of the magnet assembly or the “Lead End” of the magnet element in the magnet assembly.)

Few polarity wiring errors were observed. (3 were reported by the program over the course of the RHIC magnet construction, but only 1 appears to have been an actual error — an open or shorted lead to a corrector magnet layer — the other two were due to testing spares which had no diode installed.)

The Polarity Checker gave confidence that the elements of the magnet assemblies, as delivered, had the polarities specified in the database.